



Forschungszentrum Karlsruhe
Technik und Umwelt

Wissenschaftliche Berichte
FZKA 6099

Results of the QUENCH Commissioning Tests

**P. Hofmann, C. Homann, W. Leiling,
A. Miassoedov, D. Piel, L. Schmidt,
L. Sepold, M. Steinbrück**

**Institut für Materialforschung
Institut für Reaktorsicherheit
Hauptabteilung Ingenieurtechnik
Projekt Nukleare Sicherheitsforschung**

August 1998

Forschungszentrum Karlsruhe

Technik und Umwelt

Wissenschaftliche Berichte

FZKA 6099

Results of the QUENCH Commissioning Tests

P. Hofmann, C. Homann, W. Leiling, A. Miassoedov,
D. Piel, L. Schmidt, L. Sepold, M. Steinbrück

Institut für Materialforschung
Institut für Reaktorsicherheit
Hauptabteilung Ingenieurtechnik
Projekt Nukleare Sicherheitsforschung

Forschungszentrum Karlsruhe GmbH, Karlsruhe
1998

**Als Manuskript gedruckt
Für diesen Bericht behalten wir uns alle Rechte vor**

**Forschungszentrum Karlsruhe GmbH
Postfach 3640, 76021 Karlsruhe**

**Mitglied der Hermann von Helmholtz-Gemeinschaft
Deutscher Forschungszentren (HGF)**

ISSN 0947-8620

Abstract

The QUENCH Commissioning Tests were performed in the QUENCH test facility at the Forschungszentrum Karlsruhe in the period October 9 - 16, 1997. The QUENCH test facility was built to investigate the hydrogen source term that results from the water injection into the uncovered core of a Light-Water Reactor (LWR). The test bundle is made up of 21 fuel rod simulators each with a length of approximately 2.5 m. Twenty fuel rod simulators are heated over a length of 1024 mm, the one unheated fuel rod simulator is located in the center of the test bundle. The rod cladding is identical to that used in LWRs: Zircaloy-4, 10.75 mm outside diameter, 0.725 mm wall thickness. Heating is carried out electrically using 6 mm diameter tungsten heating elements, which are installed in the center of the rods and which are surrounded by annular ZrO₂ pellets. The test bundle is instrumented with thermocouples attached to the cladding at different elevations between -250 mm and 1350 mm and at four different orientations. Superheated steam together with argon as a carrier gas enters the test bundle at the bottom end and leaves the test section at the top together with the hydrogen that is produced in the zirconium-steam reaction. The hydrogen is analyzed by two different instruments: a mass spectrometer and a "Caldos 7 G" hydrogen detection system.

The commissioning tests consisted of (a) calibration tests, i.e. several test phases at steady-state temperatures conducted with 3 g/s argon or 3 g/s argon + 3 g/s steam, (b) a pre-oxidation phase (argon + steam), (c) a transient phase (argon + steam), and (d) a quench phase.

The pre-oxidation resulted in a maximum oxide layer thickness of 500 μm at the 900 mm elevation. The transient test phase was performed with a heatup rate of 1 K/s to a maximum rod cladding temperature of 1700 K. At this temperature level flooding of the bundle from the bottom by water was initiated. The water injection rate was 2.8 cm/s. The quench water was injected for 270 s providing a total quench water volume of 22.5 l (which is four times the void volume of the test section). During the quenching process the electrical power for the bundle heating as well as the steam supply were completely shut off. The quench temperature evaluated is between 638 and 1128 K, and the quench rate is between 0.5 cm/s (rod 21, 470/1250 mm) and 2.7 cm/s (rod 19, 350/1150 mm). The maximum cooldown rates on the basis of the thermocouple responses during quenching were determined to be 160 - 420 K/s. During

all phases of the commissioning tests a total of 105 g (corresponding to 1.2 Nm³) hydrogen was produced, most of it during the pre-oxidation and the quench phase. A part of the generated hydrogen was absorbed by the Zircaloy cladding and shroud.

The post-test appearance of the test bundle shows significant oxidation of the bundle and of the shroud inner surface between the 400 and 1300 mm elevations. The cladding is lost between 730 and 1020 mm (top of heated zone) due to embrittlement. Exactly in this region white oxide at the shroud internal surface is deposited. All rod cladding thermocouples in the hot region are destroyed.

This report presents the results of QUENCH Commissioning Tests and those of the pre-test calculations performed primarily with the SCADAP/RELAP5 computer code.

Ergebnisse der QUENCH-Inbetriebnahme-Versuche

Zusammenfassung

Die QUENCH-Inbetriebnahme-Tests wurden in der neuen QUENCH-Versuchsanlage des Forschungszentrums Karlsruhe vom 9. - 16. Oktober 1997 durchgeführt. Die QUENCH-Versuchsanlage wurde gebaut, um den Wasserstoffquellterm, der sich bei einer Einspeisung von Notkühlwasser in einen trockenen Reaktorkern eines Leichtwasserreaktors (LWR) ergibt, zu ermitteln. Das QUENCH-Testbündel besteht aus 21 Brennstabsimulatoren mit einer Gesamtlänge von ca. 2,50 m. 20 Brennstabsimulatoren sind auf einer Länge von 1024 mm beheizt. Der einzige unbeheizte Stab befindet sich in der Mitte des Versuchsbündels. Die Stabhüllen sind identisch mit LWR-Hüllrohren: Zircaloy-4, 10,75 mm Außendurchmesser und 0,725 mm Wanddicke. Die Heizung der Stäbe erfolgt elektrisch mit Hilfe eines 6 mm-Wolfram-Heizers, der sich in der Mitte der Brennstabsimulatoren befindet und von ZrO₂-Ringtabletten umgeben ist. Das Testbündel ist mit Thermoelementen instrumentiert. Sie sind an den Stabhüllen in den Ebenen von - 250 mm bis 1350 mm und in vier Umfangslagen befestigt. Überhitzter Dampf tritt zusammen mit Argon als Trägergas am unteren Ende in die Teststrecke ein und verläßt diese zusammen mit dem Wasserstoff, der sich durch die Zirkonium-Dampf-Reaktion gebildet hat am oberen Ende. Der Wasserstoff wird mit Hilfe von zwei Messgeräten analysiert: einem Massenspektrometer und einem Caldos-Analysegerät.

Die Inbetriebnahmeversuche bestanden aus: (a) Kalibrierversuchen, d. h. mehreren Phasen stationärer Temperaturen mit 3 g/s Argon bzw. 3 g/s Argon + 3 g/s Dampf, (b) einer Voroxidationsphase (3 g/s Argon + 3 g/s Dampf), (c) einer transienten Phase (Aufheizphase) und (d) einer Abschreck- bzw. Quench-Phase.

Die Voroxidation ergab eine maximale Oxidschichtdicke von 500 µm in der 900 mm-Ebene. Die transiente Phase wurde mit einer Aufheizrate von 1 K/s bis zu einer maximalen Stab-Hüllrohrtemperatur von 1700 K durchgeführt. Bei dieser Temperatur wurde das Fluten des Versuchsbündels von unten mit Wasser ausgelöst. Die Wassereinspeiserate betrug 2,8 cm/s. Das Quenchwasser wurde 270 s lang in die Teststrecke eingespeist. Damit betrug die Gesamtmenge des eingespeisten Wassers 22,5 l. (Dieser Wert entspricht dem vierfachen Leervolumen der Teststrecke).

Während des Abschreckvorgangs waren sowohl die elektrische Leistung als auch die Dampfzufuhr abgeschaltet. Die ermittelten Quench-Temperaturen lagen zwischen 638 K und 1128 K und die Abschreckgeschwindigkeiten zwischen 0,5 cm/s (Stab 21, 470/1250 mm) und 2,7 cm/s (Stab 19, 350/1150 mm). Die maximalen Abkühlraten während des Abschreckens wurden auf der Grundlage der gemessenen Temperaturen zu 160 bis 420 K/s bestimmt. Die Wasserstoffgesamtmenge, die während aller Testphasen erzeugt wurde, ergab 105 g, entsprechend 1,2 Nm³. Der Hauptanteil davon wurde in der Voroxidations- und in der Quenchphase gebildet. Ein Teil des erzeugten Wasserstoffs wurde von den Zirkaloy-Hüllen und der -Shroud absorbiert.

Nach dem Experiment läßt das Versuchsbündel und die innere Oberfläche des Shroud eine deutliche Oxidationszone zwischen 400 und 1300 mm Höhe erkennen. Zwischen 730 und 1020 mm Höhe (oberes Ende der Heizzone) sind die Stabhüllen durch die Oxidation so versprödet, dass sie weggebrochen sind. Genau in diesem Bereich hat sich eine weiße Oxidschicht auf der inneren Oberfläche des Shroud abgelagert. Alle Hüllrohr-Thermoelemente der heißen Zone sind zerstört.

Dieser Bericht beschreibt die Ergebnisse der QUENCH-Inbetriebnahmeversuche und die der Vorausrechnungen, die vor allem mit dem SCADAP/RELAP5-Rechenprogramm durchgeführt wurden.

List of Tables

- Table 1: Design characteristics of the QUENCH test bundle
- Table 2: List of instrumentation
- Table 3: QUENCH commissioning tests overview
- Table 4: Evaluation of cool-down data
- Table 5: Integral hydrogen release during the QUENCH commissioning tests
- Table 6: Experimental and calculated electrical resistance of the heated pins

List of Figures

- Fig. 1: QUENCH Test Facility, Flow Diagram
- Fig. 2: QUENCH Fuel Rod Simulator Bundle (Cross Section), Dimensions
- Fig. 3: QUENCH Test Section, Flow Lines
- Fig. 4: QUENCH Facility, H₂ Measurement with Caldos (Photograph)
- Fig. 5: QUENCH Facility, H₂ Measurement with Caldos, Flow Diagram
- Fig. 6: QUENCH Facility, H₂ Measurement, Mass Spectrometer
- Fig. 7: Heated Fuel Rod Simulator
- Fig. 8: Unheated Fuel Rod Simulator
- Fig. 9: QUENCH Test Section, TC Elevations
- Fig. 10: TC Instrumentation of the Test Bundle
- Fig. 11: QUENCH Test Bundle, TC Instrumentation and Rod Designation
- Fig. 12: TC Instrumentation of the QUENCH Test Bundle with High-Temperature Thermocouples

- Fig. 13: TC Fastening Concept for the QUENCH Test Rods
- Fig. 14: Zr Clip for Fixing the TC Tip at the Rod Cladding
- Fig. 15: QUENCH Commissioning Test, Overview, Temperature TCRC 13
- Fig. 16: QUENCH Calibration Test IBS_03 – Phase C Argon + Steam, Temperatures
- Fig. 17: QUENCH Test IBS_04 – Pre-Oxidation Axial Temperature Profile at 13000 s
- Fig. 18: QUENCH Test IBS_05 – Temperatures during Transient Phase
- Fig. 19: QUENCH Test IBS_05 – Quenching Phase, Electrical power
- Fig. 20: QUENCH Test IBS_05 – Quenching Phase, Steam flow
- Fig. 21: QUENCH Test IBS_05 – Quenching Phase, Quench water flow
- Fig. 22: Test IBS 05 – Quenching of the central rod at 570 and 950 mm
- Fig. 23: Test IBS 05 – Quenching of rods 2, 4, 6 and 8 (rod type 2)
- Fig. 24: Test IBS 05 – Quenching of rods 5 and 7 (rod type 3)
- Fig. 25: Test IBS 05 – Quenching of rods 15, 16, 18, 19 and 21 (rod type 5)
- Fig. 26: Test IBS 05 – Quenching of rods 10, 12, 19 and 21 (rod type 5)
- Fig. 27: Evaluation of Quench Rate, Example
- Fig. 28: QUENCH Test IBS_05 – Quenching Phase, Hydrogen Measured by Caldos
- Fig. 29: Hydrogen release (lower diagram) and pertinent data of the facility (upper diagram) during IBS_03
- Fig. 30: Hydrogen release (upper diagram) and data of the facility (lower diagram) during IBS_04
- Fig. 31: Hydrogen release (upper diagram) and data of the facility (lower diagram) during IBS_05
- Fig. 32: Hydrogen release (upper diagram) and data of the facility (lower diagram) during the IBS_05 quench phase
- Fig. 33: Hydrogen release and central temperature at elevation 950 mm during IBS_04

- Fig. 34: Mass spectrometer sampling position at the off-gas pipe
- Fig. 35: Cut-out of Observation Window at Shroud, Schematic
- Fig. 36: Bundle after opening the shroud (photograph)
- Fig. 37: Posttest view of the bundle
- Fig. 38: Bulging of the shroud at 900 mm elevation (photograph)
- Fig. 39: Shroud at 700 – 900 mm elevation (Pre-test, photograph)
- Fig. 40: Debris at the front end of the off-gas pipe after removal of the test section (photograph)
- Fig. 41: Oxide layer thickness of a removed oxidation calibration rod
- Fig. 42: Oxide layer thickness of a removed oxidation calibration rod at different bundle elevations
- Fig. 43: Post-test analysis of cladding tube No. 13: axial distribution of oxide layer thickness and absorbed hydrogen
- Fig. 44: Nodalization of the QUENCH facility for SCDAP/RELAP5
- Fig. 45: Pre-test calculation: power, shroud and clad temperatures, and oxide layer thicknesses for a bundle flow of 3 g/s steam and 3 g/s argon
- Fig. 46: Pre-test calculation: axial profiles of temperatures and oxide layer thicknesses for a bundle flow of 3 g/s steam and 3 g/s argon (top) and 0.3 g/s steam and 1 g/s argon (bottom)
- Fig. 47: Pre-test calculation: power, shroud and clad temperatures, and oxide layer thicknesses for a bundle flow of 0.3 g/s steam and 1 g/s argon
- Fig. 48: ICARE calculation: electrical power, shroud and clad temperatures, and oxide layer thicknesses for a bundle flow of 3 g/s steam and 3 g/s argon
- Fig. 49: Comparison of SCDAP/RELAP5 and ICARE results: axial profiles of temperatures and oxide layer thicknesses for a bundle flow of 3 g/s steam and 3 g/s argon at two different times
- Fig. 50: Commissioning test pre-calculation: power, clad, inner cooling jacket, and off-gas pipe temperatures for three power steps for a bundle flow of 3 g/s argon
- Fig. 51: Commissioning test pre-calculation: axial temperature profiles in the test section at the end of three power steps for a bundle flow of 3 g/s argon

- Fig. 52: Commissioning test pre-calculation: axial temperature profiles in the off-gas pipe at the end of three power steps for a bundle flow of 3 g/s argon
- Fig. 53: Commissioning test pre-calculation: axial temperature profiles in the bundle for three power steps for a bundle flow of 3 g/s steam and 3 g/s argon
- Fig. 54: Commissioning test pre-calculation: axial temperature profiles in the off-gas pipe for three power steps for a bundle flow of 3 g/s steam and 3 g/s argon
- Fig. 55: Commissioning test pre-calculation: power, clad temperatures, collapsed water level, and cumulated hydrogen production during quench phase assuming no shattering
- Fig. 56: Commissioning test pre-calculation: power, clad temperatures, collapsed water level, and cumulated hydrogen production during quench phase assuming complete shattering at the begin of the quench phase
- Fig. 57: IBS_02: Comparison of measured and calculated temperature developments (original modelling)
- Fig. 58: IBS_02: Comparison of measured and calculated axial temperature profiles (original modelling)
- Fig. 59: IBS_02: Comparison of measured and calculated temperature developments (improved modelling)
- Fig. 60: IBS_02: Comparison of measured and calculated axial temperature profiles (improved modelling)
- Fig. 61: Material property data for UO_2 and ZrO_2
- Fig. 62: IBS_03: Comparison of measured and calculated temperature developments (improved modelling)
- Fig. 63: IBS_03: Comparison of measured and calculated axial temperature profiles (improved modelling)

Contents

1.	Introduction.....	1
2.	Description of the Test Facility	3
3.	Test Bundle Instrumentation.....	5
4.	Hydrogen Measurement Devices	6
5.	Data Acquisition and Process Control	8
6.	Test Conduct.....	9
7.	Test Results	10
8.	H ₂ Mass Spectrometer Measurements.....	12
9.	Post-Test Appearance.....	14
10.	Calculational Support	15
10.1	Pre-Test Calculations	15
10.2	Post-Test Calculations	19
11.	References	23
12.	Acknowledgements	23

1. Introduction

One of the still open problems on early phase core degradation is the hydrogen generation during quenching. The most important accident management measure to terminate a severe accident transient in a Light-Water Reactor (LWR) is the injection of water to cool the uncovered degraded core. Analysis of the TMI-2 [1] accident and the results of integral out-of-pile (CORA) [2] and in-pile experiments (LOFT [3], PHEBUS, PBF) have shown that before the water succeeds in cooling the fuel pins there will be an enhanced oxidation of the Zircaloy cladding that in turn causes a sharp increase in temperature, hydrogen production and fission product release. Quenching is considered a worst-case accident scenario regarding hydrogen release to the containment. The increased hydrogen production worries those concerned with reactor safety. For in- and ex-vessel hydrogen management measures one has to prove that the hydrogen release rates and total amounts do not exceed safety-critical values for the considered power plant. In most of the code systems, describing severe fuel damage, the quench phenomena are either not considered or only modeled in a simplified empirical manner.

Although nobody suggests not quenching the core, it is important that the hydrogen generation rates is known so that accident mitigation measures can be designed appropriately:

- Passive autocatalytic recombiners work slowly and their surface area has to be sized.
- The concentration of hydrogen in the containment may be combustible for only a short time before detonation limits are reached. This limits the period during which igniters can be used.

No models are yet available to predict correctly the quenching processes in the CORA and LOFT LP-FP-2 tests. No experiments have been conducted that are suitable for calibrating the models. Since the increased hydrogen production during quenching cannot be determined on the basis of the available Zircaloy/steam oxidation correlations, new experiments are therefore necessary. An extensive experimental database is needed as a basis for model development and improvement.

In the earlier CORA program only a small number of quench tests could be performed. These experiments showed that quenching of the hot bundles by water resulted in a renewed temperature escalation at the top of the bundle and additional hydrogen generation, although the electric power supply was already shut off at that time.

The comparison of the quantitative data on hydrogen production measured between the CORA-16 BWR-related test (without quenching) and CORA-17 (with quenching) shows a remarkable hydrogen peak during the flooding phase of CORA-17. Similar behavior in the hydrogen response was observed in PWR-related tests, although it is assumed that in the BWR tests, additional energy and hydrogen production was caused by a steam reaction with the remnant B_4C absorber (B_4C oxidation in steam is more exothermic and produces more hydrogen per gram material than does Zircaloy) [4].

The Forschungszentrum Karlsruhe has started a QUENCH program on the determination of the hydrogen source term to investigate the generation of new metallic surfaces by cracking and fragmentation of the oxygen-embrittled cladding tubes as a result of the thermal shock during flooding and their influence on enhanced oxidation and hydrogen generation.

The main objectives of the QUENCH program are:

- The provision of an extensive experimental database of the development of detailed mechanistic quench models.
- The examination of the physico-chemical behavior of overheated fuel elements (core) under different flooding conditions.
- To provide an improved understanding of the effects of water addition at different stages of a degraded core.
- The determination of cladding failure criteria, cracking of oxide layers, exposure of new metallic surfaces to steam which results in renewed temperature escalation and hydrogen production, and
- The determination of the hydrogen source term.

The experimental part of QUENCH program consists of small-scale experiments with short Zircaloy fuel rod segments and large-scale experiments with bundle simulators under nearly adiabatic conditions.

The parameters of the test program are: Quench medium, i.e. water or steam, quench water temperature, water injection rate, cladding oxide layer thickness, and the starting temperature for quenching. Although the principal objective of the commissioning tests was to put the QUENCH facility into operation and check the various components, the testing during the different phases at different power levels resulted in an abundance of data. So, this report describes the test facility and test bundle, and the main results of the QUENCH commissioning tests. In addition, one section is dedicated to the calculational results of the computations performed with the SCADAP/RELAP5 computer code.

2. Description of the Test Facility

The QUENCH test facility consists of the following groups:

- the test section with the fuel element simulator
- the water and steam supply system
- the argon gas supply system
- the hydrogen measurement devices
- the electric power supply for the test bundle heating
- the process control system
- the data acquisition system.

A simplified flow diagram of the QUENCH test facility is given in Fig. 1. The main component of the facility is the test section with the test bundle (cross section, Fig. 2). The superheated steam from the steam generator and superheater together with argon as the carrier gas enters the test bundle at the bottom end. The steam that is not consumed, the argon, and the hydrogen produced in the zirconium-steam reaction flow from the upper bundle outlet via a water-cooled off-gas pipe to the condenser (Figs. 1 and 3). Here the steam is separated from the volatile gases argon

and hydrogen. During quenching the quench water enters the test section at the bottom via a separate line.

The design characteristics of the test bundle are given in Table 1. The test bundle is made up of 21 fuel rod simulators, each with a length of approximately 2.5 m. Twenty fuel rod simulators are heated over a length of 1024 mm, the one unheated fuel rod simulator is located in the center of the test bundle. The unheated fuel rod simulator (Fig. 8) is built with ZrO₂ pellets (bore size 2.5 mm ID) and cladding but without a tungsten heater and electrodes. Two thermocouples are inserted in its center, one thermocouple from the bottom and one from the top.

Heating is carried out electrically using 6 mm diameter tungsten heating elements, which are installed in the center of the rods and which are surrounded by annular ZrO₂ pellets (Fig. 7). The total heating power available is 70 kW distributed among the two groups of heated rods with 35 kW each, an outer ring with twelve rods and an inner ring with eight rods. In the axial direction the tungsten heater is located in the middle and connected to electrodes made of molybdenum and copper at each end of the heater. The molybdenum and copper electrodes are joined by high-frequency/high-temperature brazing performed under vacuum. For electrical insulation the surfaces of both types of electrodes are plasma-coated with 0.2 mm ZrO₂. To protect the copper electrodes and the O-ring-sealed wall penetrations against excessive heat lower and upper bundle head are water-cooled (lower and upper cooling chamber). There are sliding contacts at the top and bottom of the copper electrodes which are used to make contact to the cables connected to the electric power supply (DC).

The test bundle is surrounded by a 2.38 mm thick shroud made of Zircaloy with a 35 mm thick ZrO₂ fiber insulation and an annular cooling jacket whose walls are made of stainless steel (Fig. 2). The 7 mm annulus of the cooling jacket is cooled by argon. Above the heated zone, i.e. above the 1024 mm elevation, both test bundle and shroud are uninsulated. This region of the cooling jacket is cooled by water (Figs. 3 and 9). Both the lack of ZrO₂ insulation above the heated region and the water cooling force the axial temperature maximum downward.

Four corner positions of the bundle are occupied by three instrumentation rods, i.e. solid zircaloy rods with a diameter of 6 mm, and one instrumentation tube (6 Ø x 0.9

mm) for gas injection purposes (Fig. 2). The positioning of the four corner rods avoids an atypical large flow channel at the outer positions and, in addition, leads to a rather uniform radial temperature profile. One instrumentation rod is pulled out after pre-oxidation to determine the axial oxide thickness profile. This profile is then compared to that of another rod which was exposed for the complete experiment.

The fuel rod simulators are held in their positions by four grid spacers, three of Zircaloy, and one of Inconel at the bottom. The rod cladding is identical to that used in LWRs with respect to material and dimensions (Zircaloy-4, 10.75 mm outside diameter, 0.725 mm wall thickness). The rods are filled with helium to approx. 2.2 bar, i.e. to a pressure slightly above the system pressure. The gas filling of all rods is realized by a channel-like connection system inside the lower insulation plate which is sealed to the system by O-shaped rings. This sealing plate is, in addition, the lower boundary for the lower cooling chamber. The upper boundary of the cooling chamber is a sealing plate of stainless steel. The bundle design at the top is similar. Also here an insulation plate made of plastic (PEEK) forms the top of the upper cooling chamber, and a sealing plate of Al_2O_3 is the lower boundary of the cooling chamber (see Fig. 7). In the region below the upper Al_2O_3 plate the copper electrode is connected firmly to the cladding. This is done by hammering the cladding onto the electrode with a sleeve of boron nitride put between electrode and cladding for electrical insulation. The fixed point between cladding and electrode is in the region below the upper Al_2O_3 plate (hammered zone). The fixing of the fuel rod simulators is located directly above the upper edge of the upper insulation plate and is realized by a groove and a locking ring. So, during operation the fuel rod simulators are allowed to expand upwards and downwards. Space for expansion of the test rods is provided in the regions of the lower insulation plate. Relative movement between cladding and internal heater/electrode, however, can only take place in the region of the lower insulation plate.

3. Test Bundle Instrumentation

The test bundle is instrumented with thermocouples attached to the cladding at different elevations between – 250 mm and 1350 mm and at four different orientations (Figs. 9, 10, and 11). The elevations of the shroud thermocouples are from – 250 mm to 1250 mm. In the lower bundle region, i.e. up to the 350 mm elevation NiCr/Ni

thermocouples (1 mm outside diameter) are used for temperature measurement of rod cladding and shroud. The thermocouples of the hot zone are high-temperature thermocouples with W-5 Re/W-26 Re wires, HfO₂ insulation, and a duplex sheath of tantalum (internal)/Zircaloy (2.1 mm outside diameter, [Fig. 12](#)). The leads of the thermocouples from – 250 mm to 650 mm leave the test section at the bottom whereas the TCs above 650 mm penetrate the test section at the top. The wall of the inner tube of the cooling jacket is instrumented between – 250 mm and 1150 mm with 22 NiCr/Ni thermocouples. Five NiCr/Ni thermocouples are fixed at the outer surface of the outer tube of the cooling jacket. A list of all instruments is given in [Table 2](#). The thermocouple attachment technique is illustrated in [Figs. 13 and 14](#). The TC tip is held in place by a clamp of Zr. As this clamp is prone to oxidation and embrittlement in a steam environment an Ir-Rh wire of 0.25 mm diameter is used for support. This wire was tested together with other materials and was best with respect to melting point and handling performance [5]. As indicated in [Fig. 13](#) the wire is used for the experiments with pre-oxidation only. In a test without pre-oxidation the wire material would react with the cladding because there would be no protection of the cladding by a ZrO₂ layer.

4. Hydrogen Measurement Devices

The hydrogen is analyzed by two different instruments: (1) a mass spectrometer located at the off-gas pipe behind the test section, (2) a "Caldos 7 G" hydrogen detection system ([Fig. 4](#)) located behind the condenser, in a bypass to the off-gas line, i.e. before the argon and hydrogen exit to the outside they pass the Caldos hydrogen detection system in a bypass line ([Fig. 1](#)). Due to these different locations the mass spectrometer responds almost immediately whereas the delay time of the Caldos system is of the order of 100 s. The principle of measurement of the Caldos system is based on the different heat conductivities of different gases. The Caldos device used is calibrated for the hydrogen-argon gas mixture. To avoid any moisture in the analyzed gas a gas cooler, which is controlled at 296 K, and a drier (molecular sieve, zeolite) are connected in series before the gas analyzer ([Fig. 5](#)). The response of the gas analyzer is documented to be 2 s, i.e. the time when 90 % of the final value is reached.

The mass spectrometer (MS) "BALZERS GAM 300" used is a completely computer-controlled quadrupole MS with an 8 mm rod system which allows measurement of impurity concentrations in inert gases to better than 1 ppm. The sensitivity for hydrogen, however, is reduced due to the low molecular mass of H₂. Nevertheless, it is better than 100 ppm. The gas specimen for the MS measurement is taken at the end of the off-gas pipe in front of the throttle and the condenser (Figure 6). The sampling tube which is inserted in the off-gas pipe and has several holes at different elevations should guarantee a representative sampling gas composition. The penetration of this tube through the cooling jacket of the off-gas pipe caused partial condensation of steam at this position. Therefore, no quantitative steam concentration measurements could be performed during the commissioning tests. To avoid steam condensation the temperature of the gas at the MS inlet is controlled by a heat exchanger to be between 110 °C and 150 °C (the upper operating temperature of the MS inlet valves). Therefore, the MS can analyse the steam production rate. Additionally, it is used to control the atmosphere in the facility, e.g., to detect air ingress through a leak which is of interest from the safety point of view.

The temperature and pressure of the analysed gas are measured near the inlet valve of the MS. The MS is calibrated for hydrogen with well-defined argon/hydrogen mixtures and for steam with mixtures of argon and steam supplied by the steam generator of the QUENCH facility. Contrary to the original plan to feed the MS off-gas back into the facility, it is released to the atmosphere because the amount of hydrogen taken out of the system is negligible.

For the Caldos device as well as for the MS the hydrogen mass flow rate is calculated by referring the measured H₂ concentration to the known argon mass flow rate according to equation (1):

$$\dot{m}_{H_2} = \frac{M_{H_2}}{M_{Ar}} \cdot \frac{C_{H_2}}{C_{Ar}} \cdot \dot{m}_{Ar} \quad (1)$$

with M representing the molecular masses, C the concentrations and \dot{m} the mass flow rates of the corresponding gases.

With an argon-hydrogen (two-component) mixture that does exist at the location of the Caldos analyzer equation (1) can be written as follows

$$\dot{m}_{H_2} = \frac{M_{H_2}}{M_{Ar}} \cdot \frac{C_{H_2}}{1 - C_{H_2}} \cdot \dot{m}_{Ar} \quad (2)$$

5. Data Acquisition and Process Control

A powerful PC-based control and data acquisition system is used in the QUENCH experimental facility. Data acquisition, data storage, online visualization as well as process control, control engineering and system protection are accomplished by three computer systems that are linked in a network.

The data acquisition system allows the acquisition of about 200 measurement channels at a maximum frequency of 25 Hz per channel. The experimental data are provided with some information as far as the date and time of data acquisition are concerned and stored as raw data in the binary format. After the experiment, conversion into an ASCII format with a simultaneous recalculation into SI units takes place.

During the data acquisition of the commissioning tests, 146 channels were used by measurement signals. In the individual test phases, the data were recorded at various frequencies.

For process control, a system flow chart with the current measurement values selected is displayed on the computer screen. Furthermore, the operating mode of the active components (pumps, steam generator, superheater, DC power system, valves) is indicated. The parameter settings of the control circuits and devices can be modified online. Blocking systems and limit switches ensure safe plant operation. Pre-defined operating test phases, e.g. heatup or quenching phases, can be pre-programmed.

Online visualization allows to observe and document the current values of selected measurement positions in the form of tables or graphics. Eight diagrams with six curves each can be displayed as graphics. This means that altogether 48 measurement channels can be displayed online and selected anew during the course of the experiment.

6. Test Conduct

The commissioning tests consisted of

1. calibration tests, i.e. several test phases conducted with 3 g/s argon (IBS_02, phases A, B, C, and IBS 05, phase A) or 3 g/s argon + 3 g/s steam (IBS_03, phases A, B, C, and IBS 05, phase A) as the coolant to verify thermodynamic computations, e.g. heat losses etc.,
2. a pre-oxidation phase (argon + steam, IBS_04),
3. a transient phase (argon + steam, IBS_05, phase B),
4. a quench phase (IBS_05, phase C).

The electric power levels at the various test phases can be deduced from Ref. [6]. Table 3 describes the test conditions during the various test phases. As the thermocouples were exposed to the numerous test phases of the commissioning tests, most of them have failed. There was only one thermocouple in the hot region of the bundle (TCRC 13, 950 mm elevation) that survived the entire test due to its protection by pellets and cladding in the center of the central rod. So, with this thermocouple it is possible to provide an overview of the entire commissioning tests (Fig. 15). In general, erroneous TC signals have been eliminated from the data. Due to the extreme exposure of the thermocouples, their temperature readings should be treated with caution.

The steady-state temperatures reached during the calibration phases were between 940 K (IBS_03, phase A) and 1280 K (IBS_02, phase C). The temperatures and times during the pre-oxidation were: at 1450 K for 4000 s. The time period during which the test bundle was above 1000 K was 8000 s. The pre-oxidation resulted in a maximum oxide layer thickness of 500 μm at the 900 mm elevation. The axial distribution of the oxide layer thickness can be taken from Figs. 17 and 41, respectively.

The transient test phase was performed with a gas inlet temperature of 620 K¹ and a heatup rate of 1 K/s to a maximum rod cladding temperature of 1700 K and a maximum shroud temperature of 1600 K at the 850/950 mm bundle elevation. At this temperature flooding of the bundle from the bottom by water was initiated. To initiate the quenching phase the steam (3 g/s) and argon flow (3 g/s) through the test section were turned off and the electric power was reduced to a decay heat level. The quench water then entered the test section at the bottom. During quenching in the commissioning tests no argon was supplied as the carrier gas.

The water injection rate amounted to 2.8 cm/s and was evaluated on the basis of 300 l/h quench water (F 104) and the coolant channel cross-section of 30 cm². The quench water was injected for 270 s providing a total quench water volume of 22.5 l (which is four times the void volume of the test section). During the quenching process the electrical power for the bundle heating as well as the steam supply were completely shut off after 40 – 50 s.

7. Test Results

Figure 16 is an example of the so-called calibration data. Rod, shroud, and cooling jacket temperatures at 950 mm are plotted vs. time for IBS_03, test phase C. In Figure 17 the axial temperature profile during the pre-oxidation (at 13000 s) is compared to the axial distribution of the ZrO₂ layer thickness. Both distributions show the maximum to lie at around 900 mm. The heatup of the test rods during the transient is illustrated in Figure 18 for the 900 mm elevation. The termination of the transient at the maximum temperature of 1700 K is the onset temperature for the subsequent quench phase. The following figures present results of this final test phase. In Fig. 19 the power history is provided. The turn-off of the steam supply is illustrated in Fig. 20. The quench water flow (F 104) is given in Fig. 21.

The temperature readings during quenching are provided in Figures 22 through 26. They were taken from the thermocouples that had survived the previous test phases.

¹ Probably during the bundle assembling the thermocouple T 511 that measured the fluid temperature at the bundle inlet was displaced and measured therefore the temperature of the adjacent structure.

The temperature data were plotted according to the rod position in the bundle, i.e. temperatures of the central rod, of rod type 2 (rods 2, 4, 6, 8), of type 3 (rods 5, 7), and of rod type 5 (rods 10, 12, 15, 16, 18, 19, 21). Toward the end of the flooding phase when all rod cladding temperatures are at the lowest level the thermocouple signals of the upper elevations exhibit a renewed temperature peak (Figs. 23, 24 and 26). This peak indicates that the two-phase flow is not uniform, particularly in the upper regions (voiding effect). The shroud temperatures of the upper regions do not show this behavior.

The temperature data were evaluated to obtain the onset of cooling, quench temperatures, and cooldown rates (Table 4). In Fig. 27 the procedure of determining quench temperatures, cooldown rates, quench rates is illustrated by an example. In addition, the water injection and flooding rate are defined in this figure. Quench rates could be evaluated with help of the temperatures measured by thermocouples at the lower region and at the very top of the test section, i. e. with the help of the thermocouples that had survived the test series. The evaluation of the quench rates is of great interest because these values are a measure of how fast the test rods are flooded with water. They are defined as the velocities of the quench water level rising along the individual rods. So, the distance between a pair of thermocouples on the same test rod is related to the times of the onset of quenching.

The quench temperatures evaluated are between 638 and 1128 K, the maximum cooldown rates on the basis of the thermocouple responses were determined to be 160 – 420 K/s. The quench rates obtained are provided in Figs. 23, 25, 26. They range from 0.5 cm/s (rod 21, 470/1250 mm) to 2.7 cm/s (rod 19, 350/1150 mm).

The maximum amount of hydrogen during the quench phase was recorded by the "Caldos 7 G" device (Q 901) with 22 – 23 vol % H₂ as can be seen in Fig. 28. As the argon was turned off with the start of the quench phase there was no carrier gas flow at this time². So, this value is not reliable with respect to its time dependence.

² From the next experiment on argon will be injected at the upper bundle head, i.e. above the test section during the quench process.

8. H₂ Mass Spectrometer Measurements

The main objective of the mass spectrometric measurements (and beyond it of the QUENCH program itself) is the analysis of the hydrogen produced and released during the interaction between the Zircaloy cladding material and steam. The hydrogen absorbed by the remaining Zircaloy metal was determined in post-test analyses with the LAVA-MS installation (see section on “posttest appearance”).

The following data were recorded by the MS data acquisition system (PC) with a frequency of about 0.5 Hz: concentrations of H₂, Ar, H₂O, N₂, O₂, as well as He and temperature and pressure at the MS inlet. In the commissioning tests the MS could also be used as an indicator for the first cladding tube failure. The latter was done by the analysis of the helium concentration in the off-gas³.

The data of the MS data acquisition system and the data from the main data acquisition system are synchronised by two radio-controlled clocks. For the evaluation of the MS data the following data were extracted from the main test data files: T 401, P 401, F 401 (temperature, pressure, and flow rate at the argon inlet), T 205, P 205, F 205 (steam flow rate), TCRC 13 (TC central rod, center, 950 mm) and T 601 (TC near the MS sampling position). For the quench phase the data from TCRC 9 (TC central rod, center, 570 mm), TCR 9 (TC central rod, cladding, 570 mm) and F 104 (flow rate quench water) were additionally taken into consideration.

Due to the different sampling rates of the main and the MS data acquisition systems the two data sets were interpolated with $f = 1$ Hz.

Table 5 summarises the results of the mass spectroscopic hydrogen measurements. Altogether, 105 g (corresponding to 1.2 Nm³) hydrogen were released during the commissioning tests, most of it during the pre-oxidation and the quench phase.

Assuming a complete reaction (equation 2) and neglecting the formation of the α -Zr(O) phase, 105 g H₂ corresponds to the formation of 3.2 kg ZrO₂.



³ The fuel rod simulators were filled with helium at a low overpressure which was released into the test rig after the first cladding tube failed.

This corresponds to a ZrO_2 layer of 1 mm thickness if it is assumed that a homogeneous oxide layer has formed on 21 Zry cladding tube surfaces, 2 corner rods, 2 Zry instrumentation tubes, and the Zry shroud inner surface over a length of 500 mm.

Figures 29, 30, and 31 show the hydrogen production rate and the integral hydrogen release versus time as well as some relevant data of the facility for better understanding of the mass spectrometer data.

In Figure 33 the hydrogen production rate and the center line temperature of the central unheated rod in the hot zone (elevation 950 mm) are shown in one diagram. There is an excellent agreement between the fine structure of the two curves. The large peak in the hydrogen release at about 9800 s results from the accelerated oxidation kinetics at high temperatures (here: $T > 1200$ °C).

Figure 32 shows the hydrogen production and relevant data during the quench process. Due to a failure of a valve the constant argon feed into the facility was interrupted at the beginning of the quench phase. Therefore, there was a time-dependent argon flow rate during this phase. Since the argon flow rate is measured at the lower head of the facility (F 401) and the MS sampling position is at the end of the off-gas pipe, using equation 1 may cause problems. On the other hand, the entire gas flow rate (argon, steam, hydrogen) is very high during quenching, therefore, the delay time should be negligible.

Regarding the other species measured by the MS the following results were obtained: the oxygen concentration in the facility was about 0.002 vol % (20 vppm) during the tests IBS_03 - 05 with one exception. During test IBS_04 an oxygen (nitrogen) peak up to 2 (9) vol % was observed at 3200 s after the start of the data acquisition system. This is an indication of a small air ingress into the test section at that time.

After starting the test IBS_04 a high helium concentration was measured due to the failure of at least one cladding tube during heatup. Depending on the He pressure in the fuel rod simulators between 3 and 30 g/h helium were released from the test rods during this phase.

With respect to the hydrogen measurements the following lessons have been learned:

- In general, the MS measurements worked excellently with respect to the analysis of the hydrogen release, the detection of fuel rod simulator failure and control of the composition of the atmosphere in the facility relating to leak tightness.
- The original plan to take the gas sample for MS measurements before the condenser and to feed it back into the facility after the condenser did not work, due to the lack of a pressure gradient between these two points. Therefore, the off-gas of the MS was released into the atmosphere. Since the extracted gas quantities are very small compared to the off-gas flow rate in the facility other measurements should not be influenced. For the next tests it is planned to condense the steam in the off-gas of the MS and to measure the flow rate of the non-condensable gases in order to guarantee reproducible test conditions. If necessary, a gas pump will have to be installed to transport the MS off-gas back into the facility.
- The quantitative analysis of steam in the off-gas pipe of the facility was not possible during the commissioning tests owing to a partial steam condensation at the penetration of the gas sampling tube through the cooling jacket (Figure 34). This penetration has to be reconstructed to avoid the close proximity of the sampling gas and the cooling water. A final solution has not been defined, up to now.
- In the next tests a constant argon carrier gas flow rate up to the end of the quench phase has to be guaranteed.
- Prior to the next experiment, delay time measurements (between hydrogen production in the bundle and the measurement by MS or CALDOS) should be performed.
- The measuring gas flow rate to the MS will be regulated by a control valve.

9. Post-Test Appearance

After the experiment the test bundle was taken out of the facility and a window was cut into the shroud as illustrated in Fig. 35. So a view into the bundle was enabled: the test bundle shows significant oxidation of the rod cladding and at the shroud inner surface between 400 and 1300 mm elevation (Figs. 36 and 37). The cladding is lost between 730 and 1020 mm (top of heated zone). Exactly in this region white oxide at

the shroud internal surface is deposited. The outer surface of the shroud showed a deformation at the 900 mm elevation (Fig. 38). The maximum diameter was measured to be 90 mm compared to the pre-test dimension of 84.76 mm. The same region of the shroud seen prior to the test is shown in Fig. 39. All cladding thermocouples in the hot region are destroyed. A great part of the missing cladding material was found as debris in the off-gas pipe (Fig. 40).

There was only a limited post-test examination of the bundle, because of the untypical treatment due to the various heat-up and cool-down phases. Besides the calibration rod that was removed from the bundle during the experiment, i.e. after the pre-oxidation phase to determine the oxide layer thickness (for results see Figs. 41 and 42) rod 13 was taken out of the bundle after the experiment. The cladding tube of this latter rod has been used to determine the axial distribution of the oxide layer thickness after the quench phase. In addition, the dissolved hydrogen content has been analysed in cladding tube segments taken at various axial elevations. The results of both measurements are summarised in Figure 43. Relatively large amounts of hydrogen (up to an atomic ratio H/Zr 0.2!) were absorbed by the remaining Zircaloy metal phase above and below the hot zone of the bundle. The extrapolation of the data obtained from one cladding tube to the whole bundle gives a value of about 10 g hydrogen dissolved in Zircaloy-4 cladding and shroud material, which corresponds to 10 % of the total hydrogen release during the entire set of commissioning tests.

10. Calculational Support

10.1 Pre-Test Calculations

Within FZK institutional R&D activities calculations, mainly with SCDAP/RELAP5, (S/R5) have been made to support the construction and the operation of the QUENCH facility and to interpret results of the commissioning tests. Results concerning the design studies are reported in [7]. For the investigations reported here S/R5 mod 3.1 release F, made available for the planning of the QUENCH facility, has been used. The improved model for heat transfer in the transition boiling region [8] is included in the FZK version of the programme.

The modelling of the QUENCH facility in S/R5 is shown in Figure 44. The unheated pin, the two rows of pins to be heated independently, and the inner and outer cooling

jacket are modelled as SCDAP components. In this way two-dimensional heat conduction within the structures and radiation between adjacent structures are taken into account. The bundle flow is represented by one channel. In the radial direction the whole facility including the containment is modelled, because the ambient room temperature is the only reliable boundary condition to calculate the radial heat losses out of the bundle adequately. The containment is modelled as a heat structure, thus taking into account only radial heat conduction. The modelling of the off-gas pipe has been included during our current work by AEAT Winfrith and has been revised, updated, and extended to the whole length of 3 m by FZK. It is used for the final calculations. In particular, the orifices at the position of the mass spectrometer and at the end of the off-gas pipe are modelled. The whole modelling has been updated continually according to the state of the planning and construction of the facility. So, an additional insulation of the outer cooling jacket has been taken into account by part of the calculations, but not for the final ones.

For the fluid in the bundle an inlet temperature of 873 K was assumed. If not stated otherwise, a fluid composition of 3 g/s steam and 3 g/s argon has been assumed as a standard fluid composition. The reference pressure is 1.2 bar. The argon and the water cooling are counter-current flows with mass flow rates of 6 g/s and 100 g/s, respectively, and with an inlet temperature of 300 K. The initial structure temperatures have been assumed to be 300 K.

To fix the bundle fluid composition and mass flow rates for the experiments, a parameter study was made for the pre-oxidation phase. A power pulse was applied at the beginning of the test to reach higher temperatures as quickly as possible to avoid low temperature oxidation which may lead to breakaway effects. Then a power plateau followed to achieve the required pre-oxidation of the rods. Afterwards a power transient was applied to simulate the high rod temperatures before quenching. Besides the electrical power input and the power released due to oxidation, Figure 45 shows inner shroud wall temperatures, clad surface temperatures for the inner heated pin row and corresponding oxide layer thicknesses for the various axial elevations according to Figure 43. For the steam mass flow a minimum value of 0.3 g/s steam has been used as a lower boundary for the calculations. For the argon mass flow a value of 0.5 g/s was judged to be a minimum requirement for hydrogen production measurement.

For the standard fluid composition of 3 g/s steam and 3 g/s argon the maximum surface temperatures and hence the maximum oxide layer thicknesses are near the upper end of the heated zone (upper part of [Figure 46](#)). The radial temperature profile of the bundle is rather flat leading to nearly the same axial oxide layer profiles for all pins and the shroud. For low steam flows the calculated maximum of the temperature and hence, of the oxide layer shifts to the centre of the heated part of the bundle (lower part of [Figure 46](#)). In the upper part of the bundle steam starvation is calculated to occur. [Figure 46](#) also shows that at the bundle inlet the fluid heats up the rather cold pins and shroud. In the upper unheated zone the fluid temperature is higher than that of the pins and the shroud. This is due to radiation heat transfer to the cooling jacket. This seems possible because there is no insulation material in that region. The figure also shows the effective heat removal in the upper unheated zone of the bundle: the temperature in the bundle decreases substantially due to radiation and convection to the water flow whereas the water temperature remains nearly constant.

For all gas compositions temperature changes sensibly with power increase because of the positive feedback of local power input on temperature: local input of electrical power increases with the third power of local temperature when the electrical current is kept constant. The oxidation rate depends on an exponential function of the inverse temperature and hence also increases with temperature. So, a slight power increase may lead to a temperature escalation. Because of the low heat capacity of argon compared to steam, this effect becomes even more pronounced for small steam flows. As a consequence, oxidation rates are very small for all cases with small steam flow rates ([Figure 47](#)).

Furthermore, to avoid a temperature escalation, the electrical power has to be reduced during the pre-oxidation phase to such an extent that in larger regions of the bundle the pin temperatures decrease ([Figure 47](#)). Physically, a restructuring of the clad material to α -Zr(O) and a reduction of the oxide layer thickness result from the power decrease. However, this effect is neither typical for a reactor, nor can it be modelled in the code. In summary, the results show that it is not possible to design an axial oxide layer thickness profile by varying fluid flows and composition. Therefore the standard fluid composition of 3 g/s steam and 3 g/s argon are taken as final values for the projected tests in the QUENCH facility.

To get a more reliable basis for the planning of the experiments, calculations with ICARE were also done for the standard fluid composition. Time-dependent results with ICARE are given in Figure 48. In the axial direction the same nodalization of the facility was used as in S/R5, in the radial direction the nodalization includes the components up to the inner cooling jacket. Its surface temperature is prescribed as a boundary condition, using values from S/R5 calculations, because modelling of a counter-current flow is actually not possible in ICARE. The shroud, the shroud insulation, and the inner cooling jacket are modelled as cylindrical structures, whereas in S/R5 only a slab geometry can be considered. The temperature profiles, obtained with the two codes (Figure 49), are judged to be in sufficiently good agreement so that this activity is considered to be finished at the moment. The deviations of the oxide layer profiles show the strong sensitivity of oxidation with temperature.

For all commissioning tests pre-test calculations have been done after code error corrections which became apparent at lower temperatures. This work gave indications for the electrical power and the duration of the various test phases. Figure 50 shows results for 3 g/s of pure argon flow, where in the bundle steady state conditions could be reached at temperatures of 900, 1100, and 1300 K, respectively. The results suggest that a steady state can be reached after about one hour for each temperature level. Figure 51 shows axial temperature profiles of the bundle at the end of each power step. The cooling of the off-gas pipe is very efficient (Figure 52). So, steam condensation in the off-gas pipe is certainly a problem during the heat-up phase. Therefore it is proposed to preheat the test section and the off-gas pipe with 10 g/s of pure argon flow for one hour before using steam to avoid substantial condensation at least upstream of the measuring orifice in the off-gas pipe. Axial temperature profiles in the bundle and in the off-gas pipe at the end of the three power steps are shown in Figures 53 and 54 for the standard fluid composition. A comparison with the results for a pure argon flow (Figures 51 and 52) shows the enhanced heat transfer capabilities of steam.

Calculations for the quench phase showed a wide band of results depending on the assumptions about oxide layer shattering (Figures 55 and 56). In the first case no shattering is assumed, in the second case complete shattering at the beginning of the quench phase is assumed. However, further calculations for the quench phase

have been postponed because of code errors concerning the shattering model. The error has been notified to the code developer at INEL.

10.2 Post-Test Calculations

The aims of the commissioning tests were not only to test the QUENCH facility and ensure its safe operation, but also to assess the quality of the pre-calculations and, if necessary, to improve the modelling of the facility and fit uncertain input parameters such as material property data of the shroud insulation material. For technical reasons the tests could not be performed in the manner as it had been agreed on the basis of the pre-calculations. The inlet temperature in the tests was much lower than assumed, and some experimental procedures had to be done to test the various components of the facility. Therefore new calculations with S/R5 had to be performed using the actual experimental conditions. The range of reliable posttest calculations is limited to tests IBS_02 and IBS_03. Because of the untypical test conduct IBS_01 should not be considered for post test calculations. After the conduct of IBS_03 the pins and the shroud were partially oxidized, and calculations for the subsequent tests can only account of this fact when the whole power history of all these tests is given at the beginning of the calculation for IBS_03. This would be beyond the possibilities of the programme. Besides this the power input in test IBS_04 was controlled from temperature levels, and this test conduct led to large temperature oscillations.

As a first step post-test calculations have been done for commissioning test IBS_02, where a pure argon flow was used. With respect to the pre-test calculations only the experimental boundary conditions as inlet temperature and power history have been updated in the first calculation ([Figure 57](#)). The temperature increases in the bundle at the beginning of the power pulses are calculated to be somewhat higher than measured except in the lower unheated part. Temperature decreases at the end of the power pulses are generally underestimated.

Some more insight is given by the axial temperature profiles ([Figure 58](#)). In the lower unheated part of the bundle the axial temperature profiles at the end of each of the three power steps are met quite well, the position of the maximum bundle temperature is also met, but temperature levels are overestimated in the calculation. The relatively low temperatures measured at $z = 0.57$ m are probably due to the influence of the spacer grid at that level. The fluid outlet temperature is only given as a rough

estimate, but since the respective thermocouple was situated outside the bundle cross section, its reading was influenced by the radial temperature decrease between the bundle and the water-cooled upper plenum wall and is hence not representative for the bulk values calculated in S/R5. The radial heat losses are underestimated in the calculations as can be seen from a comparison of measured and calculated temperatures of the shroud and the cooling jackets. A comparison of experimental and calculated electrical resistance (Table 6) suggests that the heat input into the heated section is slightly overestimated.

Due to modelling restrictions in S/R5 the structures outside the bundle had to be represented in Cartesian instead of cylindrical geometry. This approximation is justified when the thickness of the component is small in comparison to its inner radius. For the first SCDAP component "shroud" which contains the shroud itself, the shroud insulation and the inner cooling jacket this assumption is not justified. So its volume is about 40 % larger than for a Cartesian geometry, and for the same temperature difference the average heat flux is larger by about 40 % than for a Cartesian geometry. Since the major part of this domain is filled by the insulation material, both its specific heat capacity and the thermal conductivity have been increased by 40 % to compensate for this geometry effect. This treatment is, however, only an approximation because average values for the whole domain are considered, and for a better representation the use of cylindrical co-ordinates to solve the heat conduction equation is mandatory.

In spite of the relatively low temperature level outside the outer cooling jacket radiation may not be neglected. Therefore the containment is modelled as a SCDAP component for further calculations so that radiation between the outer cooling jacket and the containment can be accounted for. Its effect will be demonstrated later.

Another reason for the deviations between calculated and measured temperatures may lie in the difficulty to model adequately the complicated design of the QUENCH facility. For example the pins and the shroud must be modelled to have the same axial extension to account for the radiation heat transfer between these components, but in the QUENCH facility the pins are longer than the shroud section. During the pre-calculations it was felt that the correct modelling of geometry of the shroud and the shroud insulation is predominant. As a consequence of this modelling, the portion of electrical energy released into the heated zone is overestimated. To improve

this situation with not too large an effort, some input changes are made. Only molybdenum is considered in the unheated part instead of molybdenum and copper, so increasing the electrical resistance of the unheated part of the pins. Besides this the length of the three upper unheated nodes was modelled to be 0.2 m instead of 0.15 m. With these two changes the calculated electrical power input into the unheated zone is increased and hence the portion of electrical energy release into the heated part of the bundle decreased, the total amount of electrical power being given from experimental values.

Further investigations showed that the thermal conductivity of the insulation material should be increased by another 40 % to fit the measured temperatures in IBS_02. This may have to do with experimental uncertainties.

A calculation has been done with all changes mentioned above (Figures 59 and 60). The measured temperatures in the bundle are now met much better. The remaining difference between measured and calculated pin temperatures at the end of the three power steps can be attributed to experimental uncertainties. Separate investigations [4] show that at high temperatures the measured temperature might be about 100 K above the clad surface temperature due to the method of fixing the thermocouples on the pins, and measured pin temperatures are now between calculated pin surface and fluid temperatures as it should be for such experimental arrangement.

For the three power steps the calculated electrical resistance is about 1 m Ω above the experimental values (Table 6). Therefore the electrical power input should be correct. Temperatures in the cooling jackets are also met, indicating that the radial heat losses are reasonably well modelled. In particular, a comparison of the outer cooling jacket temperatures with those in Figure 57 demonstrates the role of radiation heat transfer between the outer cooling jacket and the containment. While the measured temperatures are overestimated in the original modelling, i. e. the deviations increase with increasing temperature level, there is no such effect for the improved modelling.

The still somewhat overestimated temperature rise at the begin of the power pulse may be due to the material property data of the pins. In the experiment ZrO₂ pellets with a theoretical density of 90 % were used, in the calculation UO₂ pellets with a theoretical density of 95 % are modelled; an improvement of the S/R5 would be rather elaborate, because changes would be necessary at many programme steps.

The influence of the wrong modelling can be assessed from a comparison of the material property data. Figure 61 shows that for the interesting temperature range the specific heat capacity of ZrO_2 is somewhat higher such explaining the lower measured temperature increase. The thermal conductivity of ZrO_2 is lower than that of UO_2 for the whole temperature range. Since the radial temperature profile in the pins is rather low this difference may be neglected at the moment.

In principle there is an uncertainty leading to a systematic error: the thermocouple to measure the fluid temperature at bundle inlet was displaced, probably during the bundle assembly and measured the temperature of the adjacent structure. A comparison of measured and calculated temperatures near the bundle inlet shows, however, that for IBS_02 this uncertainty cannot be large.

Based on the final modelling of IBS_02 calculations for commissioning test IBS_03 have been made, only adjusting the parameters that were specific for the test conduct. The fluid bundle inlet temperature has been assessed to be constant at 600 K except for the cool-down phase. Time- and space-dependent results (Figures 62 and 63) compare quite well for IBS_02 if one keeps in mind that the thermocouples in the bundle measure a temperature between the clad surface and the fluid temperature. The difference between calculated and measured electrical resistance is also comparable to the results for IBS_02 (Table 6) indicating that the electrical power input is correct.

11. References

- [1] J.M. Broughton, P. Kuan, and D.A. Petti, "A Scenario of the Three Mile Island Unit 2 Accident," Nuclear Technology, 87, 34, 1989.
- [2] P. Hofmann, S. Hagen, V. Noack, G. Schanz, L. Sepold, "Chemical-Physical Behavior of Light Water Reactor Core Components Tested under Severe Reactor Accident Conditions in the CORA Facility", Nuclear Technology, Vol. 118, 1997, pp. 200.
- [3] R.R. Hobbins and G.D. McPherson, "A Summary of Results from the LOFT LP-FP-2 Test and Their Relationship to Other Studies at the Power Burst Facility and of the Three Mile Island Unit 2 Accident", OECD/LOFT Final Event, ISBN 92-64-03339-4, 1991.
- [4] S. Hagen, P. Hofmann, V. Noack, L. Sepold, G. Schanz, G. Schumacher, "Comparison of the Quench Experiments CORA-12, CORA-13, CORA-17", FZKA 5679, Forschungszentrum Karlsruhe, 1996.
- [5] L. Sepold, S. Horn, W. Leiling, FZK Internal Report, 1997
- [6] L. Sepold, S. Horn, W. Leiling, FZK Internal Report, 1997
- [7] T. J. Haste et al. "Design Studies for FZK Degraded Core Bundle Quench Experiments", Report AEAT-1360, May 1997.
- [8] V. Sanchez, E. Elias, Ch. Homann, W. Hering, D. Struwe, "Development and Validation of a Transition Boiling Model for the RELAP5/MOD3 Reflood Simulation", FZKA 5954, Sep. 1997.

12. Acknowledgements

This work was executed under the multi-partners research contract FI4S-CT95-0013 (Investigation of Core Degredation) co-financed by the European Commission under the Euratom Fourth Framework Programme on Nuclear Fission Safety 1994 – 1998 (Report No. INV-COBE (98)-D009). It is also part of the cooperation with the German nuclear industry, co-financed by Siemens/KWU.

At the Forschungszentrum Karlsruhe a variety of support needed for preparation, conduct and evaluation of the experiment is hereby gratefully acknowledged. In particular, the authors would like to thank E. Mackert for the assembly of the test rods and J. Moch for the assembly and instrumentation of the test bundle. We would like to express our gratitude to S. Horn for the preparation of the hydrogen measurement with the Caldos system and the support for the test data evaluation.

The thorough review of the manuscript by T. Haste, AEA Technology, on attachment to JRC Ispra, is gratefully acknowledged.

Table 1: Design characteristics of the QUENCH test bundle

Bundle type		PWR
Bundle size		21 rods
Number of heated rods		20
Number of unheated rods		1
Pitch		14.3 mm
Rod outside diameter		10.75 mm
Cladding material		Zircaloy-4
Cladding thickness		0.725 mm
Rod length	heated rods (elevation) unheated rods (elevation)	2480 mm (-690 to 1790 mm) 2842 mm (-827 to 2015 mm, incl. extension)
Heater material		Tungsten (W)
Heater length		1024 mm
Heater diameter		6 mm
Annular pellet	heated rods unheated rods	ZrO ₂ ; Ø 9.15/6.15 mm; L=11 mm ZrO ₂ ; Ø 9.15/2.5 mm; L=11 mm
Pellet stack	heated rods unheated rods	0 to 1020 mm 0 to 1553 mm
Grid spacer	material length location of the lower edge	Zircaloy-4, Inconel 718 Zry 42 mm, Inc 38 mm -200 mm Inconel 50 mm Zircaloy-4 550 mm Zircaloy-4 1050 mm Zircaloy-4
Shroud	material wall tickness outside diameter length (elevation)	Zircaloy-4 2.38 mm 84.76 mm 1600 mm (-300 to 1300 mm)
Shroud insulation	material insulation thickness elevation	ZrO ₂ fiber 35 mm -300 to 1000 mm
Molybdenum-copper electrodes:		
length of upper electrodes		766 mm (576 Mo, 190 mm Cu)
length of lower electrodes		690 mm (300 Mo, 390 mm Cu)
diameter of electrodes:		
- prior to coating		8.6 mm
- after coating by ZrO ₂		9.0 mm
Cooling jacket	material inner tube outer tube	Stainless steel, 1.4541 Ø 158.3 / 168.3 mm Ø 181.7 / 193.7 mm

Table 2: List of instrumentation of the QUENCH calibration tests

Channel	Designation	Instrument, location
0	TCRC 9	TC (W/Re) central rod, center, 570 mm
1	TCRC13	TC (W/Re) central rod, center, 950 mm
2	TCR 9	TC (W/Re) central rod, cladding, 570 mm
3	TCR 13	TC (W/Re) central rod, cladding, 950 mm
4	TFS 2/11	TC (W/Re) fuel rod simulator 8 (type 2), 750 mm, 135°
5	TFS 2/13	TC (W/Re) fuel rod simulator 2 (type 2), 950 mm, 225°
6	TFS 2/15	TC (W/Re) fuel rod simulator 4 (type 2), 1150 mm, 315°
7	TFS 2/17	TC (W/Re) fuel rod simulator 6 (type 2), 1350 mm, 45°
8	TFS 3/8	TC (W/Re) fuel rod simulator 5 (type 3), 470 mm, 45°
9	TFS 3/10	TC (W/Re) fuel rod simulator 7 (type 3), 670 mm, 135°
10	TFS 3/12	TC (W/Re) fuel rod simulator 9 (type 3), 850 mm, 225°
11	TFS 3/13	TC (W/Re) fuel rod simulator 3 (type 3), 950 mm, 315°
12	TFS 3/14	TC (W/Re) fuel rod simulator 5 (type 3), 1050 mm, 45°
13	TFS 3/16	TC (W/Re) fuel rod simulator 7 (type 3), 1250 mm, 135°
14	TFS 4/11	TC (W/Re) fuel rod simulator 14 (type 4), 750 mm, 45°
15	TFS 4/13	TC (W/Re) fuel rod simulator 20 (type 4), 950 mm, 135°
16	TFS 5/8	TC (W/Re) fuel rod simulator 21 (type 5), 470 mm, 225°
17	TFS 5/9	TC (W/Re) fuel rod simulator 10 (type 5), 570 mm, 315°
18	TFS 5/10	TC (W/Re) fuel rod simulator 12 (type 5), 670 mm, 225°
19	TFS 5/11	TC (W/Re) fuel rod simulator 13 (type 5), 750 mm, 45°
20	TFS 5/12	TC (W/Re) fuel rod simulator 15 (type 5), 850 mm, 315°
21	TFS 5/13	TC (W/Re) fuel rod simulator 16 (type 5), 950 mm, 135°
22	TFS 5/14	TC (W/Re) fuel rod simulator 18 (type 5), 1050 mm, 45°
23	TFS 5/15	TC (W/Re) fuel rod simulator 19 (type 5), 1150 mm, 225°
24	TFS 5/16	TC (W/Re) fuel rod simulator 21 (type 5), 1250 mm, 225°
25	TFS 5/17	TC (W/Re) fuel rod simulator 10 (type 5), 1350 mm, 315°
26	TSH 9/270	TC (W/Re) shroud outer surface, 570 mm, 270°
27	TSH 11/270	TC (W/Re) shroud outer surface, 750 mm, 270°
28	TSH 13/270	TC (W/Re) shroud outer surface, 950 mm, 270°
29	TSH 14/270	TC (W/Re) shroud outer surface, 1050 mm, 270°
30	TSH 11/180	TC (W/Re) shroud outer surface, 750 mm, 180°

Chan-nel	Designation	Instrument, location
31	TSH 12/180	TC (W/Re) shroud outer surface, 850 mm, 180°
32	TSH 13/180	TC (W/Re) shroud outer surface, 950 mm, 180°
33	TSH 15/180	TC (W/Re) shroud outer surface, 1150 mm, 180°
34	TSH 16/180	TC (W/Re) shroud outer surface, 1250 mm, 180°
35	TSH 9/90	TC (W/Re) shroud outer surface, 570 mm, 90°
36	TSH 11/90	TC (W/Re) shroud outer surface, 750 mm, 90°
37	TSH 13/90	TC (W/Re) shroud outer surface, 950 mm, 90°
38	TSH 14/90	TC (W/Re) shroud outer surface, 1050 mm, 90°
39	TSH 11/0	TC (W/Re) shroud outer surface, 750 mm, 0°
40	TSH 12/0	TC (W/Re) shroud outer surface, 850 mm, 0°
41	TSH 13/0	TC (W/Re) shroud outer surface, 950 mm, 0°
42	TSH 15/0	TC (W/Re) shroud outer surface, 1150 mm, 0°
43	TSH 16/0	TC (W/Re) shroud outer surface, 1250 mm, 0°
44	T 512	Gas temperature bundle outlet
45	-	
46	-	
47	Ref. T 01	Reference temperature 1
48	TFS 2/1	TC (NiCr/Ni) fuel rod simulator 4 (type 2), 250 mm, 315°
49	TFS 2/2	TC (NiCr/Ni) fuel rod simulator 6 (type 2), 150 mm, 45°
50	TFS 2/3	TC (NiCr/Ni) fuel rod simulator 8 (type 2), 50 mm, 135°
51	TFS 2/5	TC (NiCr/Ni) fuel rod simulator 2 (type 2), 150 mm, 225°
52	TFS 2/6	TC (NiCr/Ni) fuel rod simulator 4 (type 2), 250 mm, 315°
53	TFS 2/7	TC (NiCr/Ni) fuel rod simulator 6 (type 2), 350 mm, 45°
54	TFS 5/4/0	TC (NiCr/Ni) fuel rod simulator 15 (type 5), 50 mm, 315°
55	TFS 5/4/180	TC (NiCr/Ni) fuel rod simulator 21 (type 5), 50 mm, 135°
56	TFS 5/5	TC (NiCr/Ni) fuel rod simulator 16 (type 5), 150 mm, 225°
57	TFS 5/6	TC (NiCr/Ni) fuel rod simulator 18 (type 5), 250 mm, 45°
58	TFS 5/7	TC (NiCr/Ni) fuel rod simulator 19 (type 5), 350 mm, 225°
59	TSH 4/270	TC (NiCr/Ni) shroud outer surface, 50 mm, 270°
60	TSH 3/180	TC (NiCr/Ni) shroud outer surface, 50 mm, 180°
61	TSH 4/180	TC (NiCr/Ni) shroud outer surface, 50 mm, 180°
62	TSH 7/180	TC (NiCr/Ni) shroud outer surface, 350 mm, 180°
63	TSH 4/90	TC (NiCr/Ni) shroud outer surface, 50 mm, 90°
64	TSH 1/0	TC (NiCr/Ni) shroud outer surface, 250 mm, 0°

Channel	Designation	Instrument, location
65	TSH 4/0	TC (NiCr/Ni) shroud outer surface, 50 mm, 0°
66	TSH 7/0	TC (NiCr/Ni) shroud outer surface, 350 mm, 0°
67	TCI 9/270	TC (NiCr/Ni) cooling jacket inner tube wall, 550 mm, 270°
68	TCI 10/270	TC (NiCr/Ni) cooling jacket inner tube wall, 650 mm, 270°
69	TCI 11/270	TC (NiCr/Ni) cooling jacket inner tube wall, 750 mm, 270°
70	TCI 13/270	TC (NiCr/Ni) cooling jacket inner tube wall, 350 mm, 270°
71	-	
72	TCI 1/180	TC (NiCr/Ni) cooling jacket inner tube wall, 250 mm, 180°
73	TCI 4/180	TC (NiCr/Ni) cooling jacket inner tube wall, 50 mm, 180°
74	TCI 7/180	TC (NiCr/Ni) cooling jacket inner tube wall, 350 mm, 180°
75	TCI 11/180	TC (NiCr/Ni) cooling jacket inner tube wall, 750 mm, 180°
76	TCI 12/180	TC (NiCr/Ni) cooling jacket inner tube wall, 850 mm, 180°
77	TCI 13/180	TC (NiCr/Ni) cooling jacket inner tube wall, 950 mm, 180°
78	TCI 15/180	TC (NiCr/Ni) cooling jacket inner tube wall, 1150 mm, 180°
79	-	
80	TCI 9/90	TC (NiCr/Ni) cooling jacket inner tube wall, 550 mm, 90°
81	TCI 10/90	TC (NiCr/Ni) cooling jacket inner tube wall, 650 mm, 90°
82	TCI 11/90	TC (NiCr/Ni) cooling jacket inner tube wall, 750 mm, 90°
83	TCI 13/90	TC (NiCr/Ni) cooling jacket inner tube wall, 850 mm, 90°
84	-	
85	TCI1/0	TC (NiCr/Ni) cooling jacket inner tube wall, 250 mm, 0°
86	TCI 4/0	TC (NiCr/Ni) cooling jacket inner tube wall, 50 mm, 0°
87	TCI 7/0	TC (NiCr/Ni) cooling jacket inner tube wall, 350 mm, 0°
88	TCI 11/0	TC (NiCr/Ni) cooling jacket inner tube wall, 750 mm, 0°
89	TCI 12/0	TC (NiCr/Ni) cooling jacket inner tube wall, 850 mm, 0°
90	TCI 13/0	TC (NiCr/Ni) cooling jacket inner tube wall, 950 mm, 0°
91	TCI 15/0	TC (NiCr/Ni) cooling jacket inner tube wall, 1150 mm, 0°
92	-	
93	TCO 9/270	TC (NiCr/Ni) cooling jacket outer tube surface, 550 mm, 270°
94	TCO 4/180	TC (NiCr/Ni) cooling jacket outer tube surface, 50 mm, 180°
95	-	
96	TCO 1/0	TC (NiCr/Ni) cooling jacket outer tube surface, 250 mm, 0°
97	TCO 7/0	TC (NiCr/Ni) cooling jacket outer tube surface, 350 mm, 0°
98	TCO 13/0	TC (NiCr/Ni) cooling jacket outer tube surface, 950 mm, 0°

Channel	Designation	Instrument, location
99	T 601	Temperature before off-gas flow instrument F 601
100	T 513	Temperature bundle head top (wall)
101	T 514	Temperature bundle head, at outlet (wall)
102	-	
103	-	
104	T 104	Temperature quench water
105	T 201	Temperature steam generator heating pipe
106	T 204	Temperature before steam flow instrument location 50 g/s
107	T 205	Temperature before steam flow instrument location 10 g/s
108	T 301A	Temperature behind superheater
109	T 302	Temperature superheater heating pipe
110	T 303	Temperature before total flow instrument location
111	T 401	Temperature before gas flow instrument location
112	T 403	Temperature at inlet cooling gas
113	T 404	Temperature at outlet cooling gas
114	T 501	Temperature at containment
115	T 502	Temperature at containment
116	T 503	Temperature at containment
117	T 504	Temperature at containment
118	T 505	Temperature at containment
119	T 506	Temperature at containment
120	T 507	Temperature at containment
121	T 508	Temperature at containment
122	T 509A	Temperature bundle head outside (wall)
123	T 510	Temperature at containment
124	T 511	Gas temperature at bundle inlet
125	T 901	Temperature before off-gas flow instrument F 901
126	-	
127	Ref. T 02	Reference temperature 2
128	P 201	Pressure steam generator
129	P 204	Pressure at steam flow instrument location 50 g/s
130	P 205	Pressure at steam flow instrument location 10 g/s
131	P 303	Pressure before total flow instrument location
132	P 401	Pressure before gas flow instrument location

Chan- nel	Designation	Instrument, location
133	P 511	Pressure at bundle inlet
134	P 512	Pressure at bundle outlet
135	P 601	Pressure before off-gas flow instrument F 601
136	P 901	Pressure before off-gas flow instrument F 901
137	L 201	Liquid level steam generator
138	L 501	Liquid level quench water
139	L 701	Liquid level main condenser
140	Q 901	H2 concentration, off-gas (Caldos)
141	P 411	Pressure helium supply
142	-	
143	-	
144	F 104	Flow rate quench water
145	F 204	Flow rate steam 50 g/s
146	F 205	Flow rate steam 10 g/s
147	F 303	Flow rate at bundle inlet (steam + argon), orifice
148	F 401	Argon gas flow rate
149	F 403	Flow rate cooling gas
150	F 601	Flow rate off-gas (orifice)
151	F 901	Off-gas flow rate before Caldos (H2)
152	E 201	Electric current steam generator
153	E 301	Electric current superheater
154	E 501	Electric current inner ring of fuel rod simulators
155	E 502	Electric current outer ring of fuel rod simulators
156	E 503	Electric voltage inner ring of fuel rod simulators
157	E 504	Electric voltage outer ring of fuel rod simulators

Table 3: QUENCH Commissioning Test Overview

Test	Phase	Argon [g/s]	Steam [g/s]	Inlet temp.*) [K]	Maximum temperature [K]	Time at temp. [s]
IBS_01	A	3.6	-	350	950	4000
	B	3.6	-	390	1150	2500
	C	3.6	-	390	1440	3000
IBS_02	A	3.3	-	325	990	2500
	B	3.3	-	360	1120	2500
	C	3.3	-	360	1280	3000
IBS_03	A	3.1	3.0	600	940	2000
	B	3.1	3.0	610	1120	2000
	C	3.1	3.0	610	1270	1000
IBS_04	Heatup (< 0.1 K/s; 0 – 7000 s)	2.8	4.7	650	≤ 1100	7000
	Heatup (< 0.15 K/s; 7000 – 10000 s)	2.8	2.9	610	≤ 1500	3000
	Plateau	2.8	2.9	610	1500	4000
IBS_05	A (1500 – 2250 s)	3.1	-	325	1200**)	750
	B (4000 – 5000 s)	3.1	2.9	500	800**)	1000
	C (7000 – 8500 s)	3.1	2.9	500	1050**)	1500
	D (10500 – 12500 s)	3.1	2.9	530	1270**)	2000
	Transient (1 K/s)	3.1	2.9	620	1750**)	-
	Quenching	- ***)	-	350	-	-

*) Based on T 511 that was attached to the wall of the inlet annulus. So, temperatures given tend to be somewhat too low.

***) Max. temperatures of IBS_05 extrapolated due to TC failures.

***) Ar flow turned off accidentally due to a malfunction of a magnetic valve.

Table 4: Evaluation of cool-down data

Cladding Thermo-couple	Elevation Rod number	Onset of cooling		Onset of quenching		Max. cooldown during quenching (K/s)
		Time (s)	Temp. (K)	Time (s)	Temp. (K)	
TFS2/1	- 250 mm (rod 4)	-	-	19	638	420
TFS2/2	- 150 mm (rod 6)	-	-	19	737	420
TFS2/3	- 50 mm (rod 8)	-	-	19	815	320
TFS2/5	150 mm (rod 2)	19	1034	35	943	260
TFS2/6	250 mm (rod 4)	19	1171	42	1040	210
TFS2/7	350 mm (rod 6)	19	1231	62	977	280
TFS2/17	1350 mm (rod 6)	46	1341	92	834	420
TFS3/8	470 mm (rod 5)	18	1220	55,5	971	300
TFS3/16	1250 mm (rod 7)	43	1483	92	767	320
TFS5/4/0	50 mm (rod 15)	19	877	33	803	230
TFS5/4/180	50 mm (rod 21)	19	867	33	803	160
TFS5/5	150 mm (rod 16)	19	1015	34	946	200
TFS5/6	250 mm (rod 18)	19	1133	50	896	280
TFS5/7	350 mm (rod 19)	19	1222	69	881	260
TFS5/8	470 mm (rod 21)	19	1166	35	1128	300
TFS5/9	570 mm (rod 10)	19	1209	40	1094	280
TFS5/10	670 mm (rod 12)	19	1338	39	1036	370
TFS5/15	1150 mm (rod 19)	43	1500	99	900	220
TFS5/16	1250 mm (rod 21)	43	1416	92	870	310
TFS5/17	1350 mm (rod 10)	43	1310	82	735	340
TCR9	570 mm (rod 1)	19	1259	46	1000	350

Table 5: Integral hydrogen release during the QUENCH commissioning tests

Test	Type	Integral H ₂ -production, g
IBS_03	Calibration test in steam	13
IBS_04	Pre-oxidation at 1500 K	35
IBS_05	a) Repetition of the calibration test in steam	17
	b) Quench scoping test	40
Σ		105

Table 6: Experimental and calculated electrical resistance of the heated pins in mΩ.

exp/run	step 1	step 2	step 3
IBS_02	9.9/10.1	11.2/11.4	12.4/12.7
i02r01	11.7	13.1	14.4
i02r06	11.1	12.4	13.5
IBS_03	11.2/11.4	12.5/12.8	14.1/14.4
i03r01	12.1	13.6	15.7

Note: For the experiments the results for the inner and outer heated pin rows are given, for the calculations the results for the inner heated pins are given.

QUENCH Test Facility

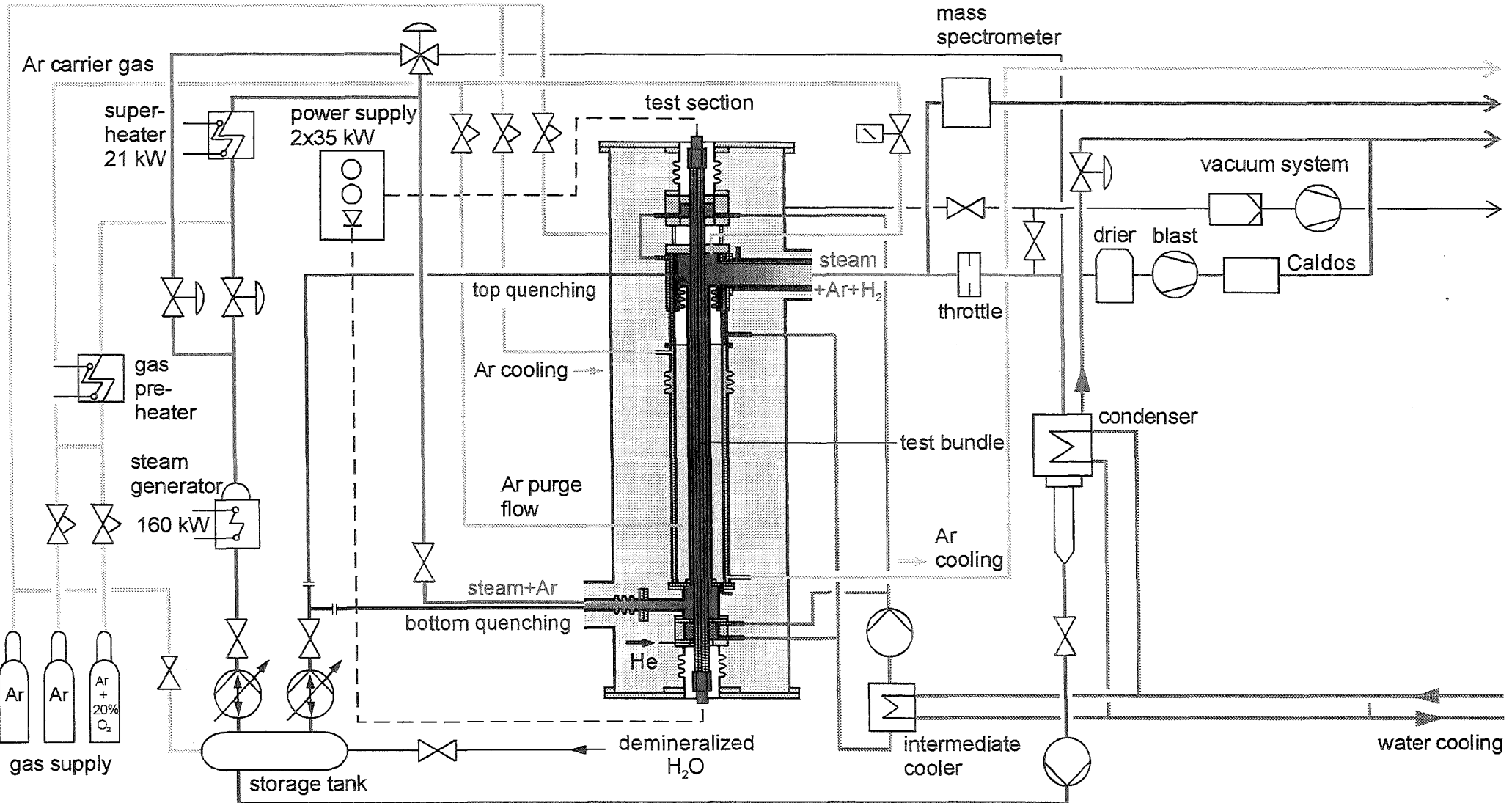


Fig. 1

QUENCH Fuel Rod Simulator Bundle (Top View)

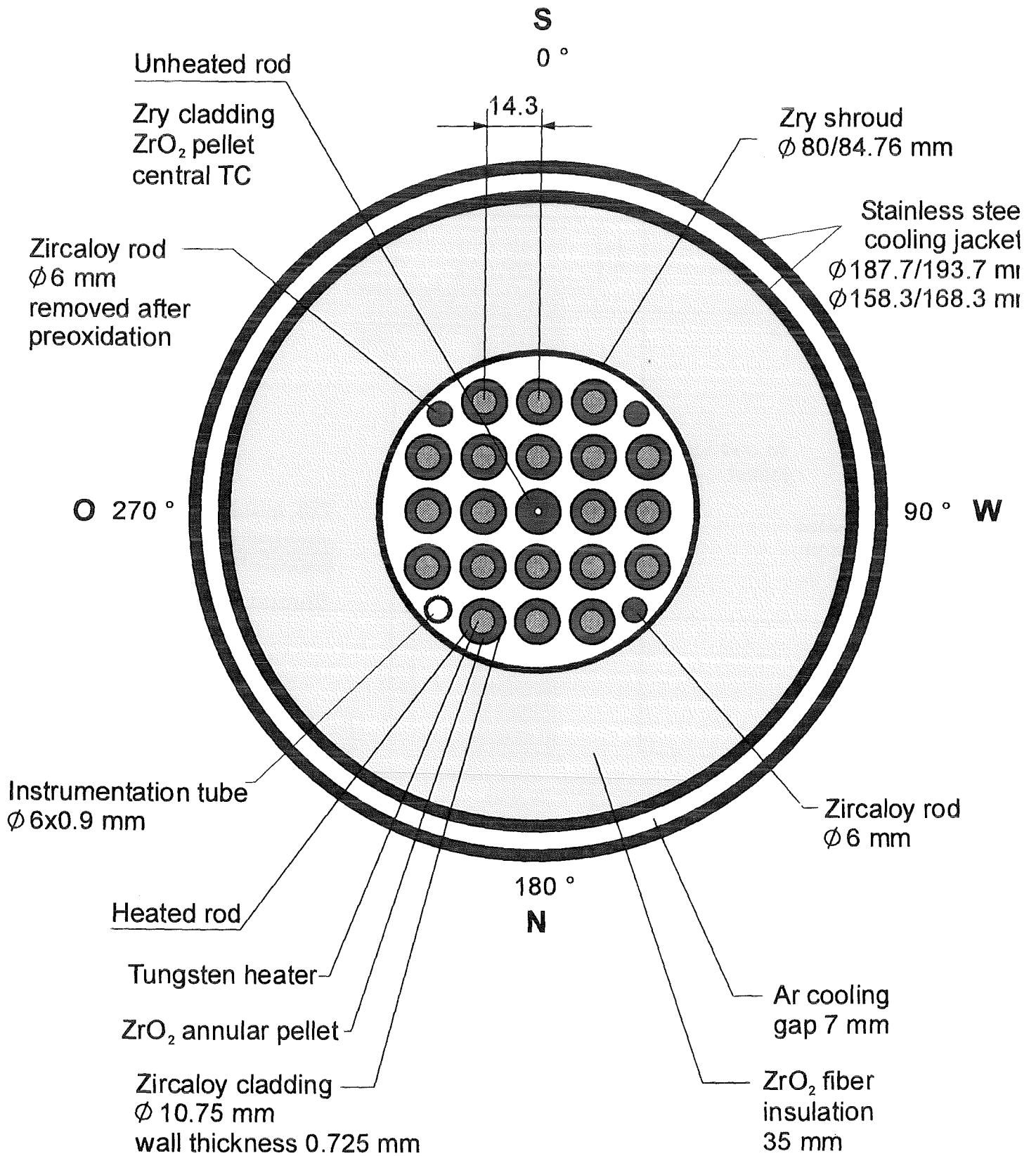


Fig. 2

QUENCH Test Section - Flow Lines

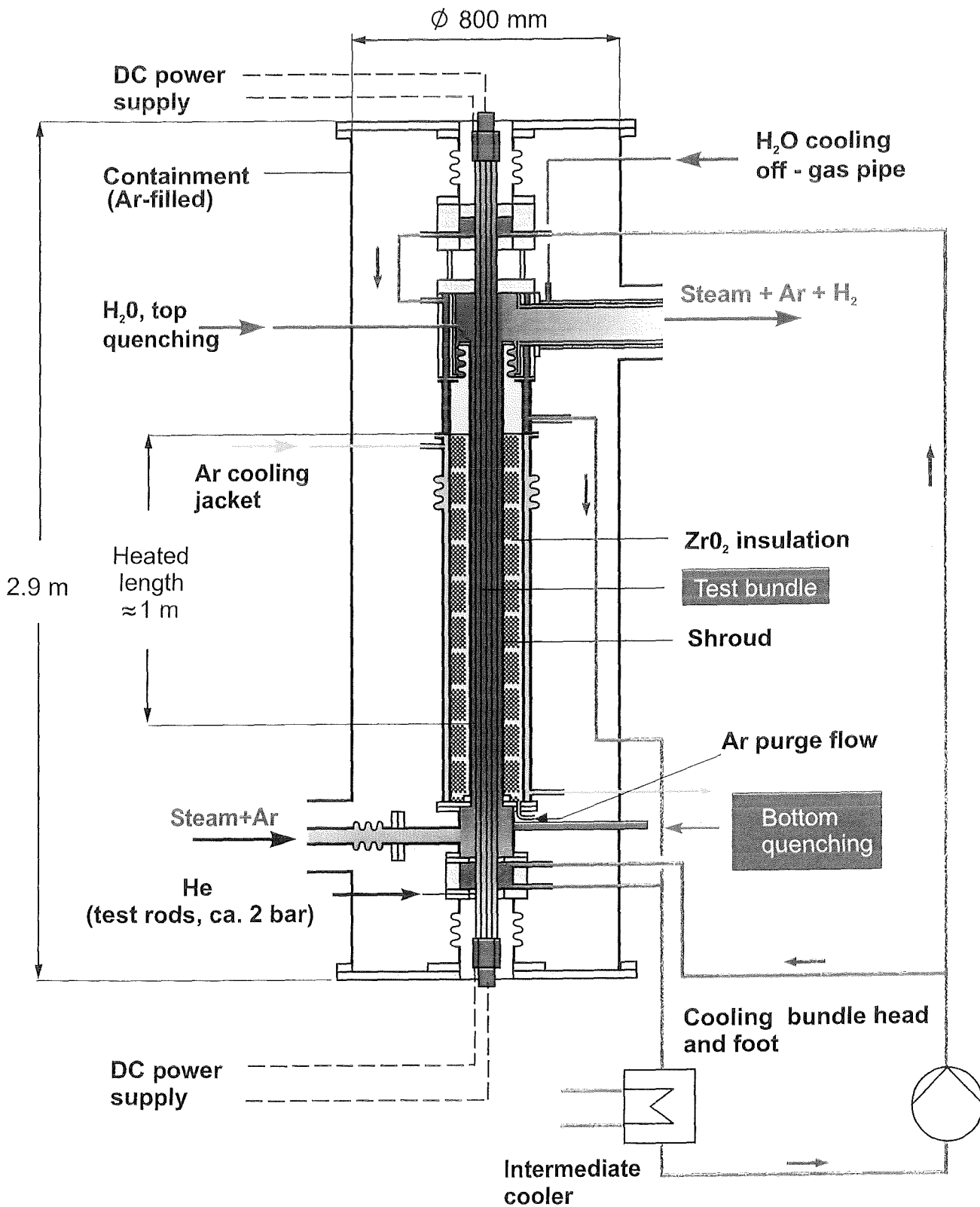


Fig. 3

QUENCH Test Facility H₂ Measurement by CALDOS

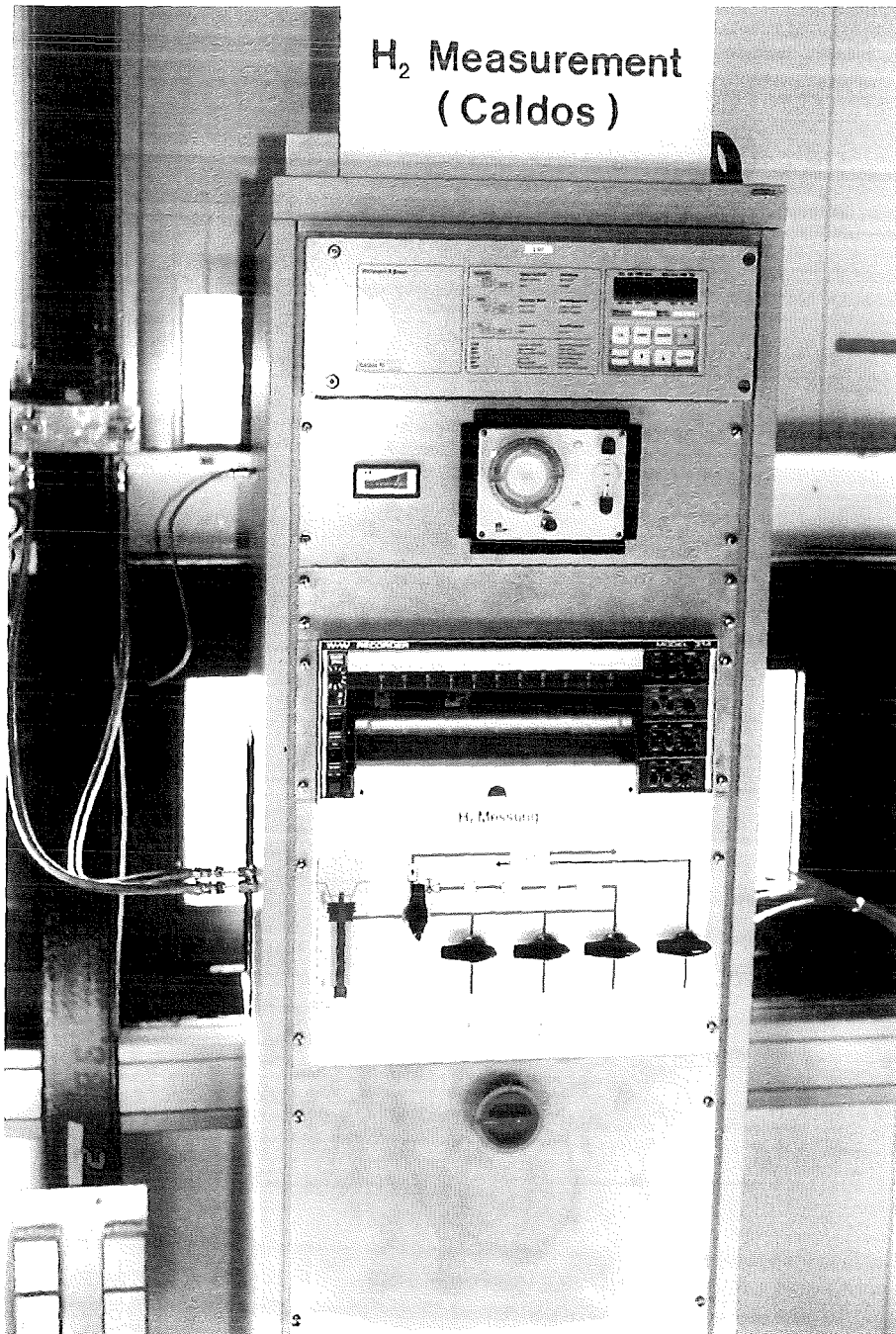


Fig. 4

QUENCH Facility

H₂ measurement with CALDOS (bypass to off-gas line)

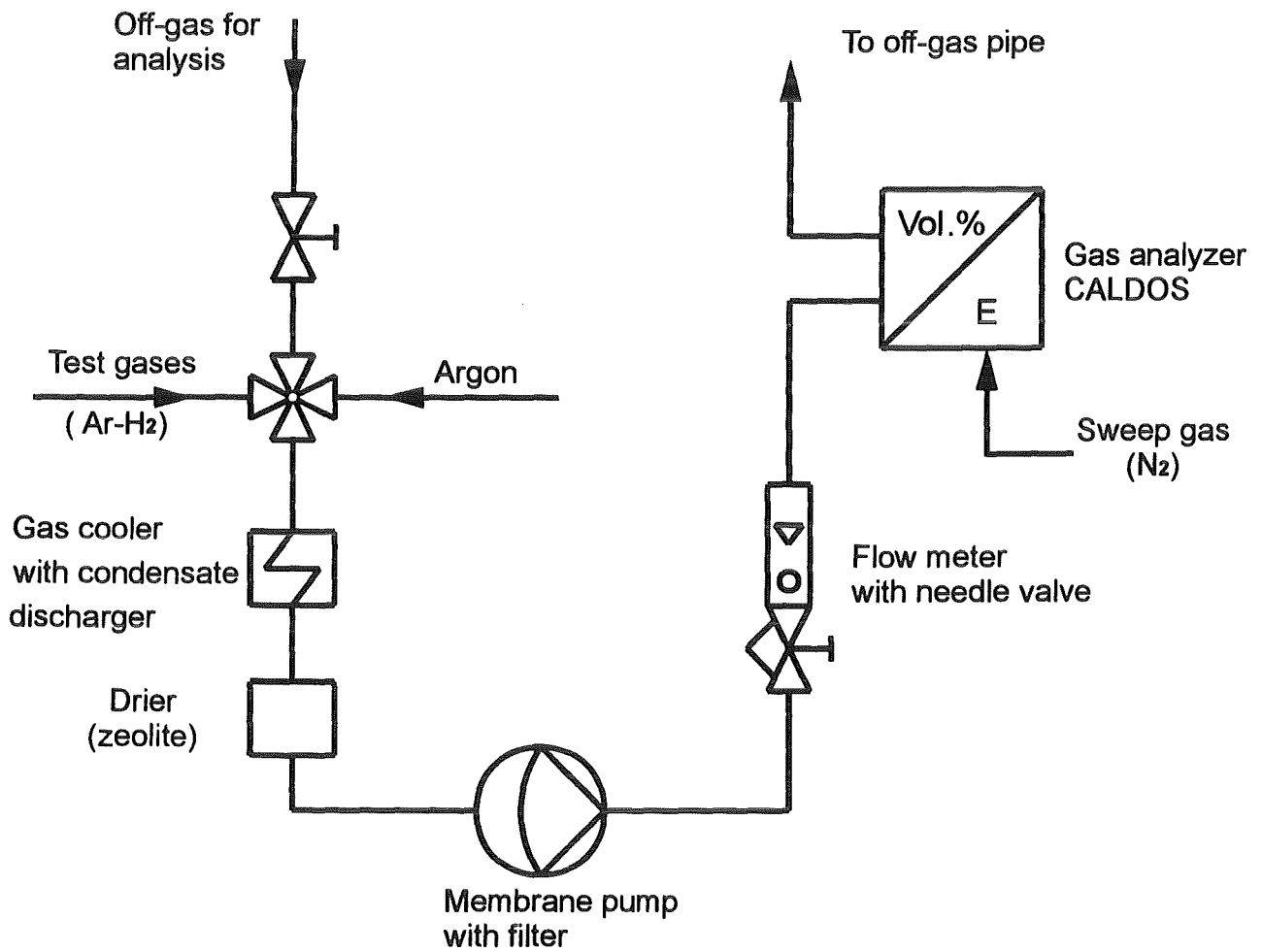


Fig. 5

QUENCH - Facility

H₂ - Measurement mass spectrometer

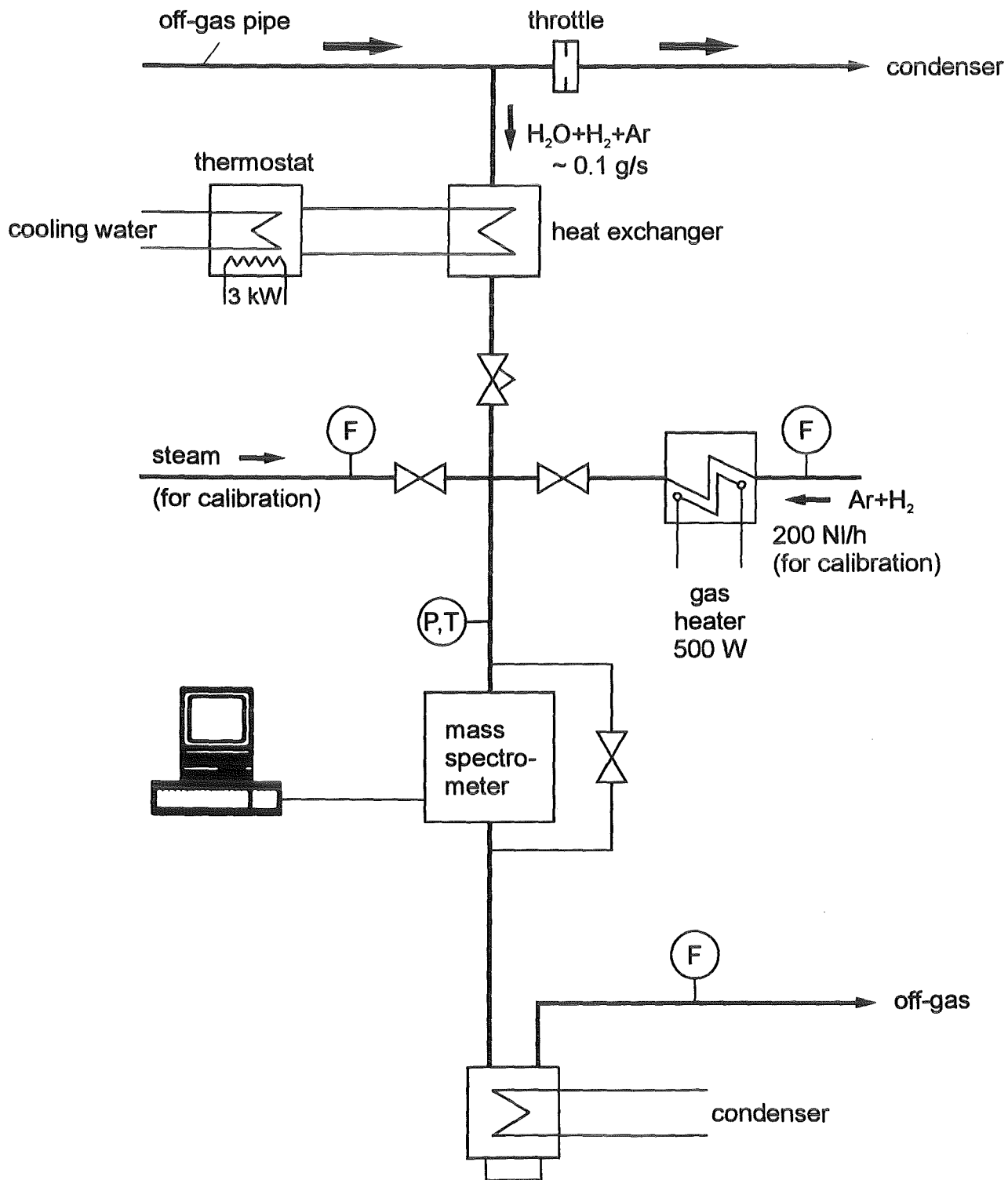


Fig. 6

Heated Fuel Rod Simulator

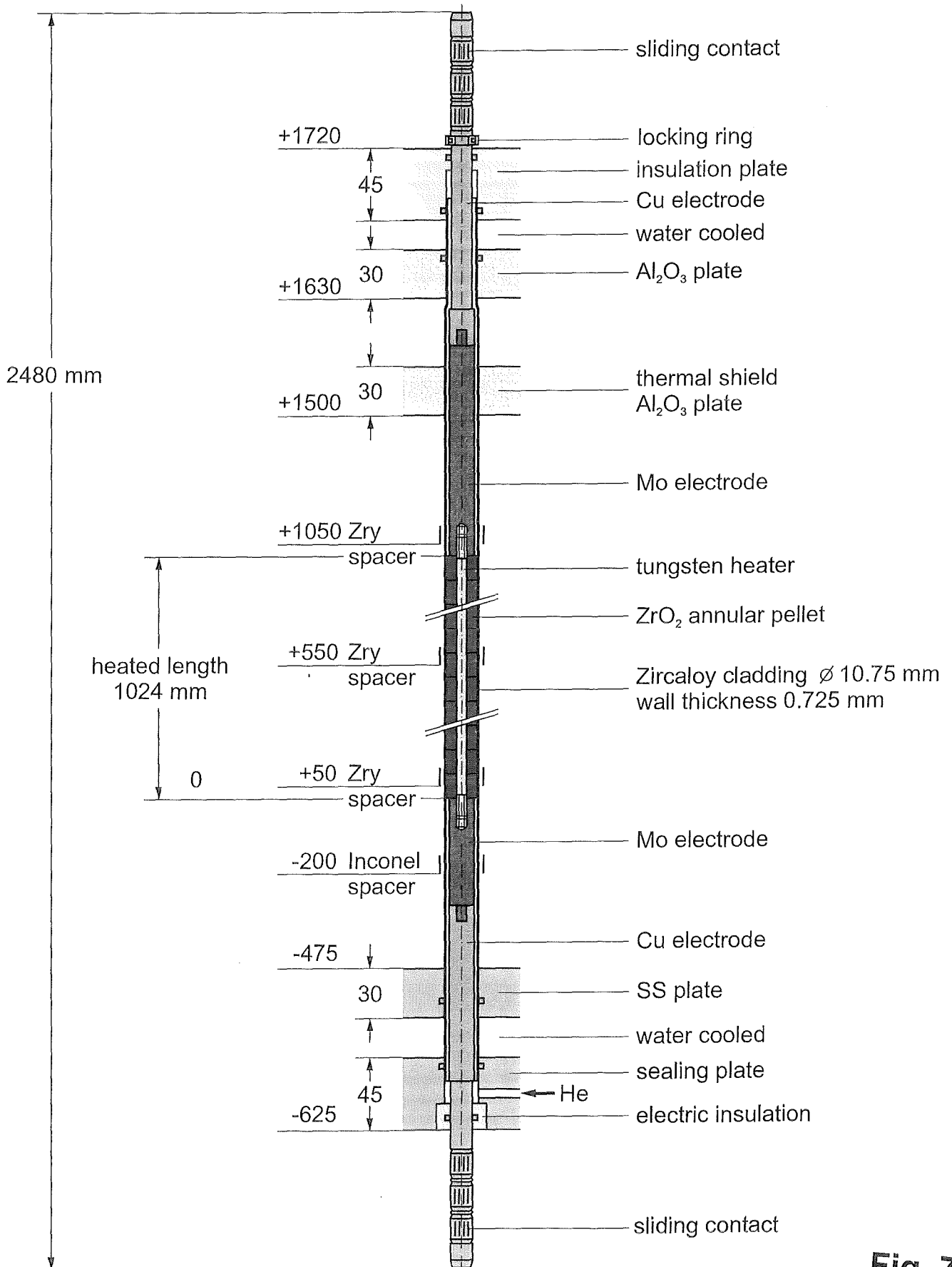


Fig. 7

Unheated Fuel Rod Simulator

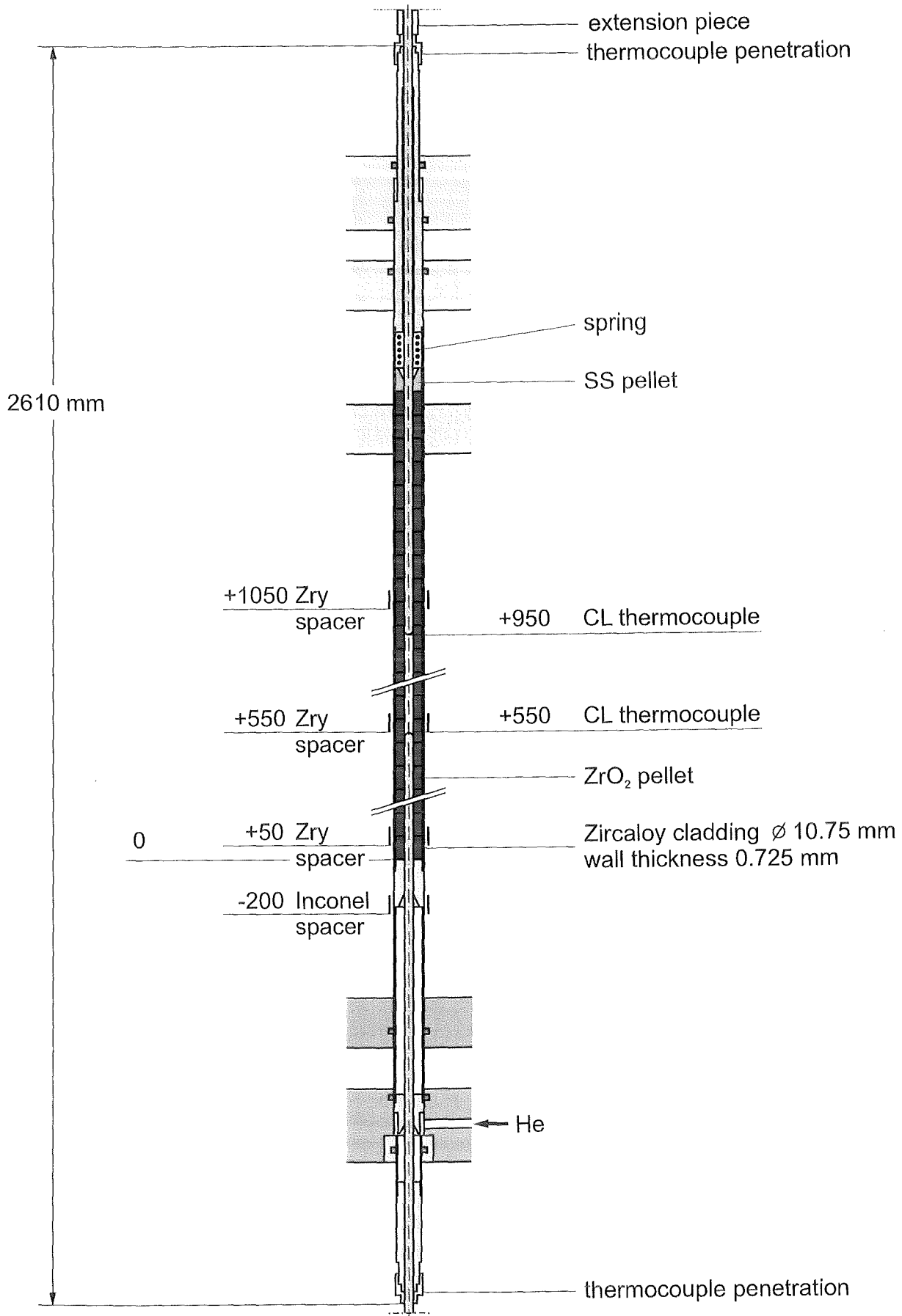


Fig. 8

QUENCH Test Section Instrumentation

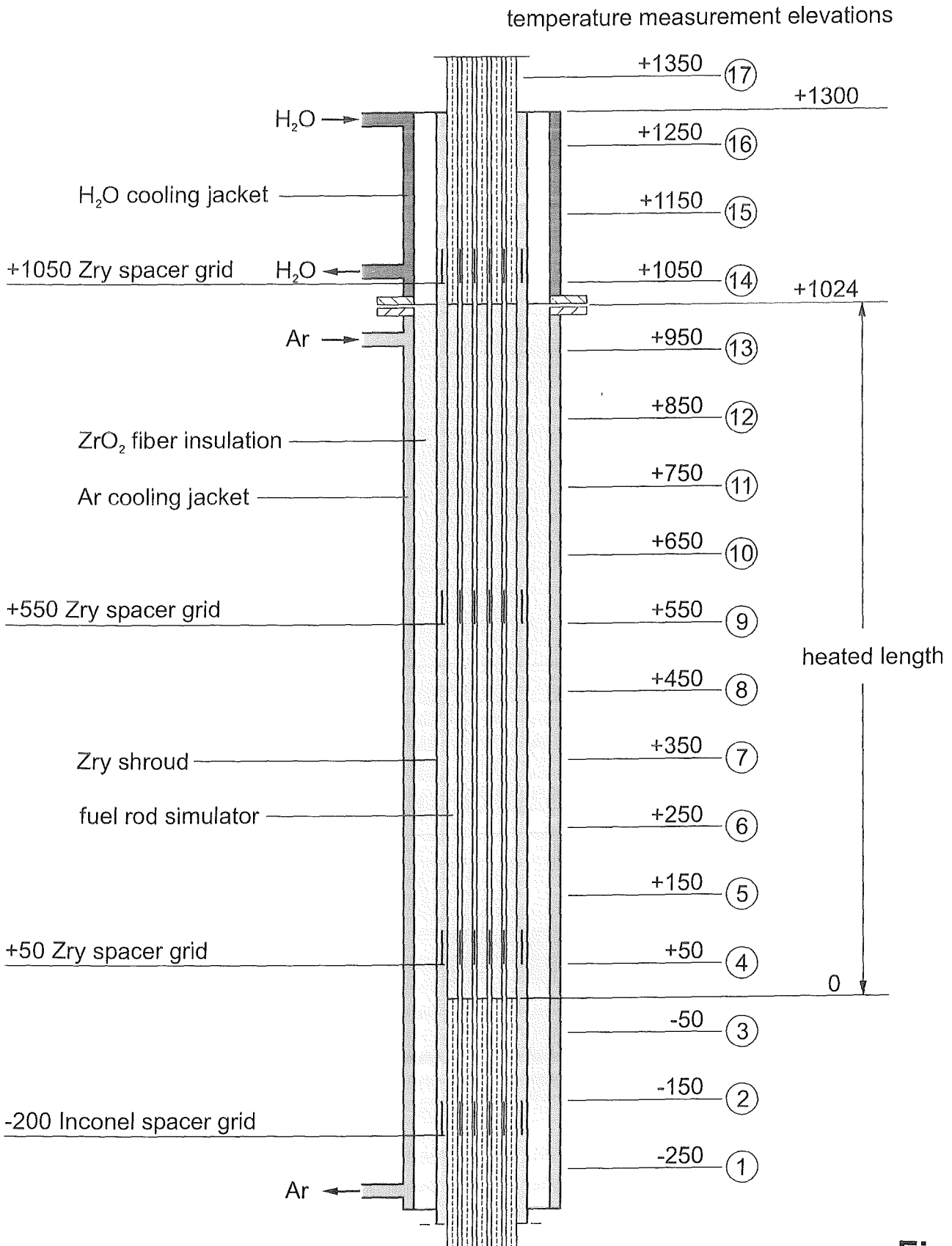


Fig. 9

TC Instrumentation of the Test Bundle

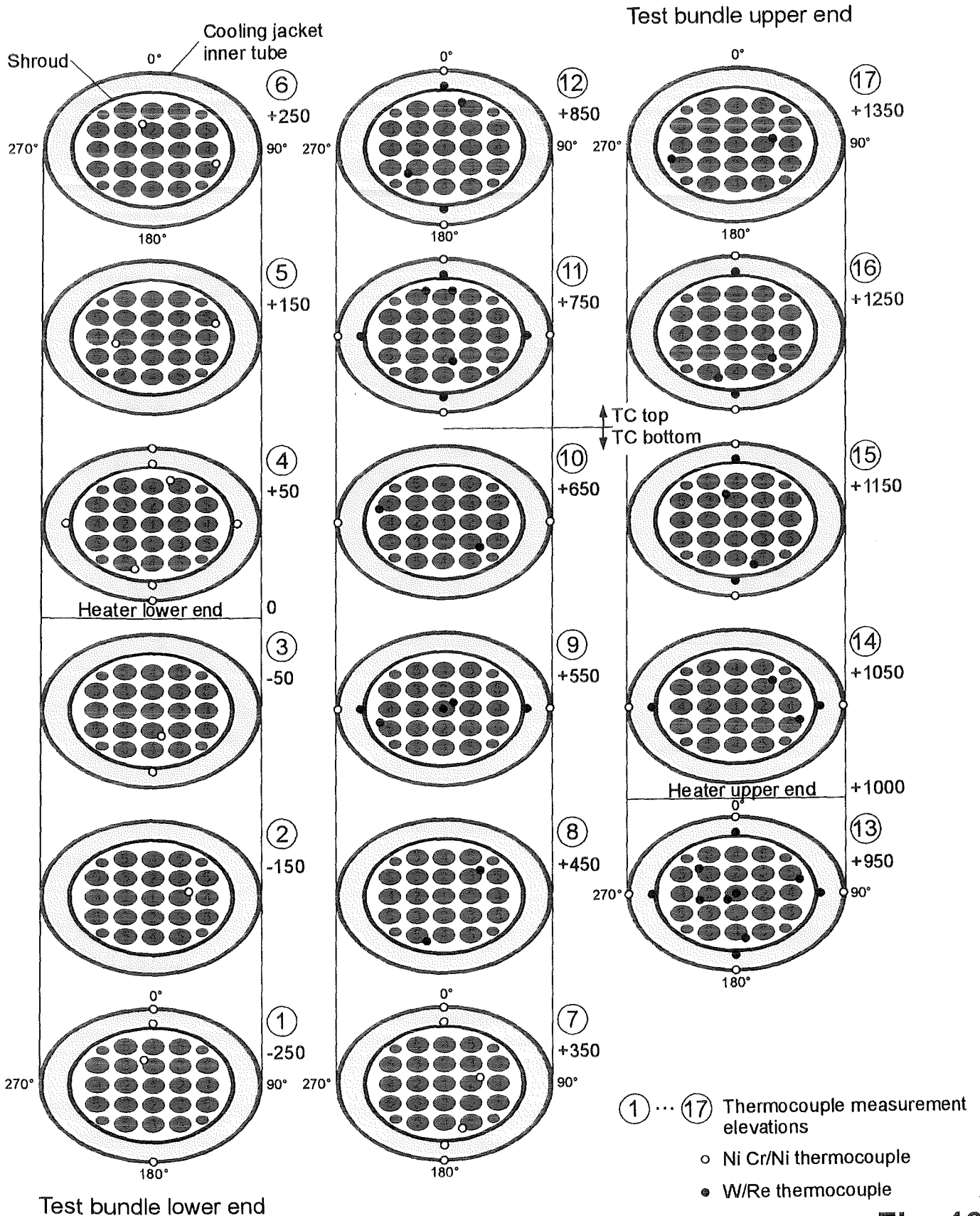
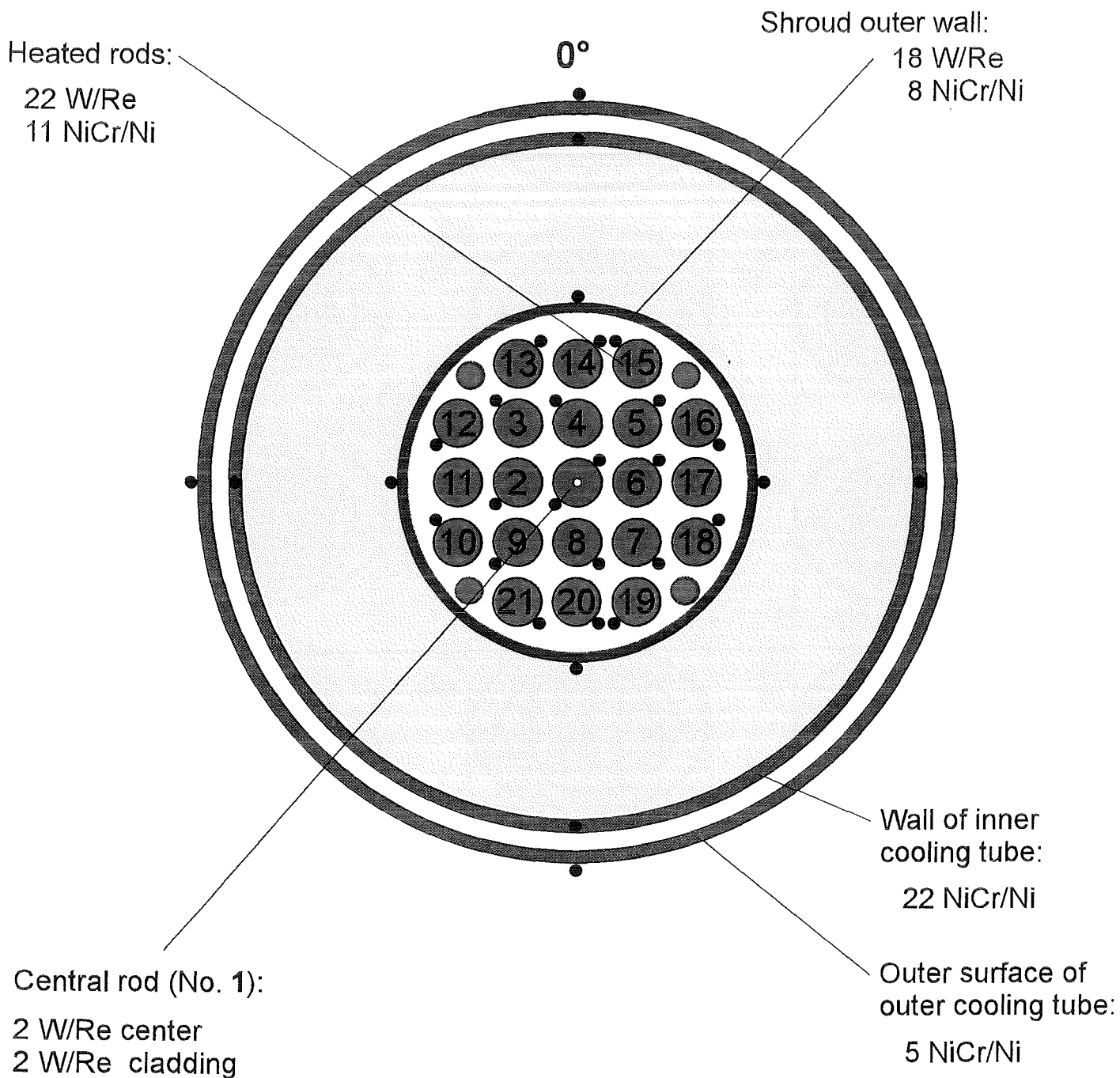


Fig. 10

QUENCH Test Bundle

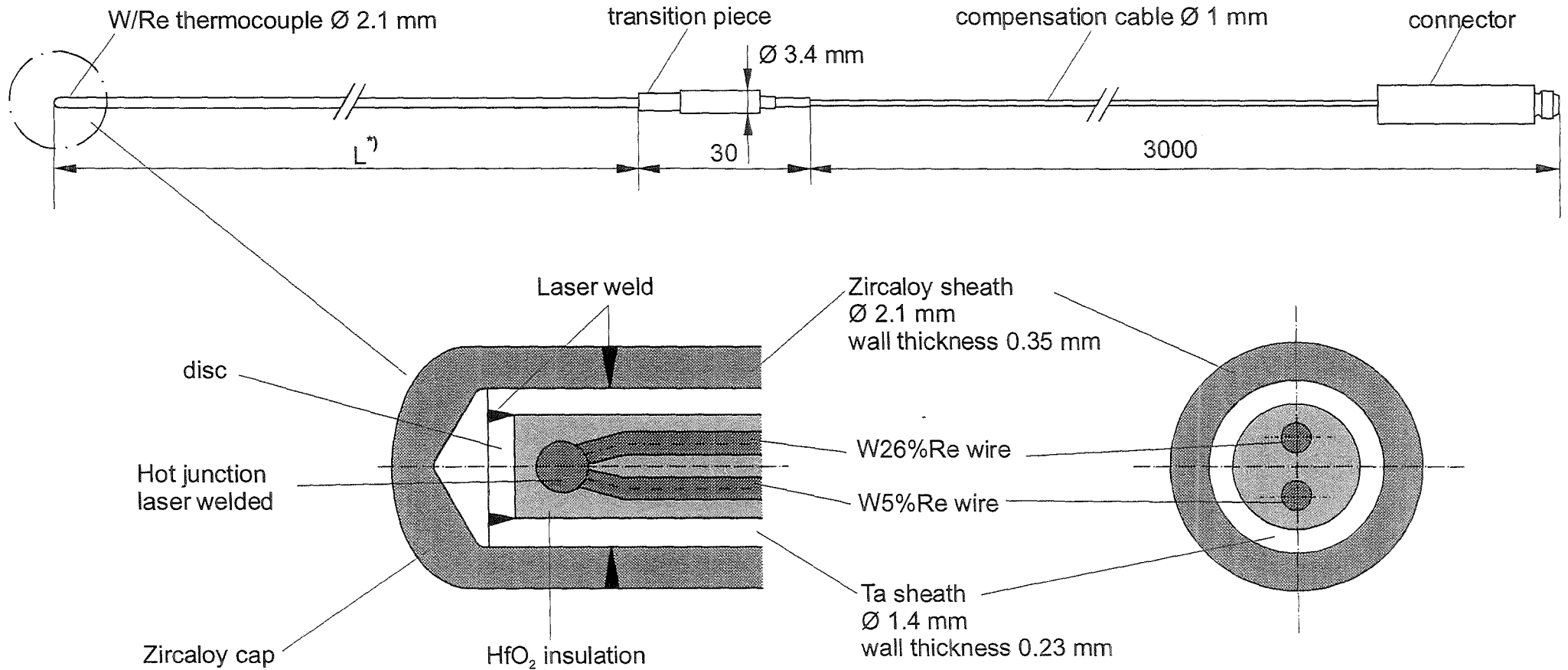
TC Instrumentation and Rod Designation (Top View)



Thermocouples at 17 axial elevations:
From -250 mm to +1350 mm with distances of 100 mm

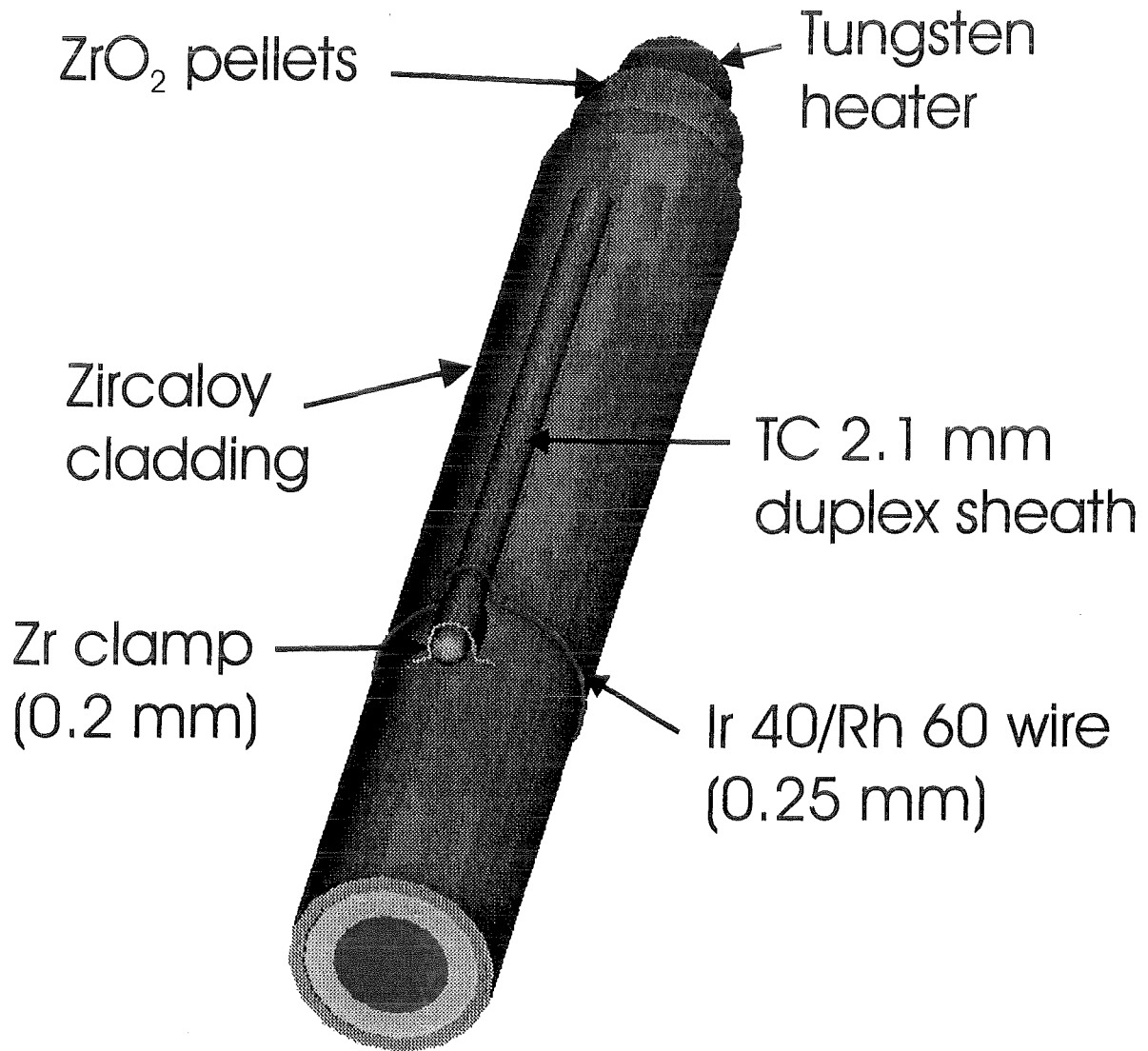
Fig. 11

QUENCH High-temperature thermocouple



*) L: high-temperature section length dependent on the TC position in the test bundle 500 mm - 1800 mm

TC Fastening Concept for the QUENCH Test Rods

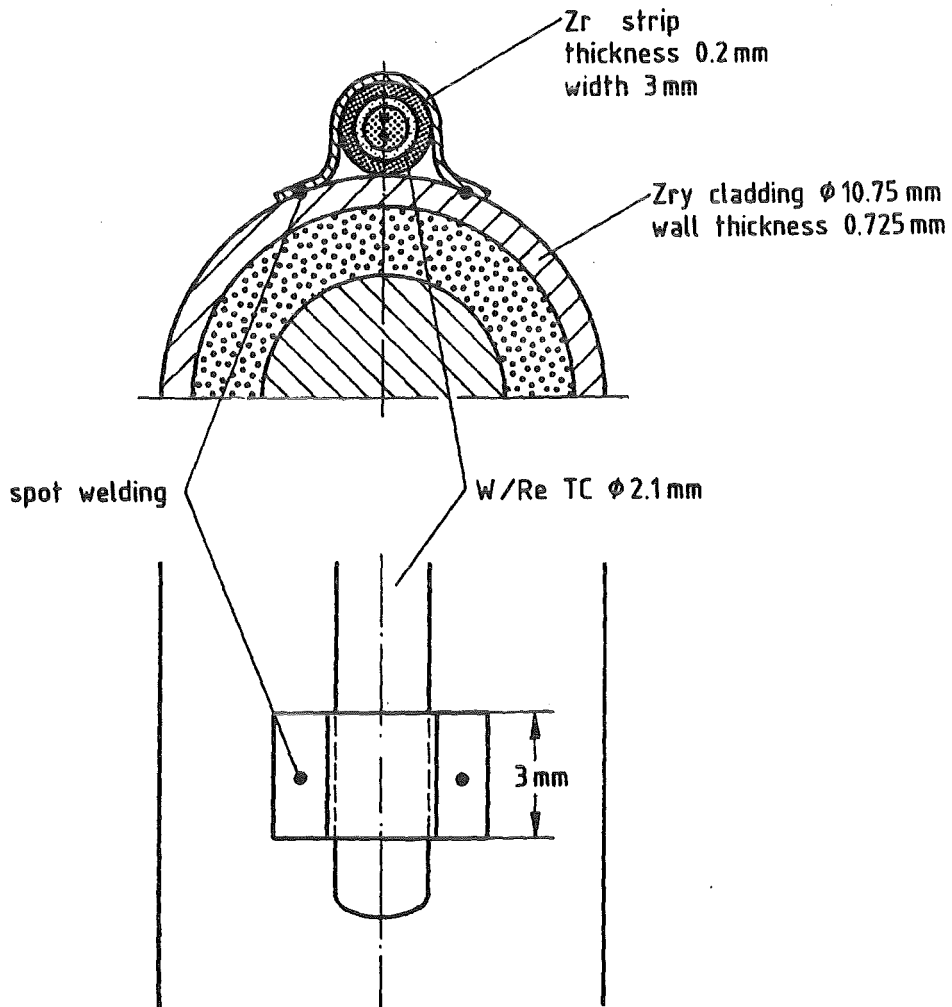


With pre-oxidation: Zr clamp + wire

Without pre-oxidation: Zr clamp

Fig. 13

Zr Clip for Fixing the TC Tip at the Rod Cladding



IMF III / 02.97

Fig. 14

QUENCH Commissioning Test 9 - 16 Oct., 1997

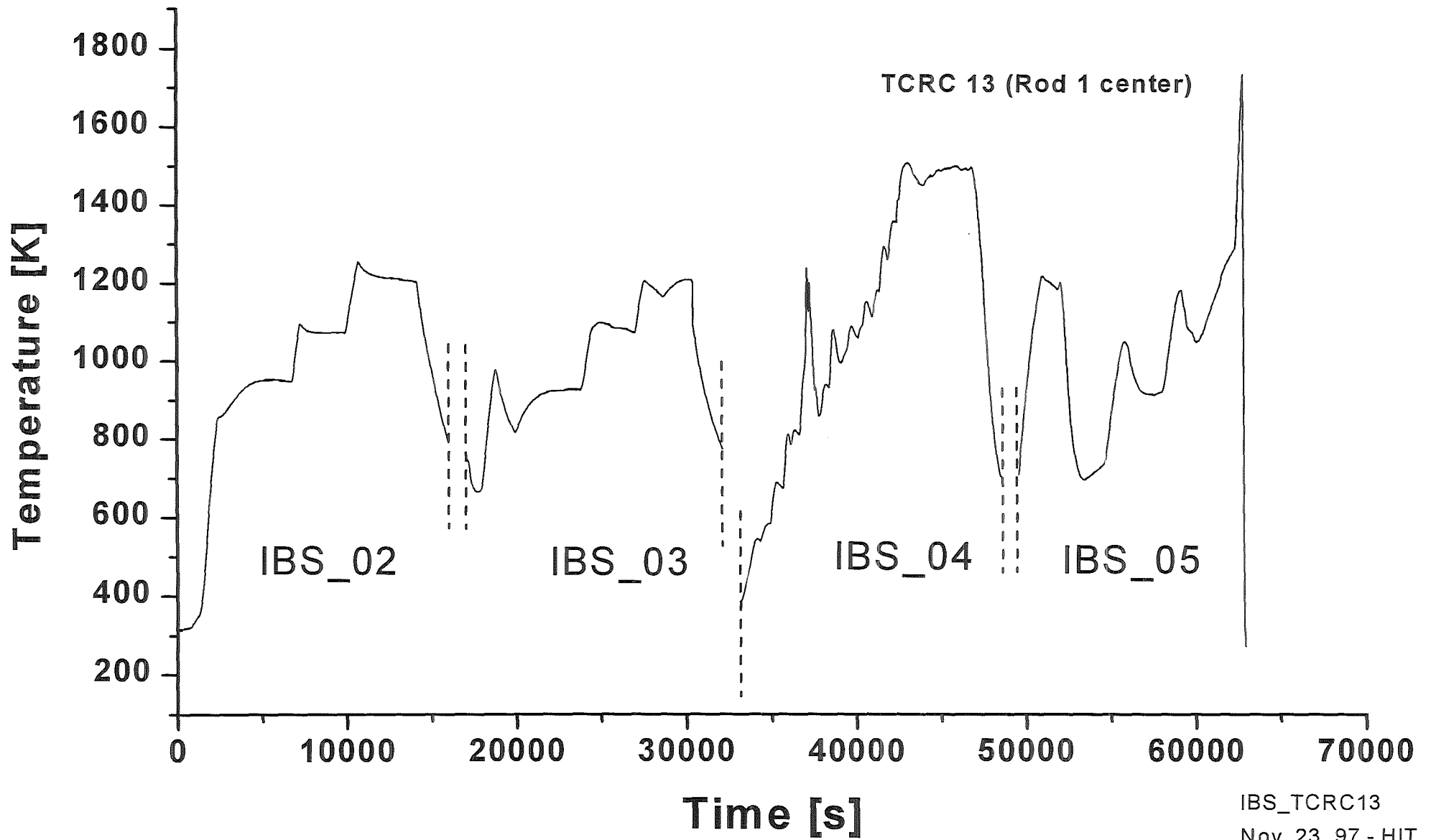


Fig. 15

IBS_TCRC13
Nov. 23, 97 - HIT

QUENCH Calibration Test IBS_03 (Oct. 10, 1997) - Phase C Argon + Steam

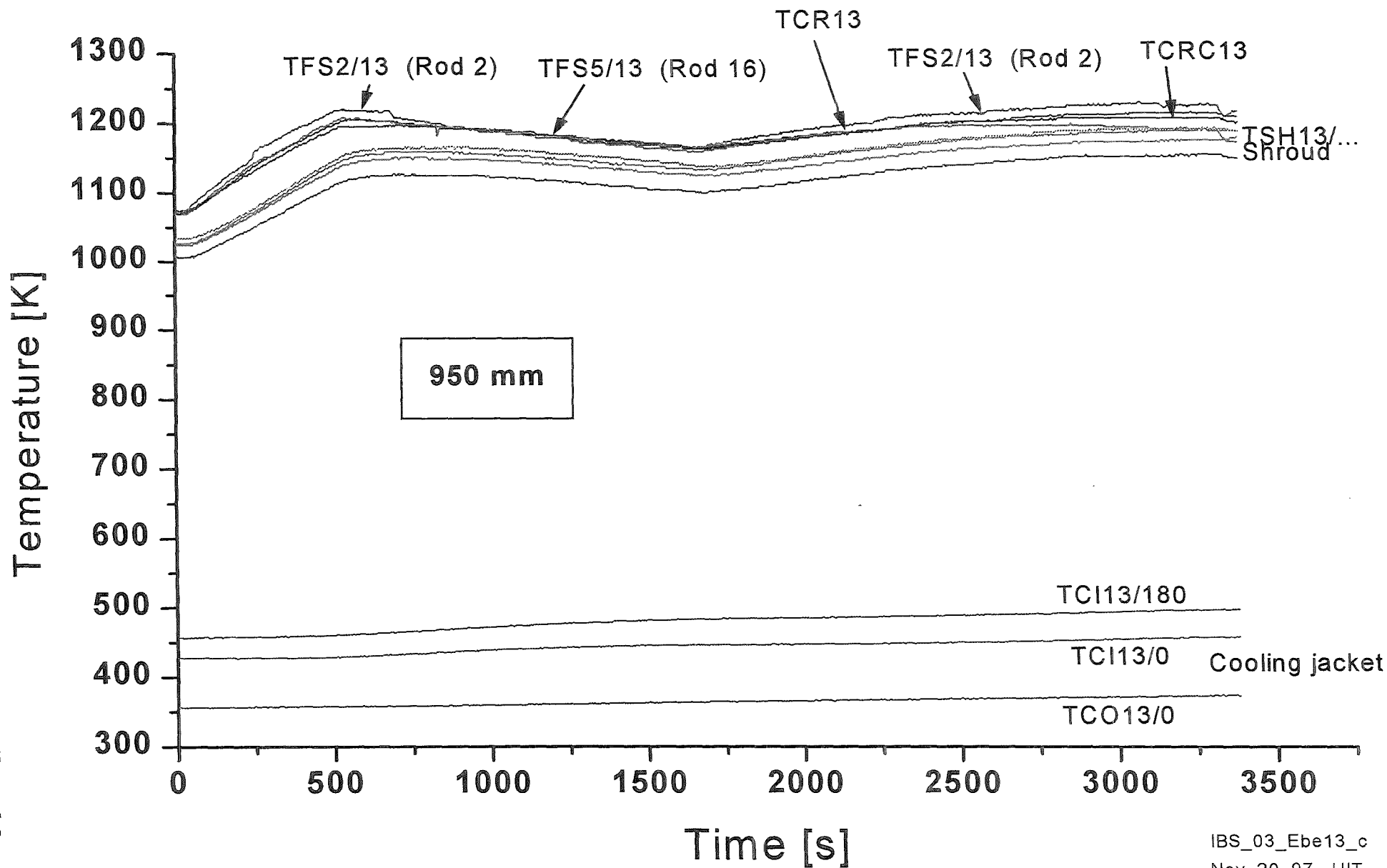
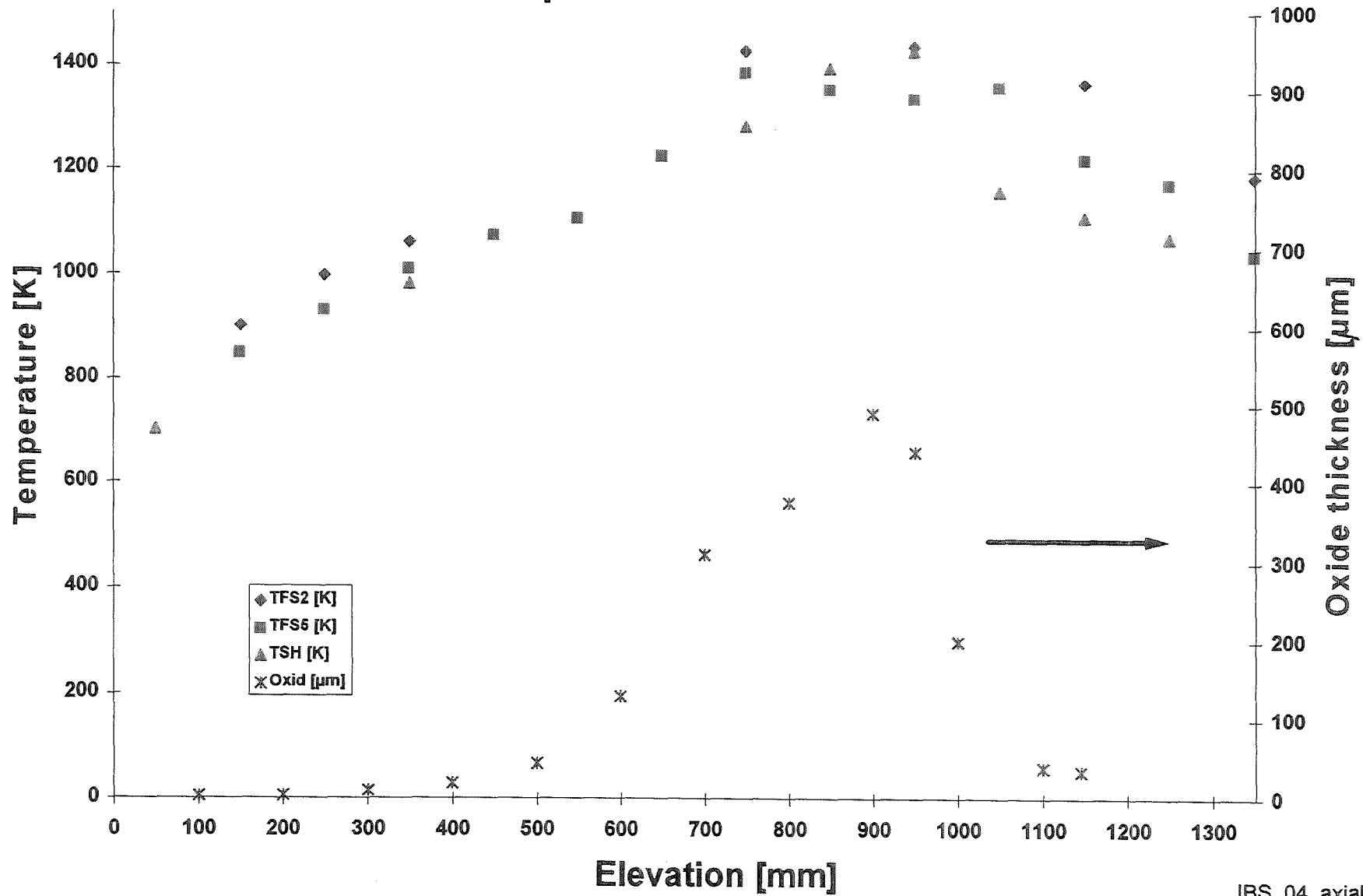


Fig. 16

QUENCH Test IBS_04 - Pre-oxidation

Axial Temperature Profile at 13000 s



IBS_04_axial_zeit
Nov. 11, 97 - HIT

Fig. 17

QUENCH Test IBS_05 (Oct. 16, 1997) - Transient Phase

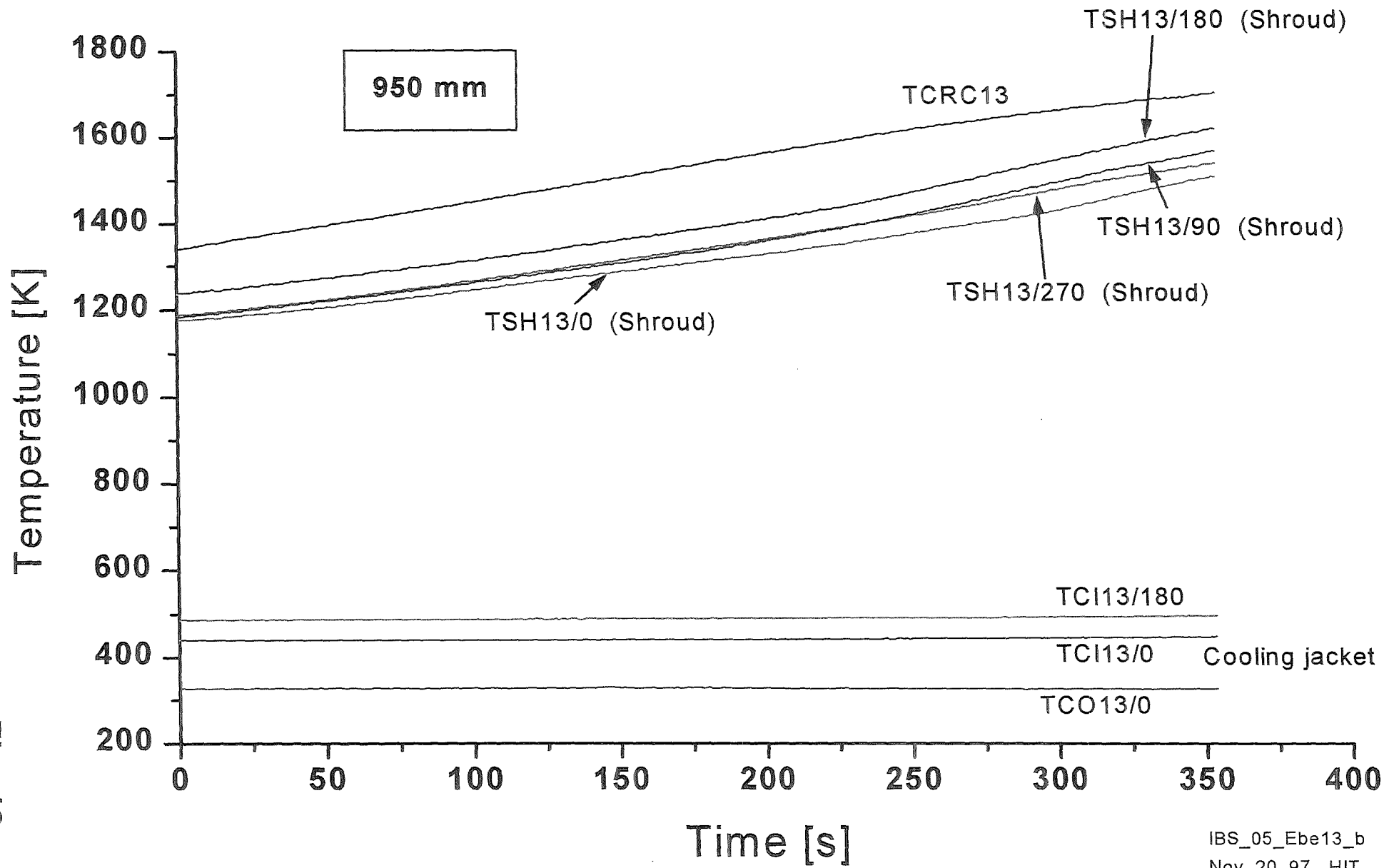


Fig. 18

QUENCH Test IBS_05 (Oct. 16, 1997) - Quenching Phase

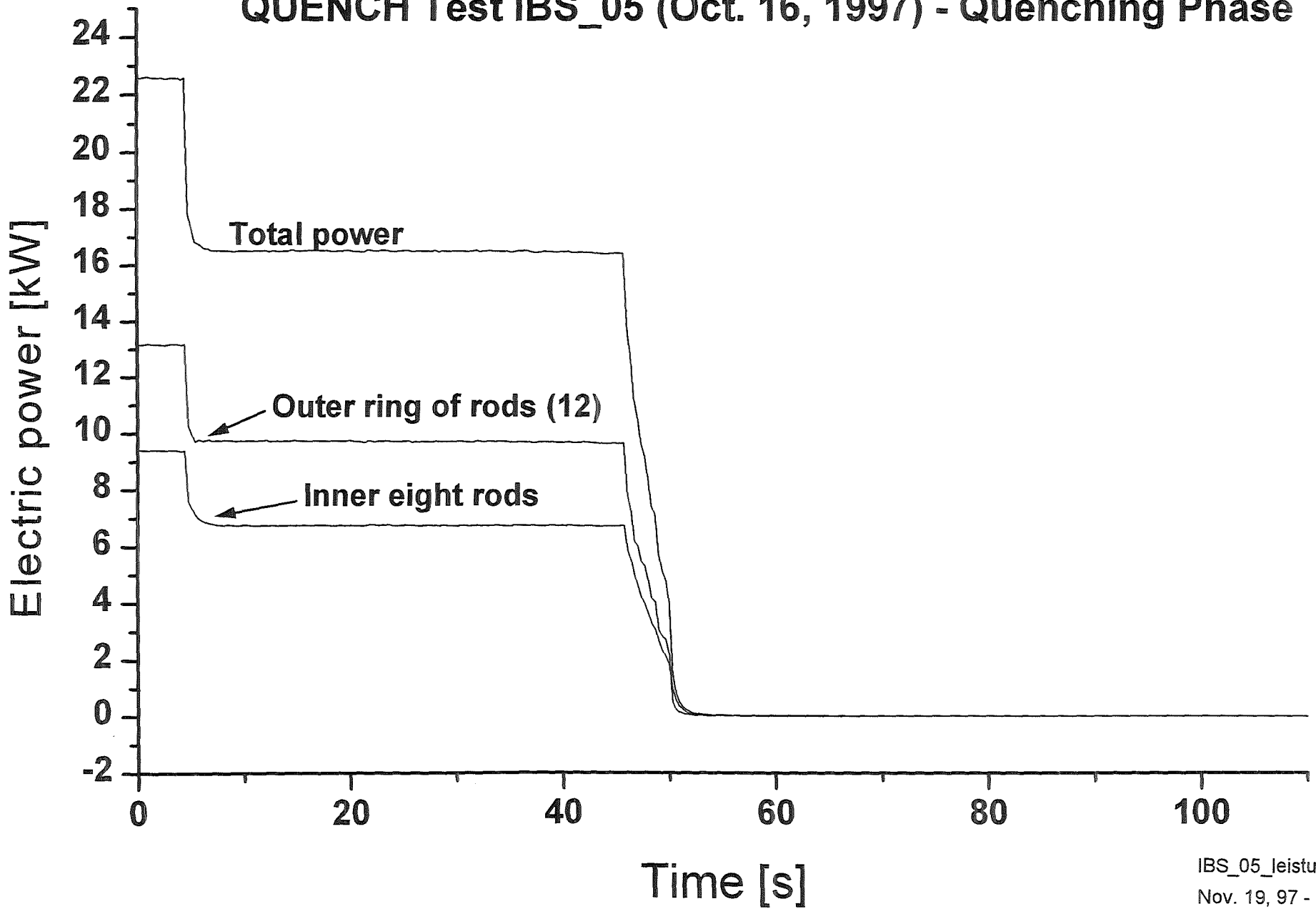


Fig. 19

QUENCH Test IBS_05 (Oct. 16, 1997) - Quenching Phase

Volumetric flow, standard [m³/h]

Steam flow (F 205)

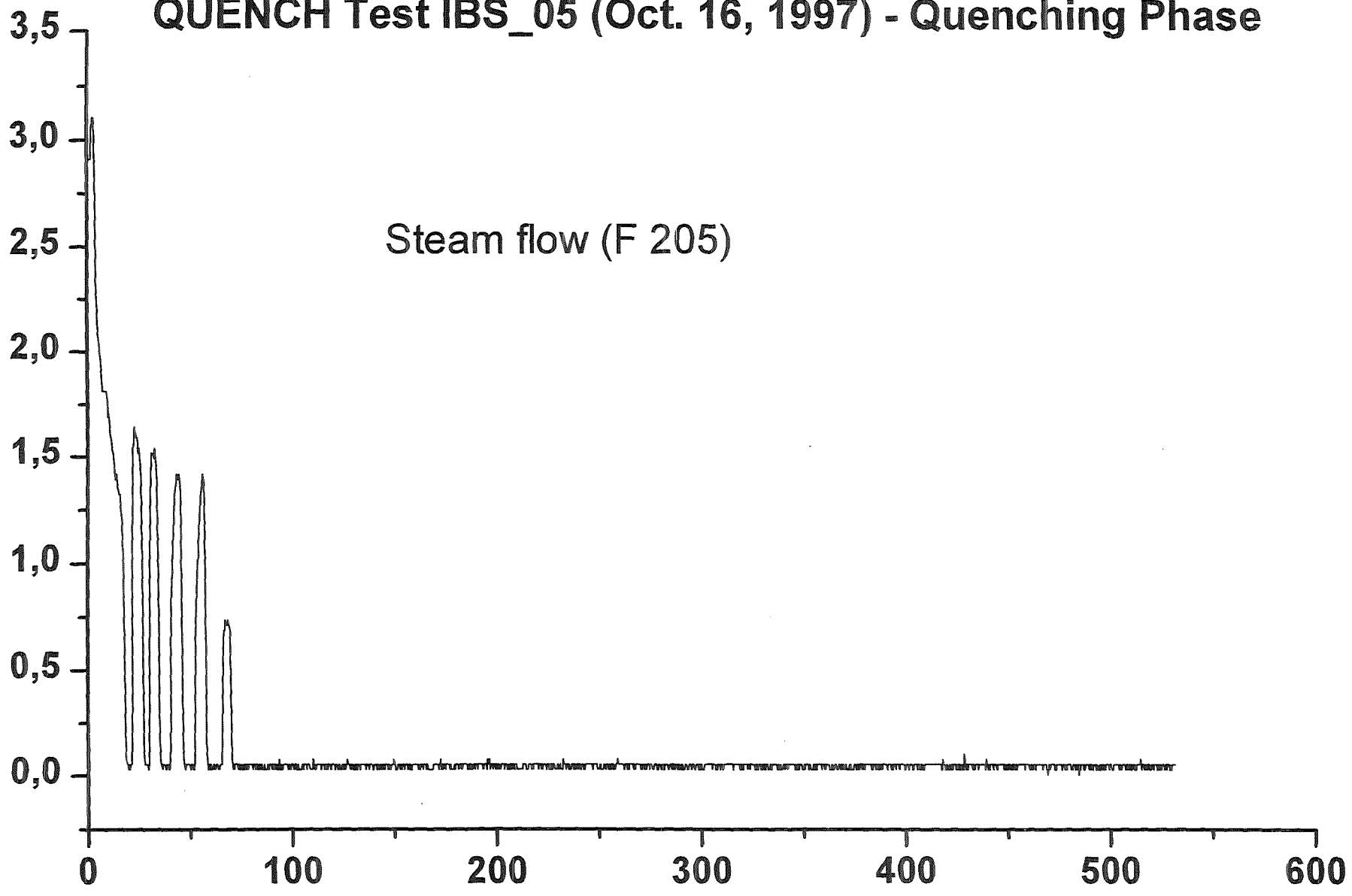


Fig. 20

Time [s]

IBS_05_F205_c
Nov. 4, 1997 - HIT

QUENCH Test IBS_05 (Oct. 16, 1997) - Quenching Phase

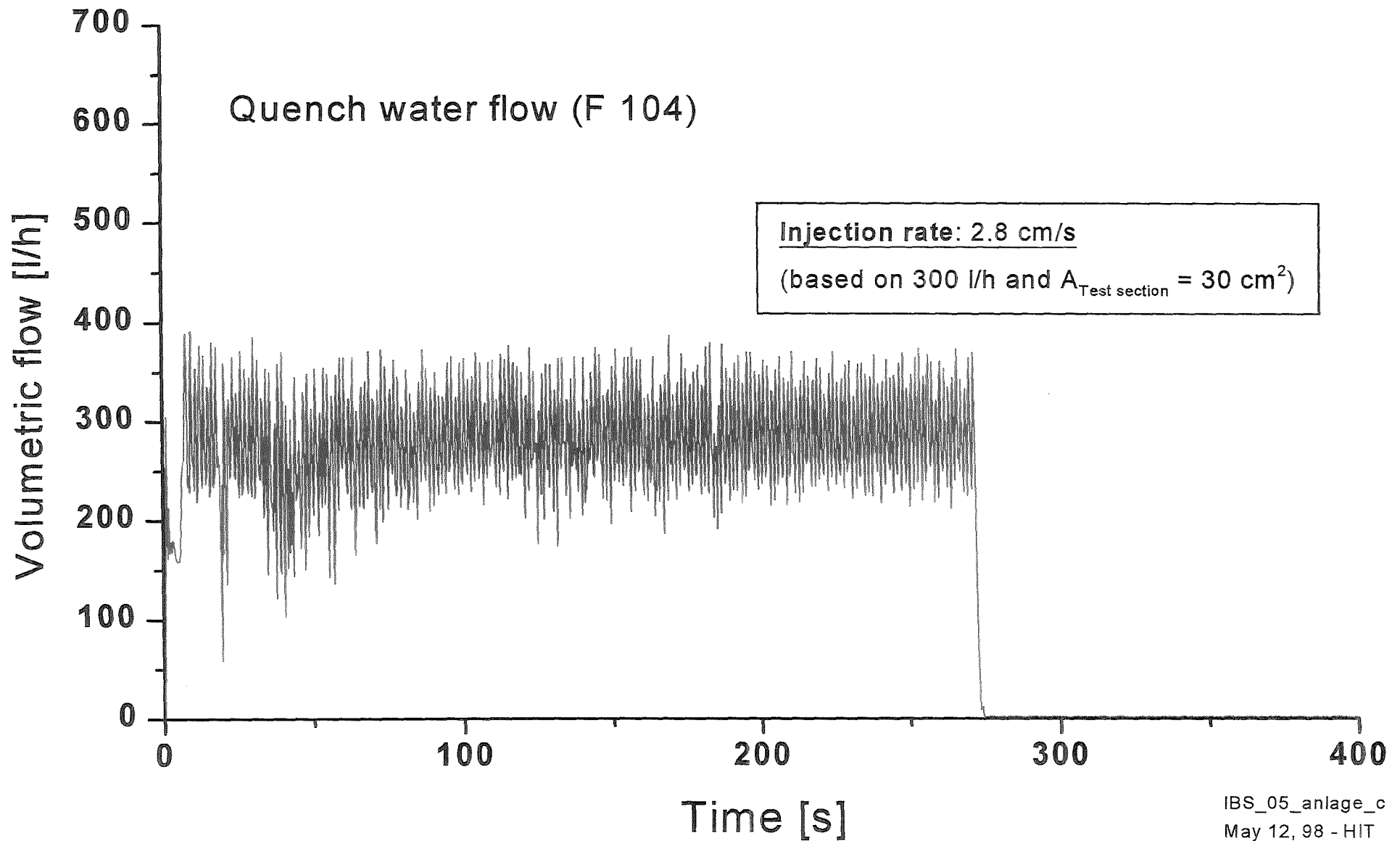


Fig. 21

Test IBS 05 - Quenching of the central rod at 570 and 950 mm

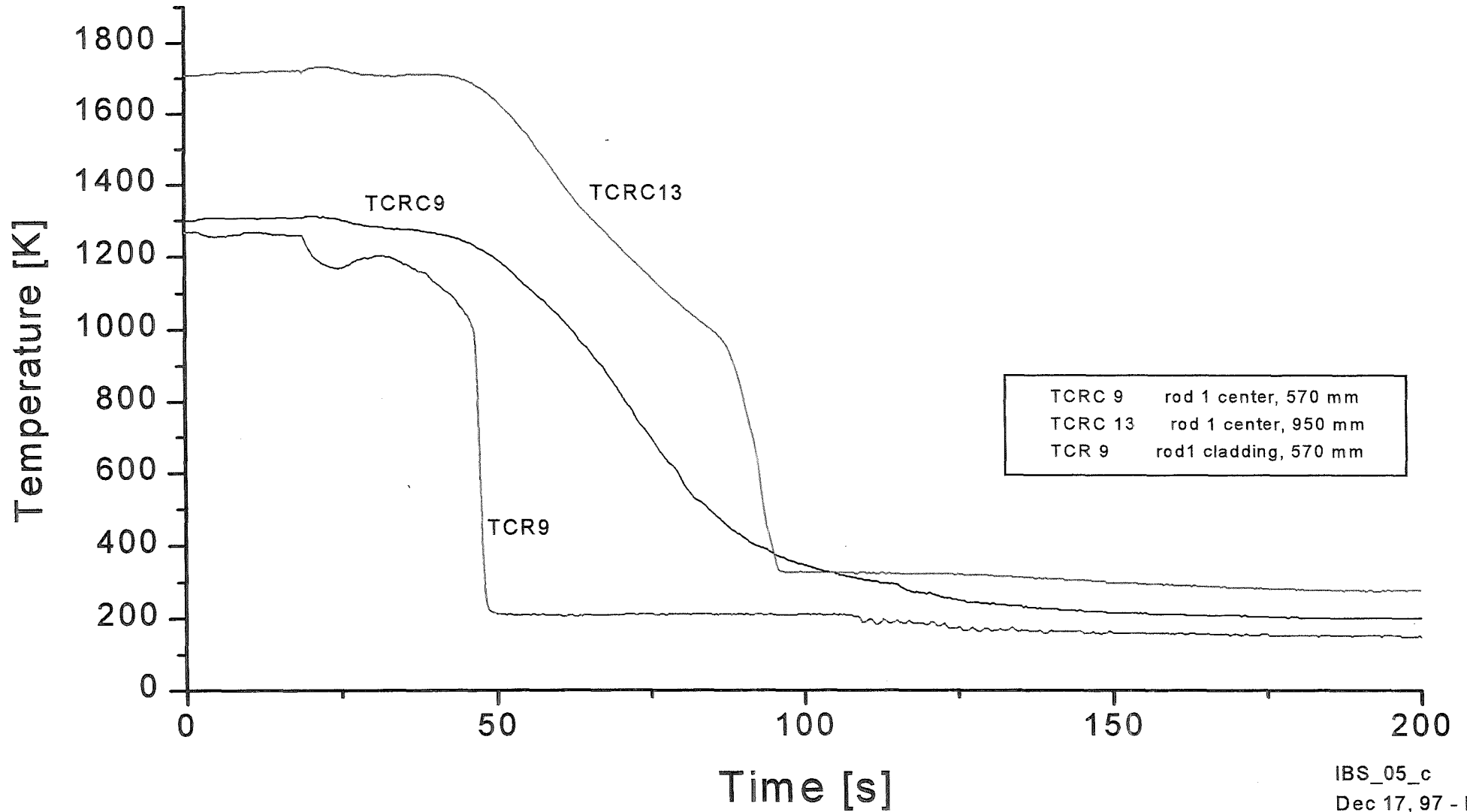


Fig. 22

Test IBS 05 - Quenching of rods 2, 4, 6 and 8 (rod type 2)

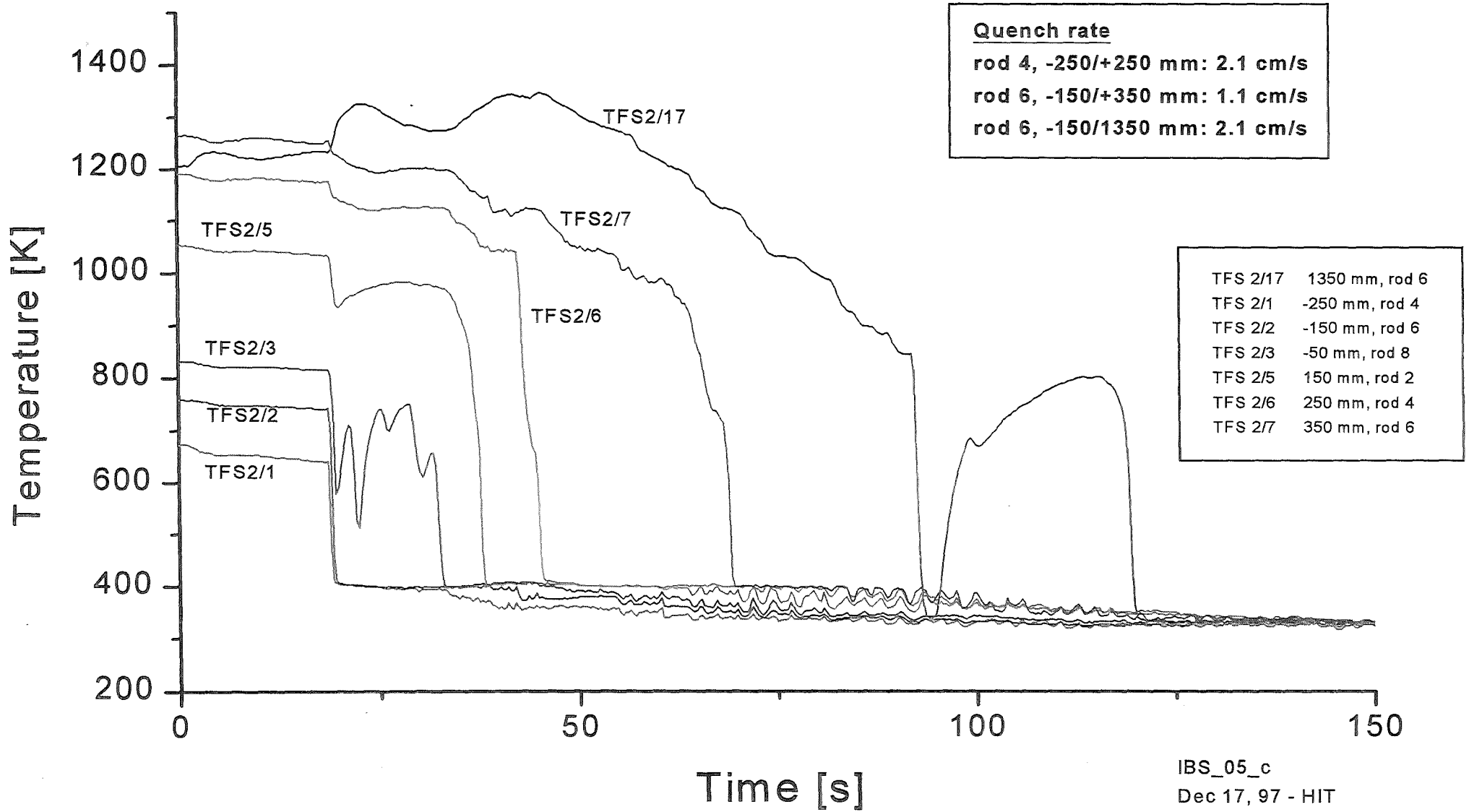


Fig. 23

Test IBS 05 - Quenching of rods 5 and 7 (rod type 3)

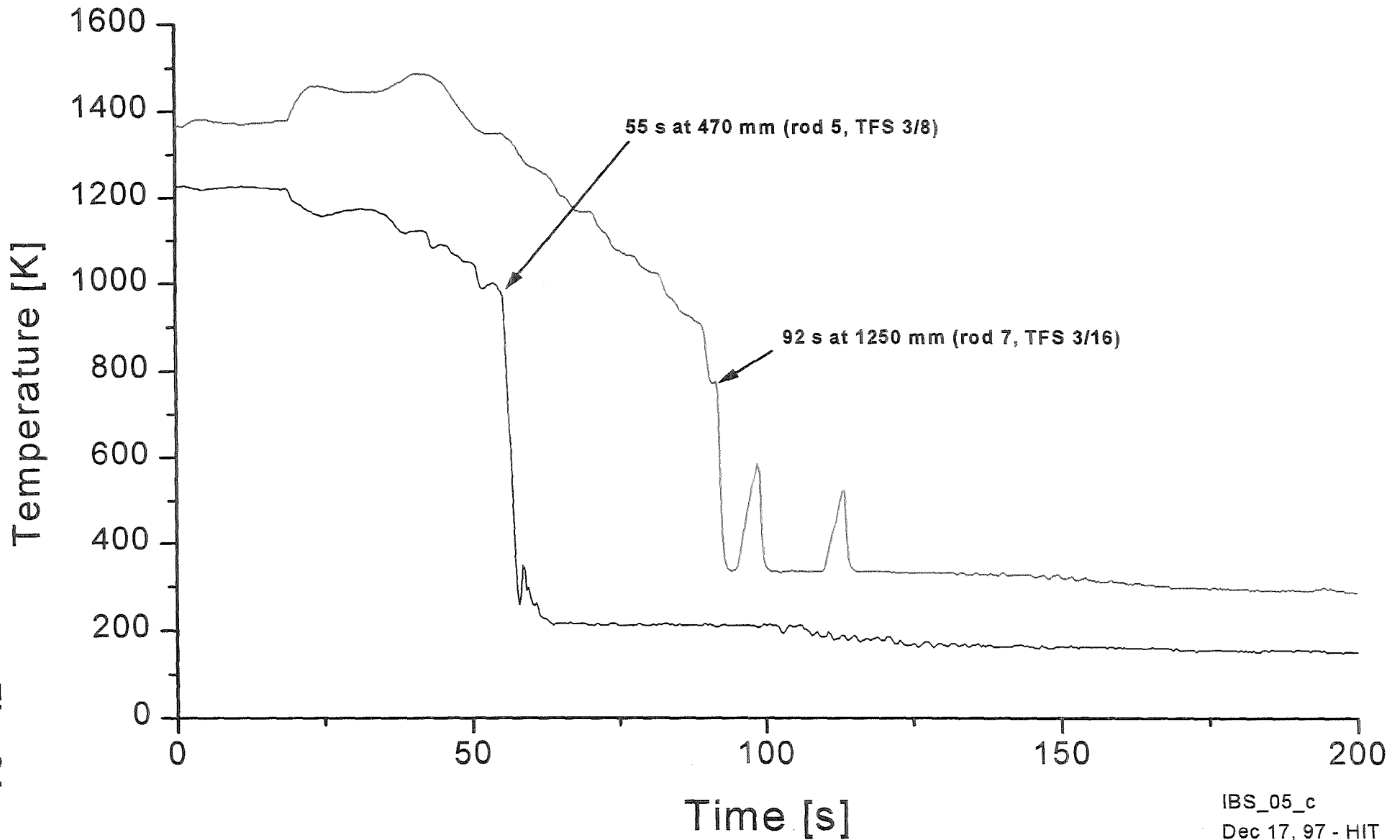


Fig. 24

Test IBS 05 - Quenching of rods 15, 16, 18, 19 and 21 (rod type 5)

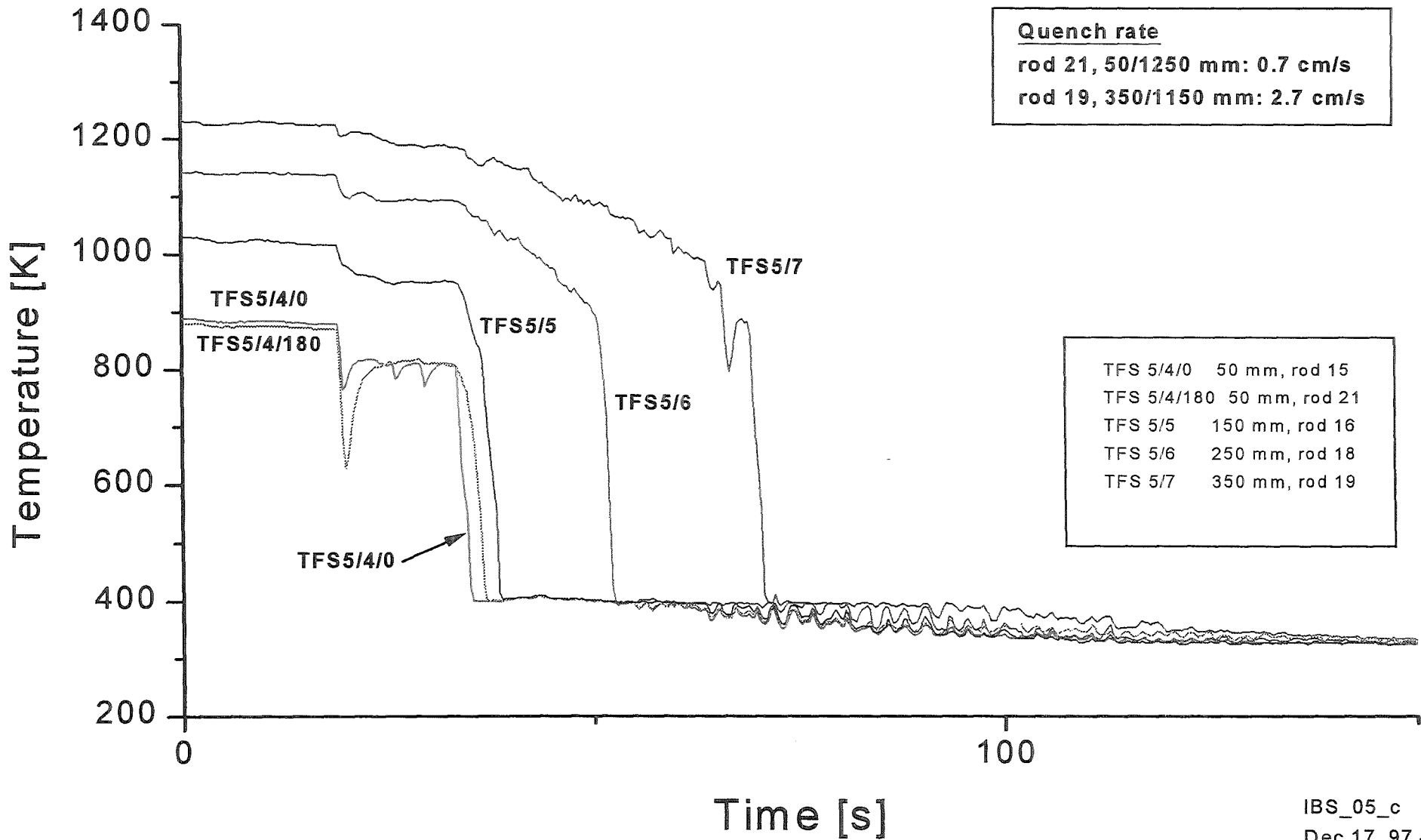


Fig. 25

Test IBS 05 - Quenching of rods 10, 12, 19 and 21 (rod type 5)

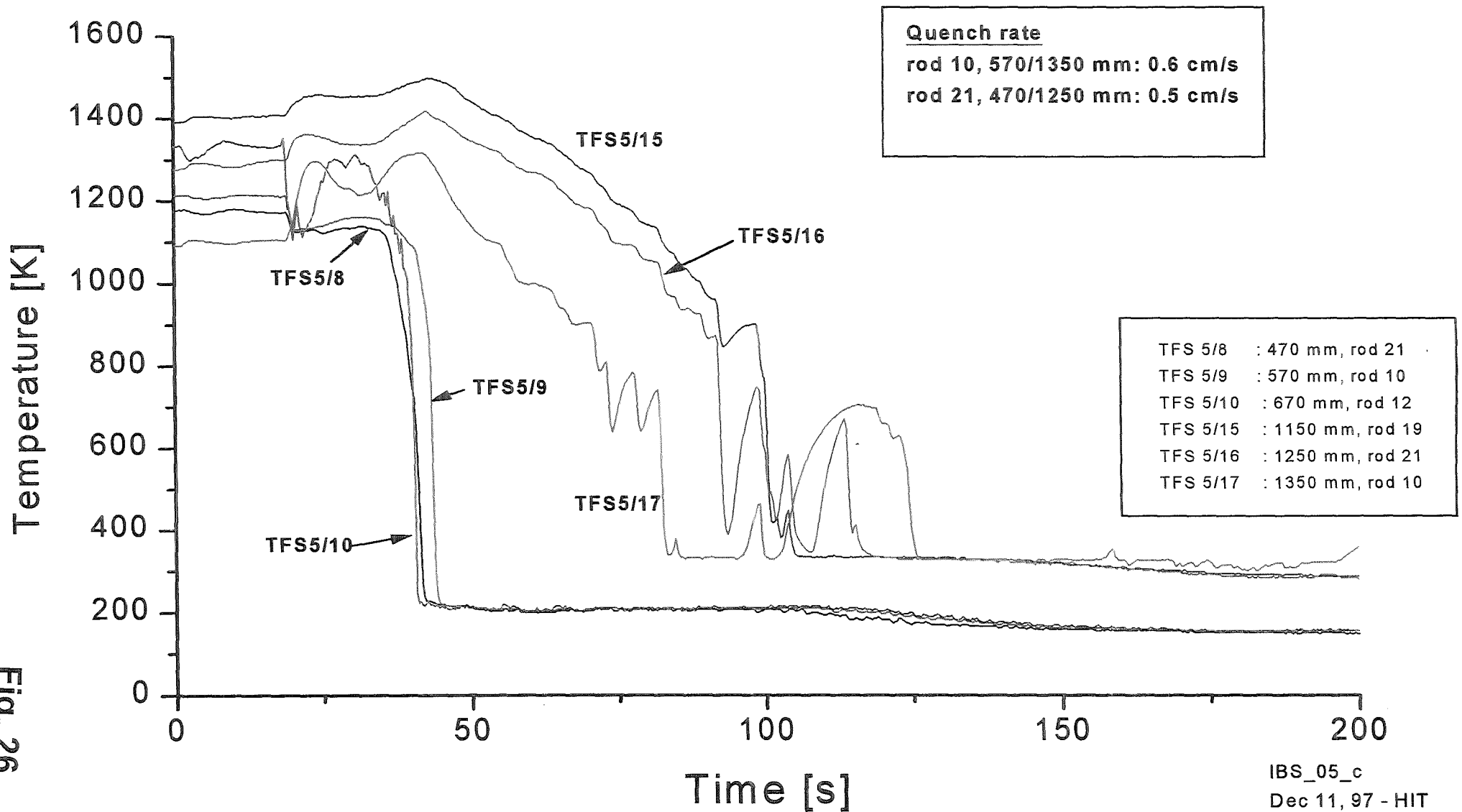
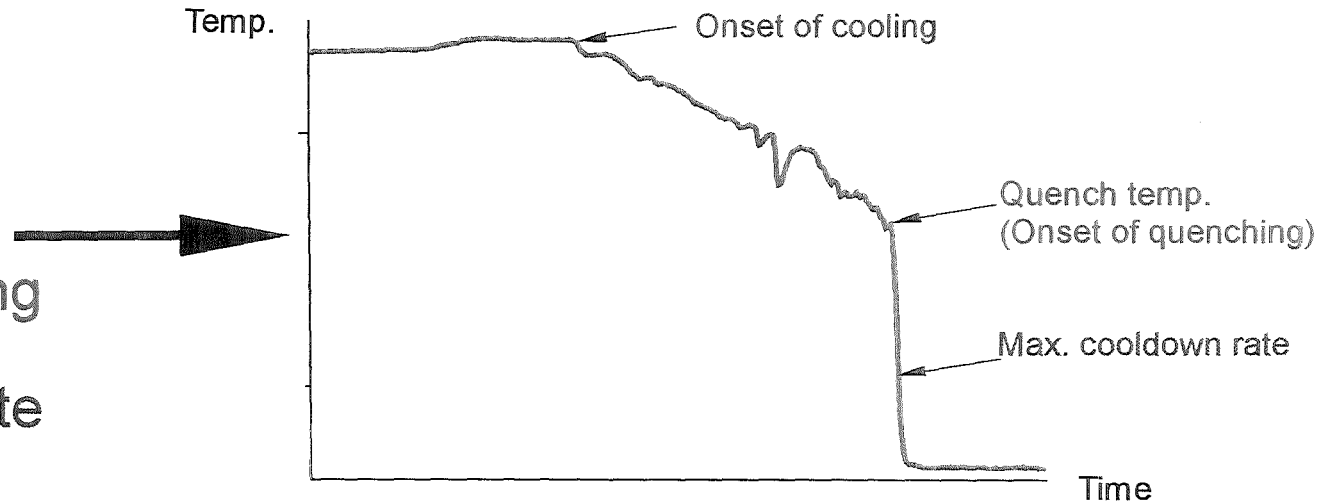


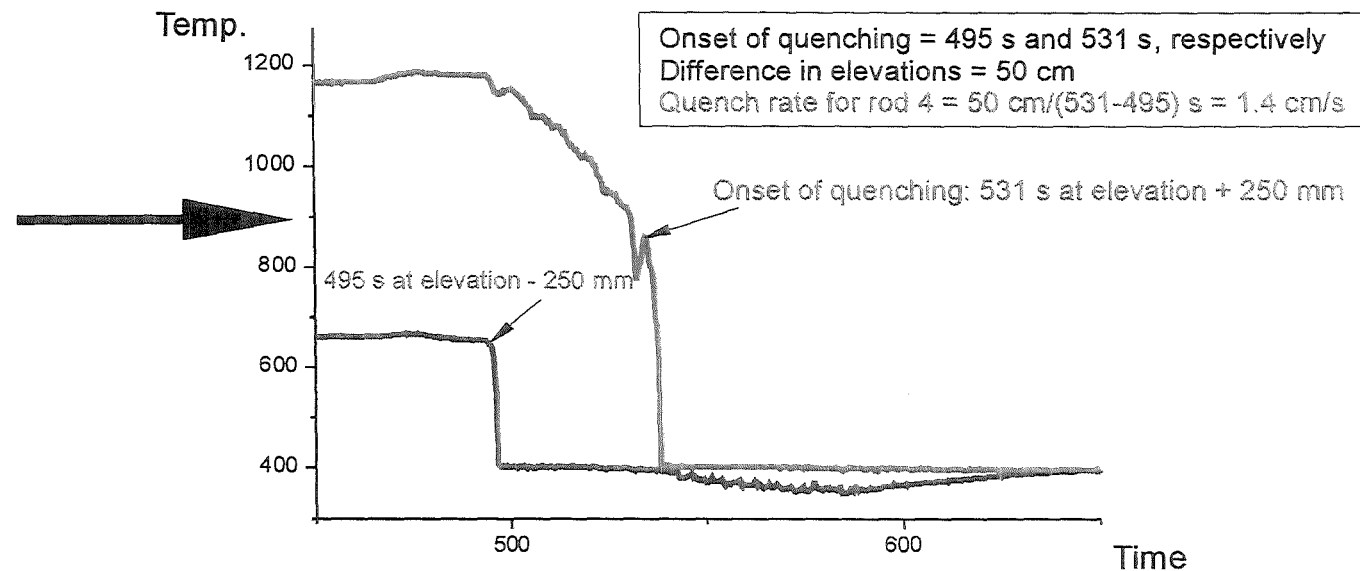
Fig. 26

Definitions

- Onset of cooling
- Onset of quenching
- Max. cooldown rate



- Quench rate



- Injection rate = Quench water flow entering the bottom of the test section determined by quench pump rate
- Flooding rate = Injection rate minus water evaporation in the test section; function of elevation

QUENCH Test IBS_05 (Oct. 16, 1997) - Quenching Phase

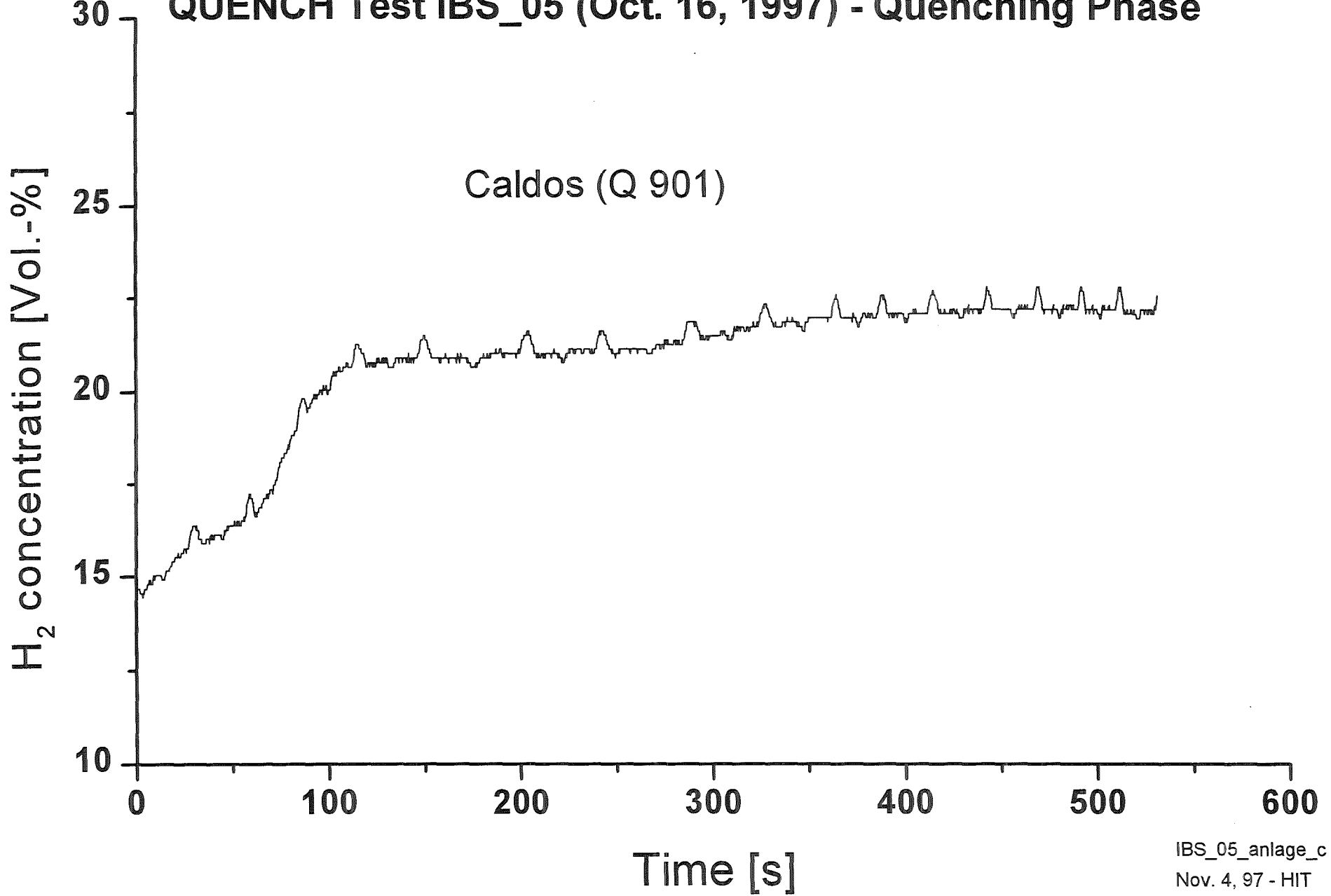


Fig. 28

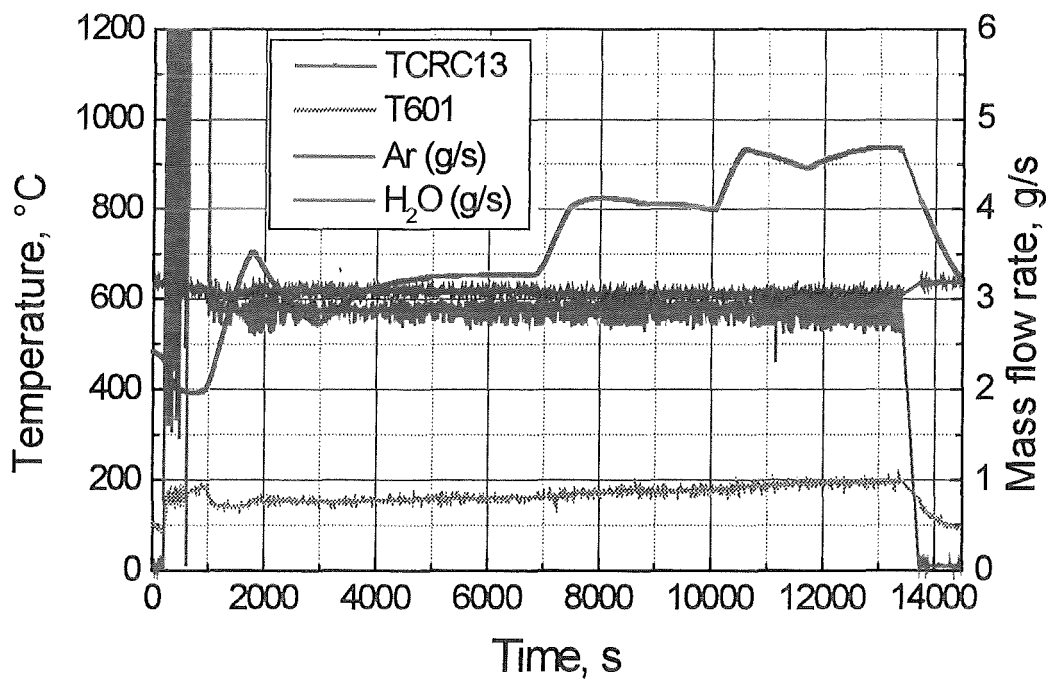
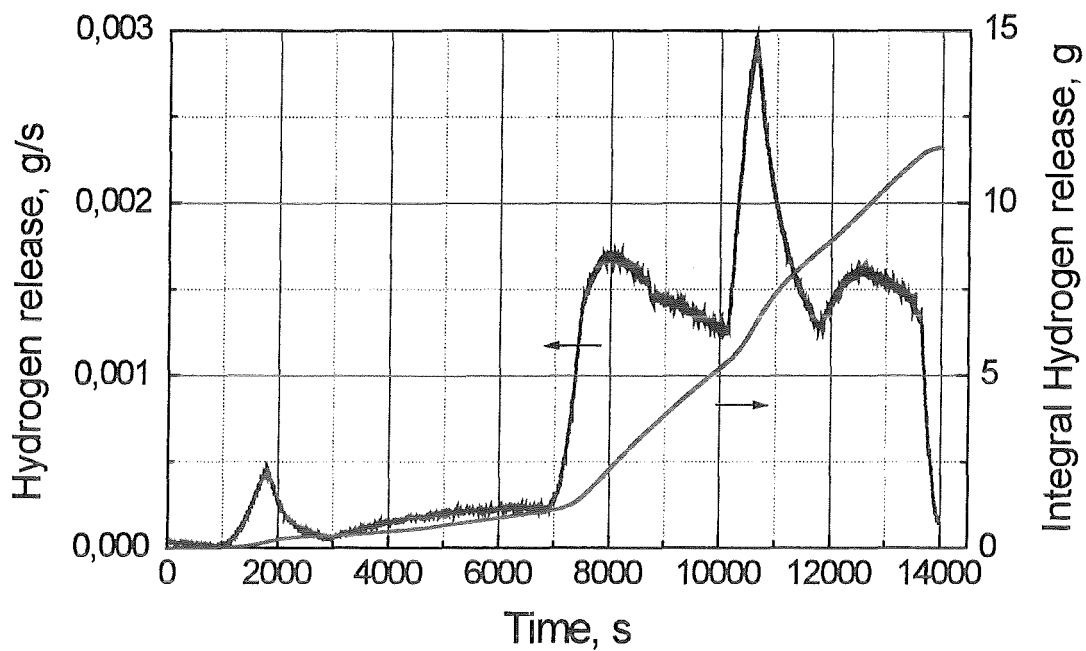


Fig. 29: Hydrogen release (lower diagram) and pertinent data of the facility (upper diagram) during IBS_03

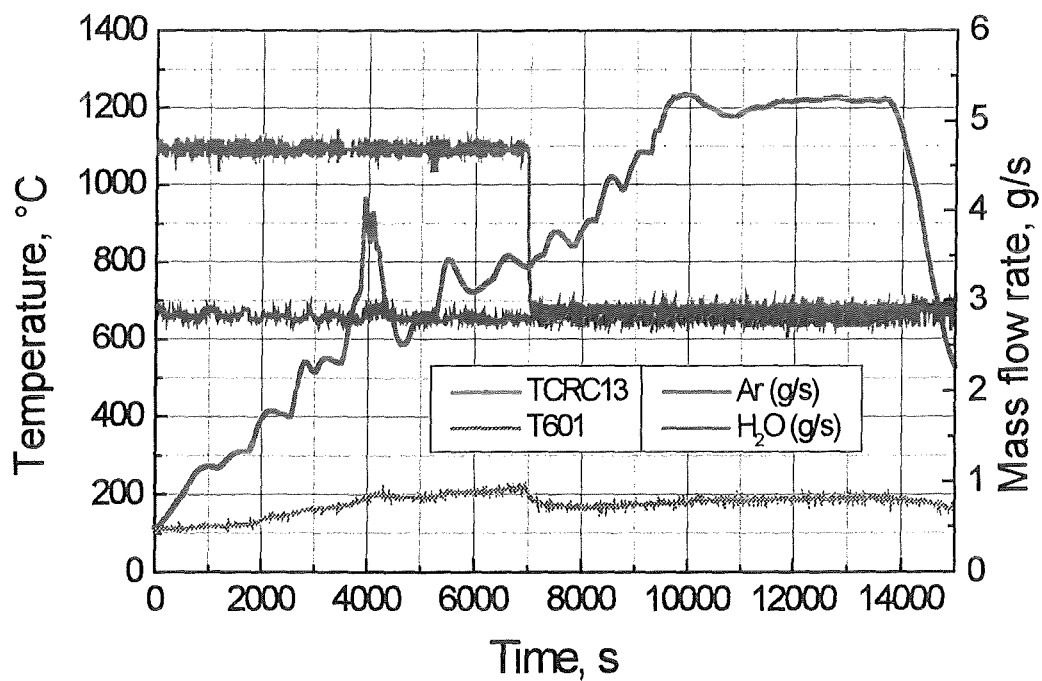
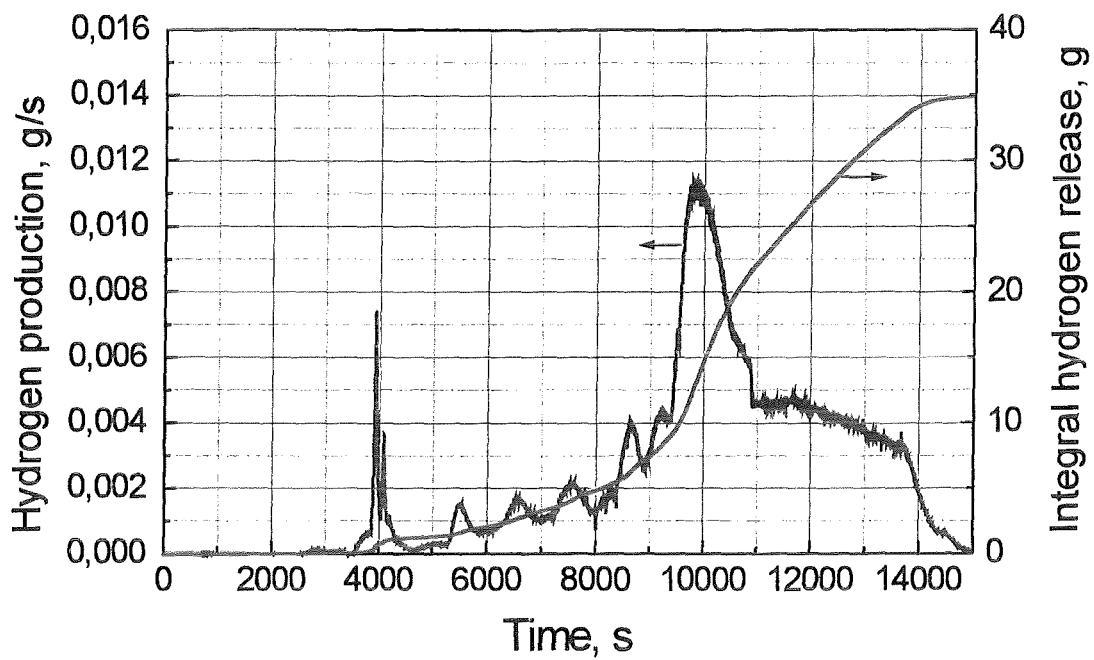


Fig. 30: Hydrogen release (upper diagram) and data of the facility (lower diagram) during IBS_04

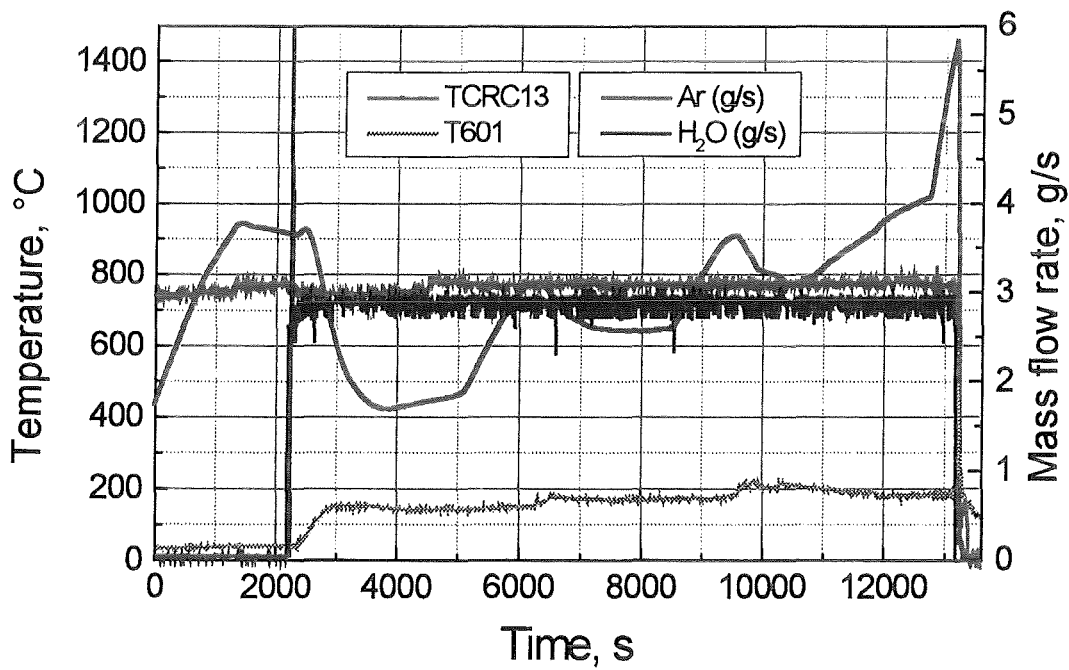
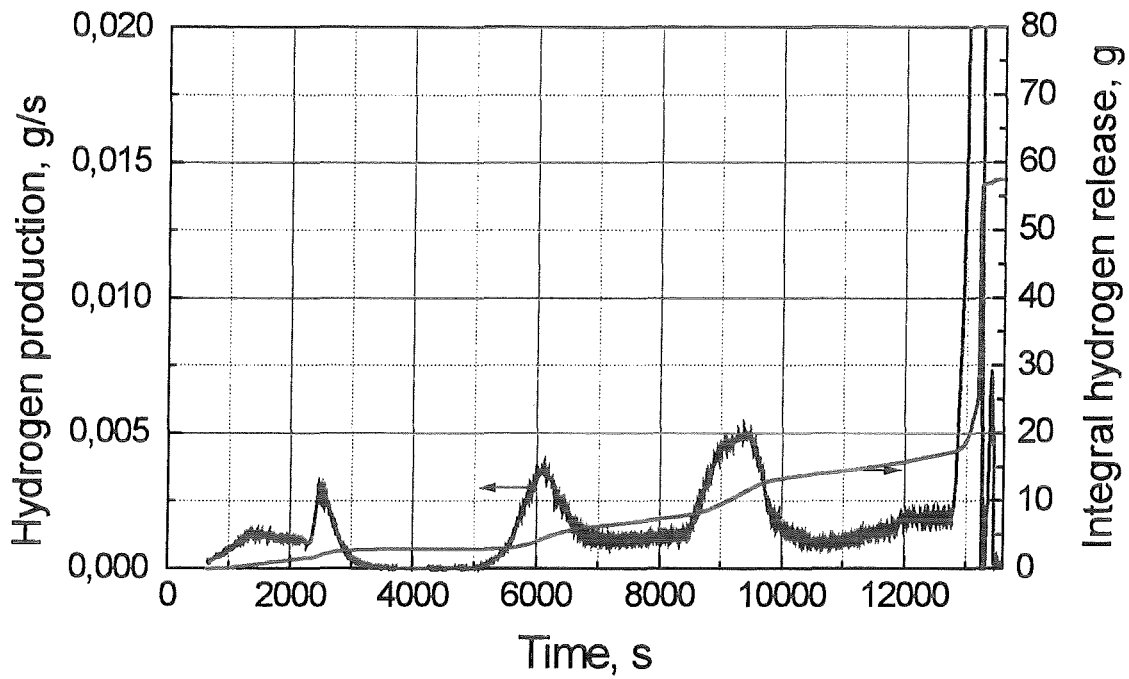


Fig. 31: Hydrogen release (upper diagram) and data of the facility (lower diagram) during IBS_05

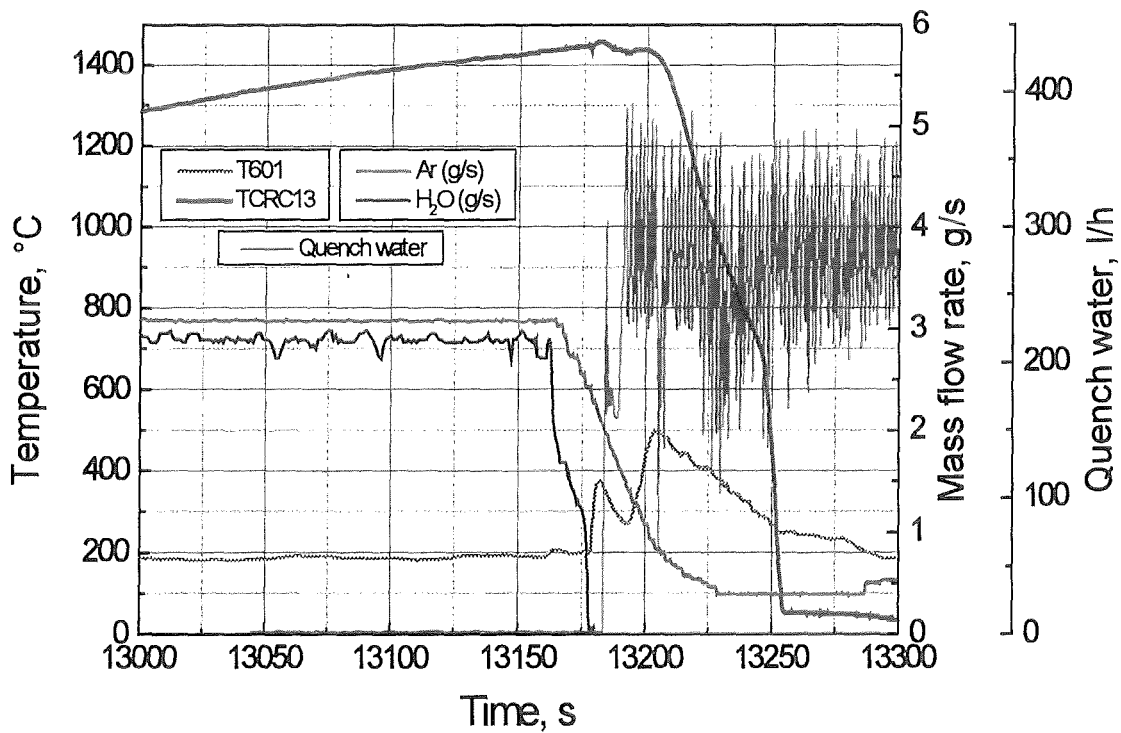
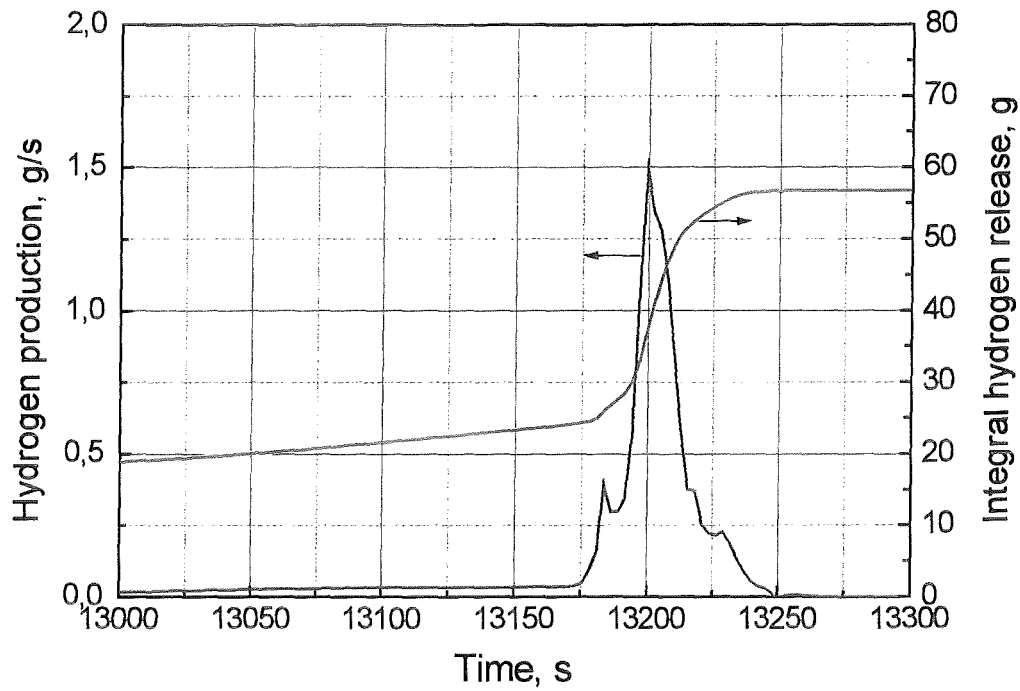


Fig. 32: Hydrogen release (upper diagram) and data of the facility (lower diagram) during the IBS_05 quench phase

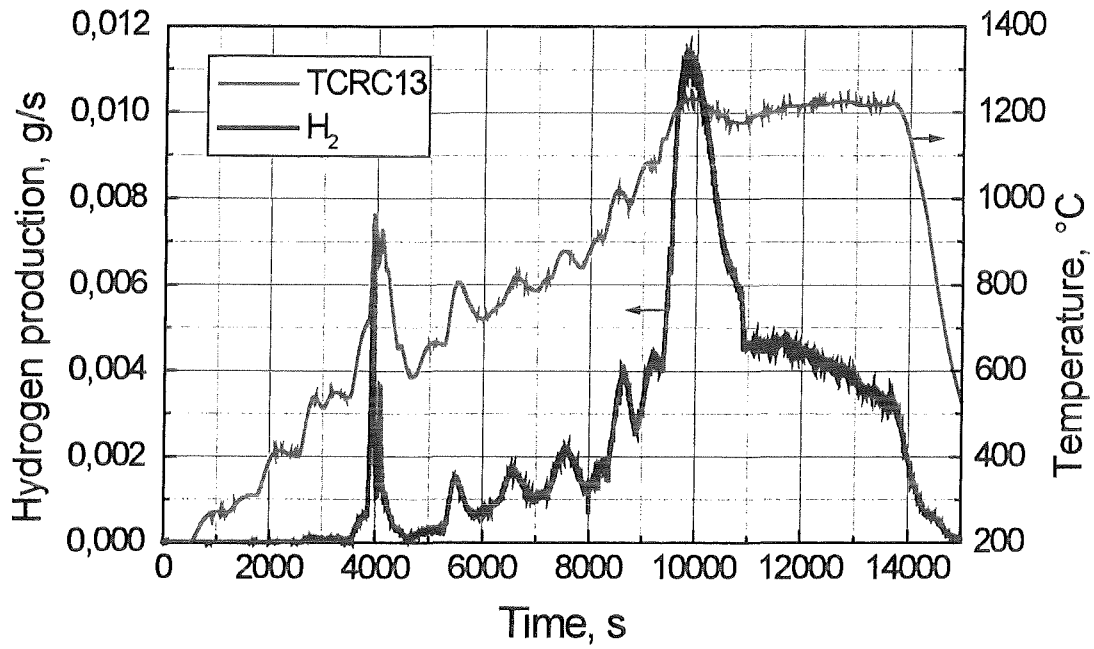


Fig. 33: Hydrogen release and central temperature at elevation 950 mm during IBS_04

Mass spectrometer sampling position at the off-gas pipe

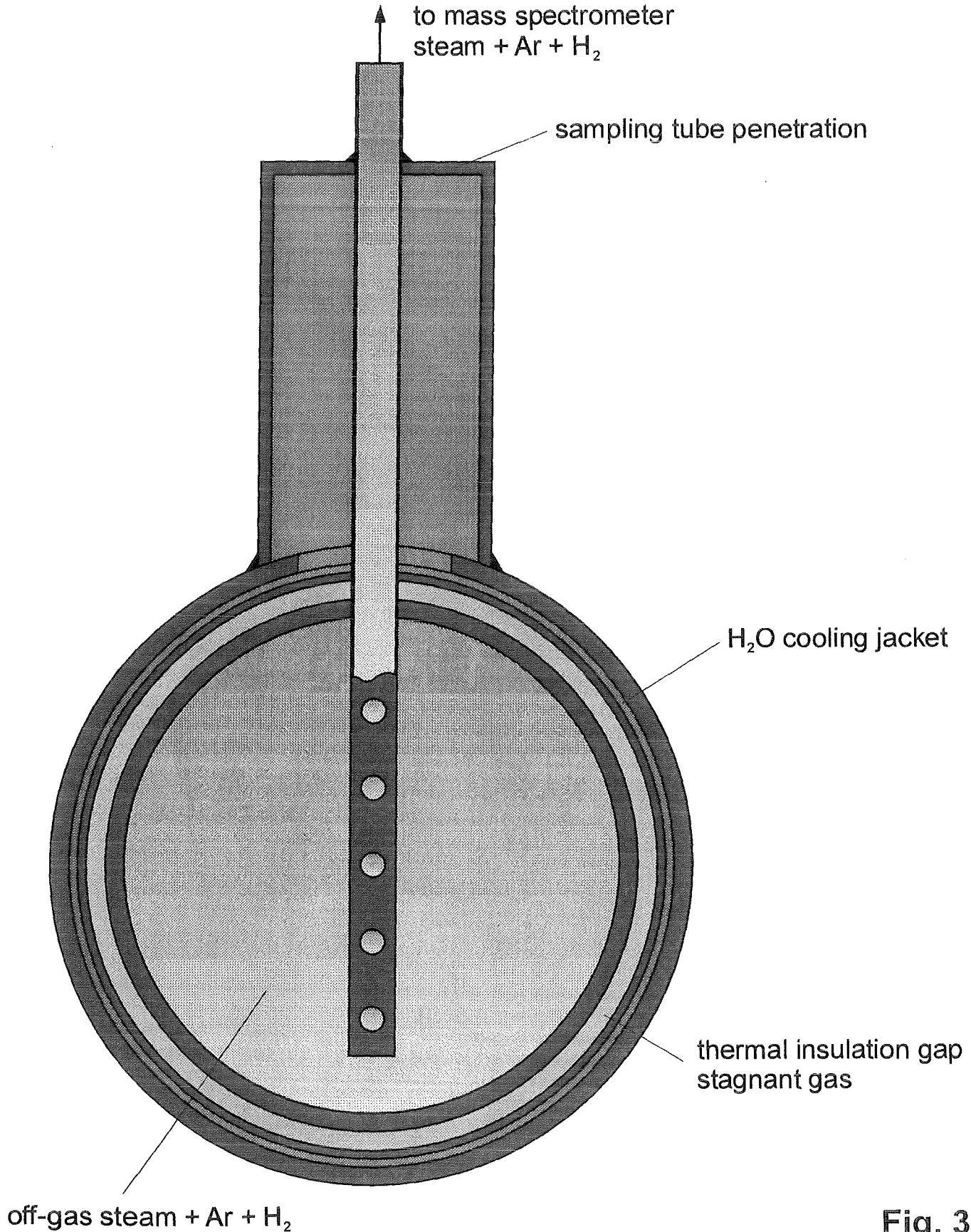
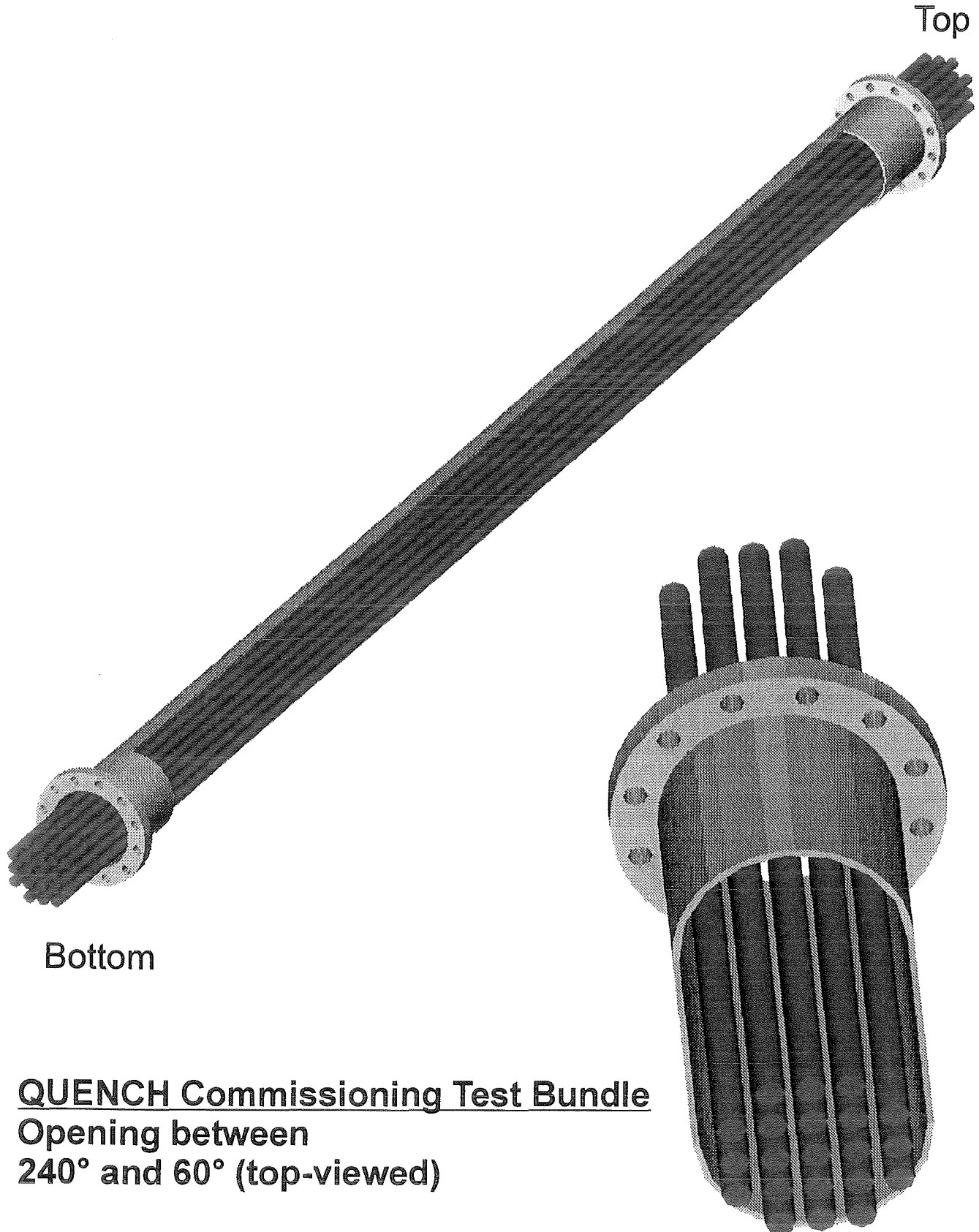


Fig. 34

Cut-out of an Observation Window at the Shroud, Schematic



QUENCH Commissioning Test Bundle
Opening between
240° and 60° (top-viewed)

Fig. 35

QUENCH Commissioning Tests

Bundle after opening the shroud

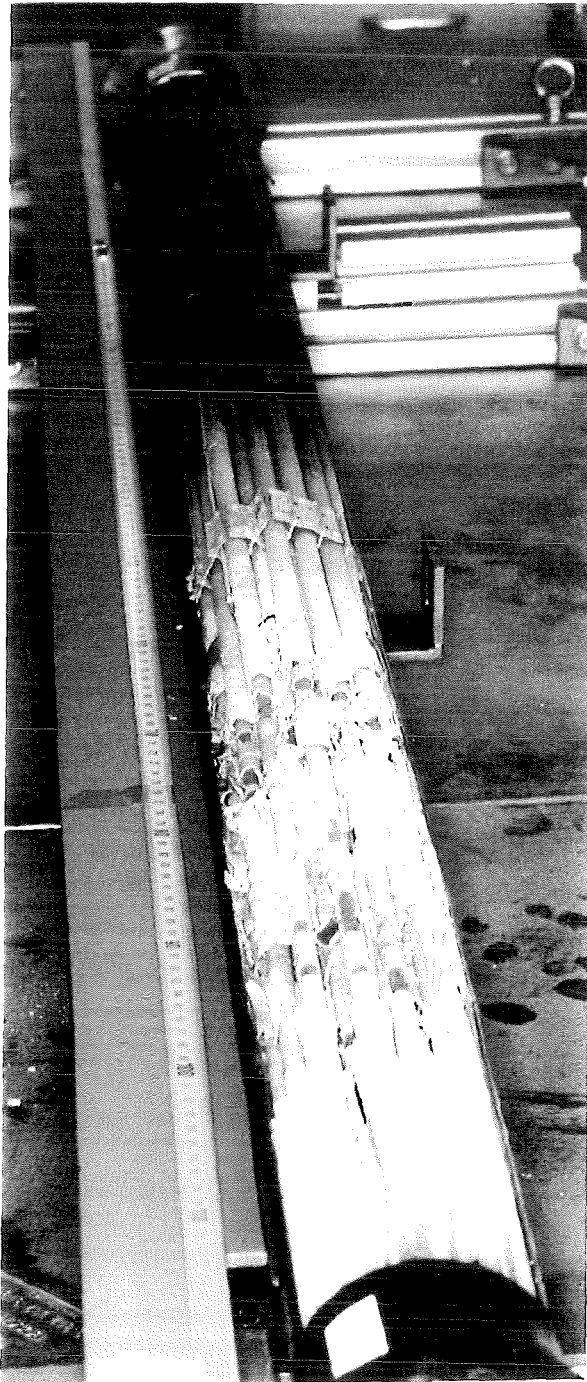


Fig. 36

QUENCH Commissioning Tests
Posttest view of the bundle



Fig. 37

QUENCH Commissioning Tests
Bulging of the shroud at 900 mm elevation



Max. shroud temp.: 1600 K at 850/950 mm

Max. deformation: 90/84.76 mm

Fig. 38

QUENCH Commissioning Tests

Shroud at 700 - 900 mm elevation (Pre-test)

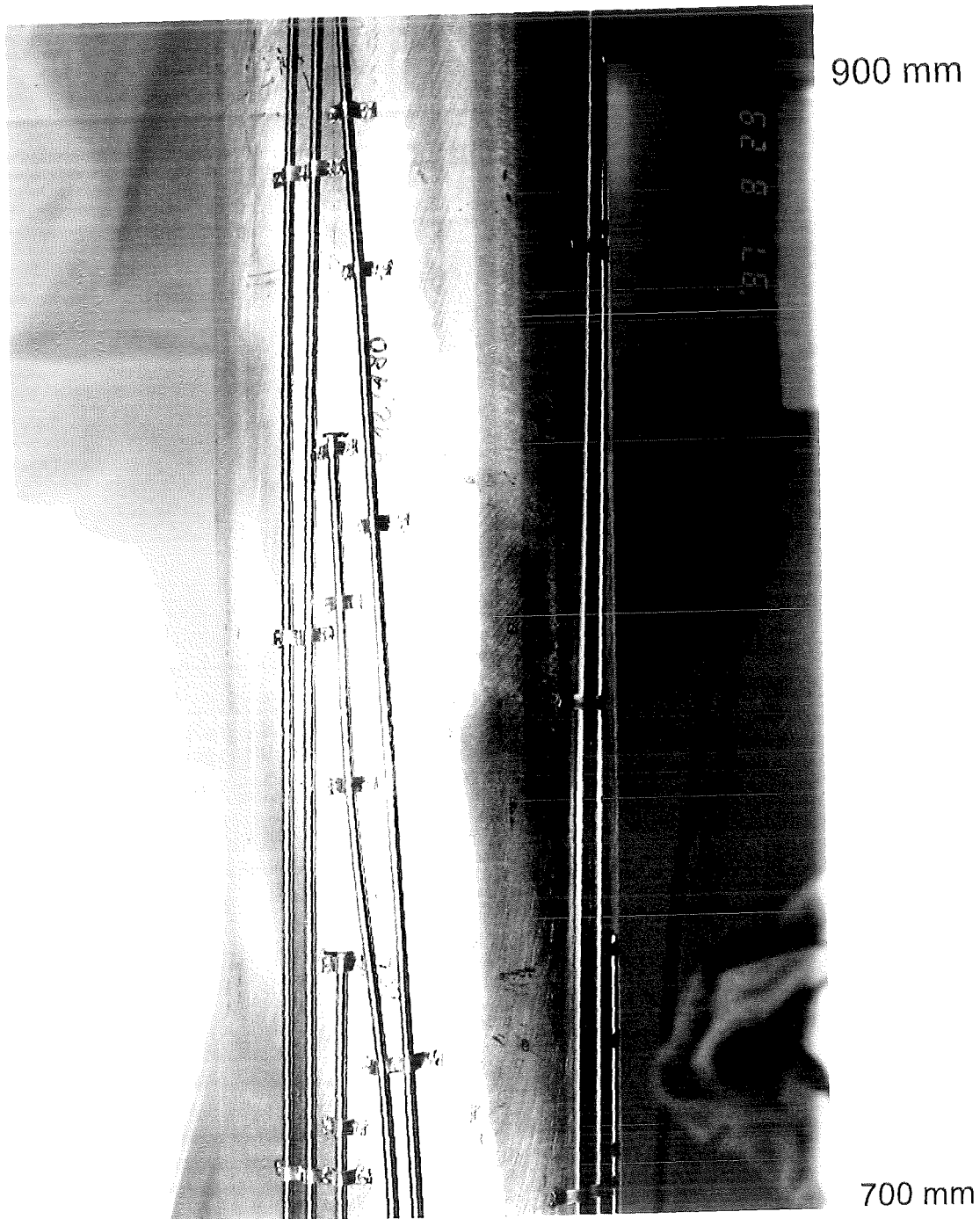


Fig. 39

QUENCH Commissioning Tests

Debris at the front end of the off-gas pipe
after removal of the test section



Fig. 40

Oxide layer thickness of a removed oxidation calibration rod

Commissioning tests performed in October 1997

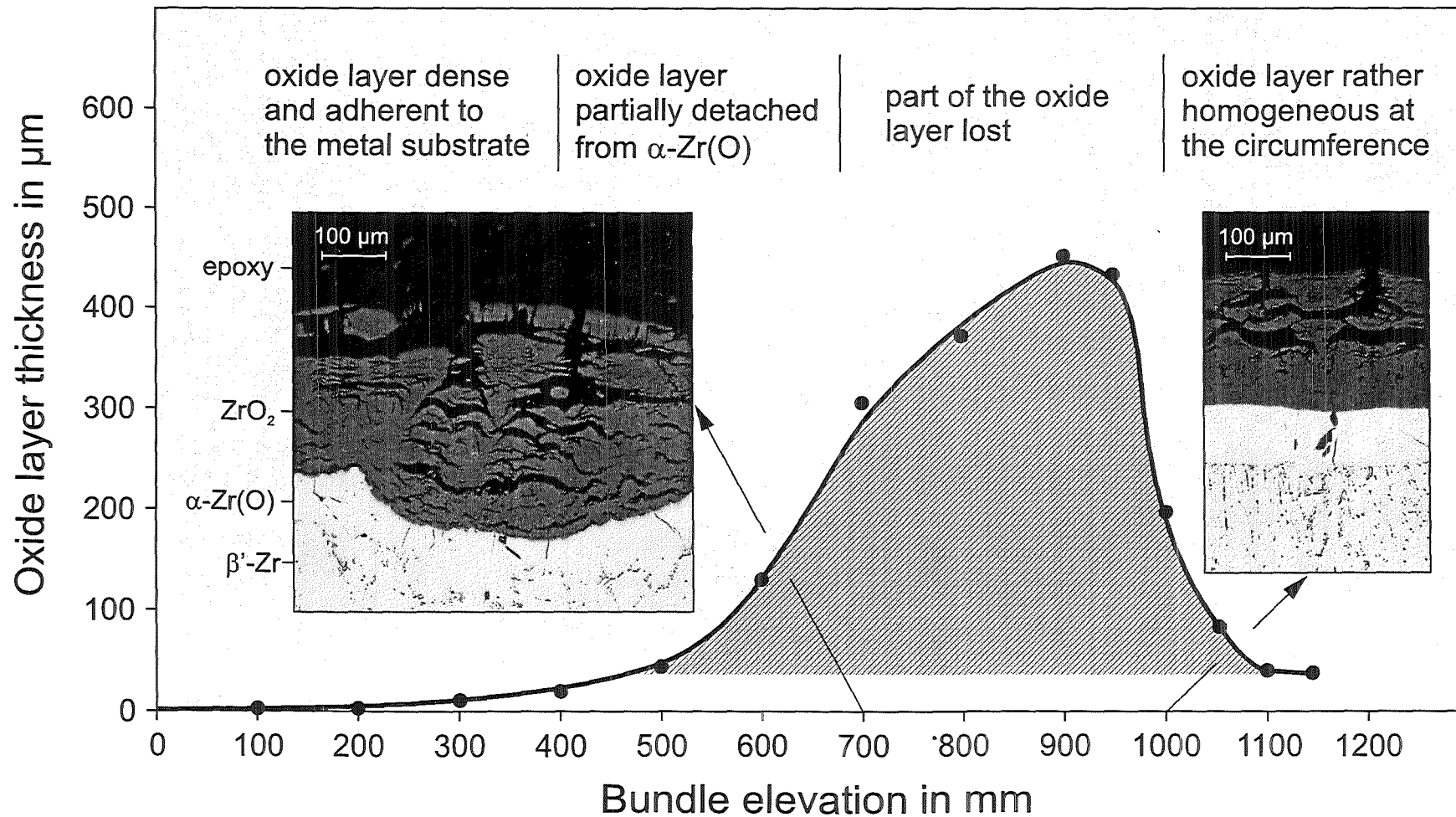
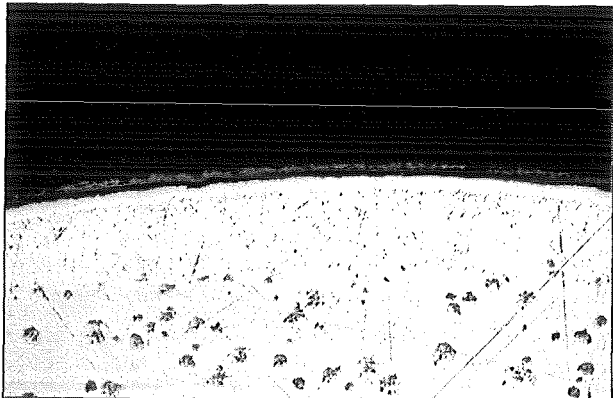
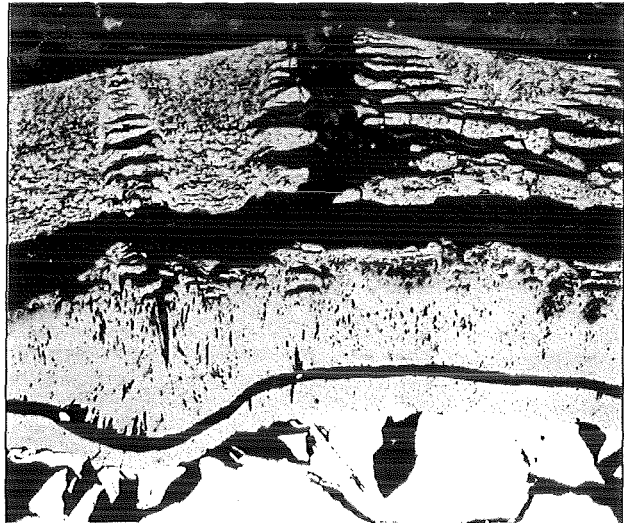


Fig. 41

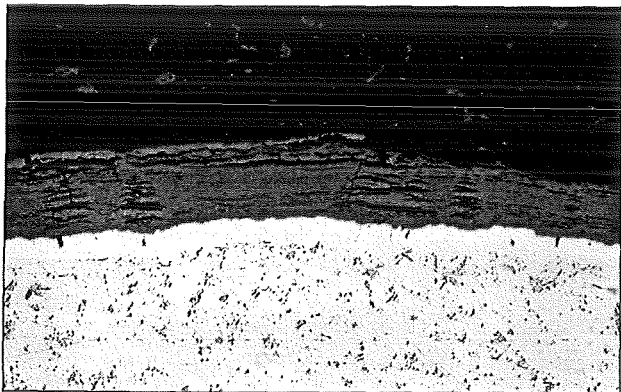
100μm



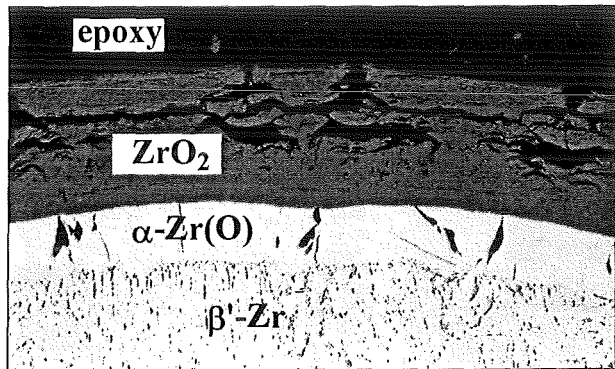
axial bundle elevation: 500 mm



900 mm



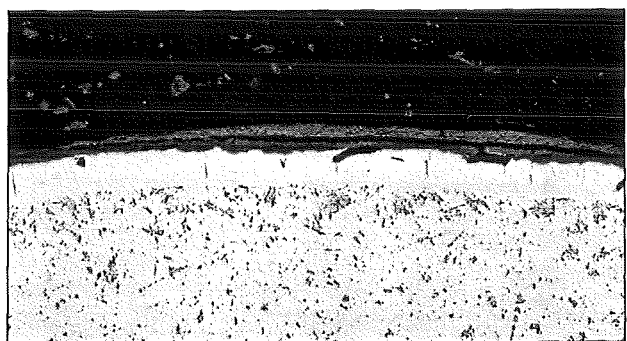
600 mm



1000 mm



700 mm



1100 mm

Oxide layer thickness of a removed oxidation calibration rod at different bundle elevations

QUENCH Commissioning Tests

Hydrogen absorbed in cladding tube #13
and oxide thickness after quenching

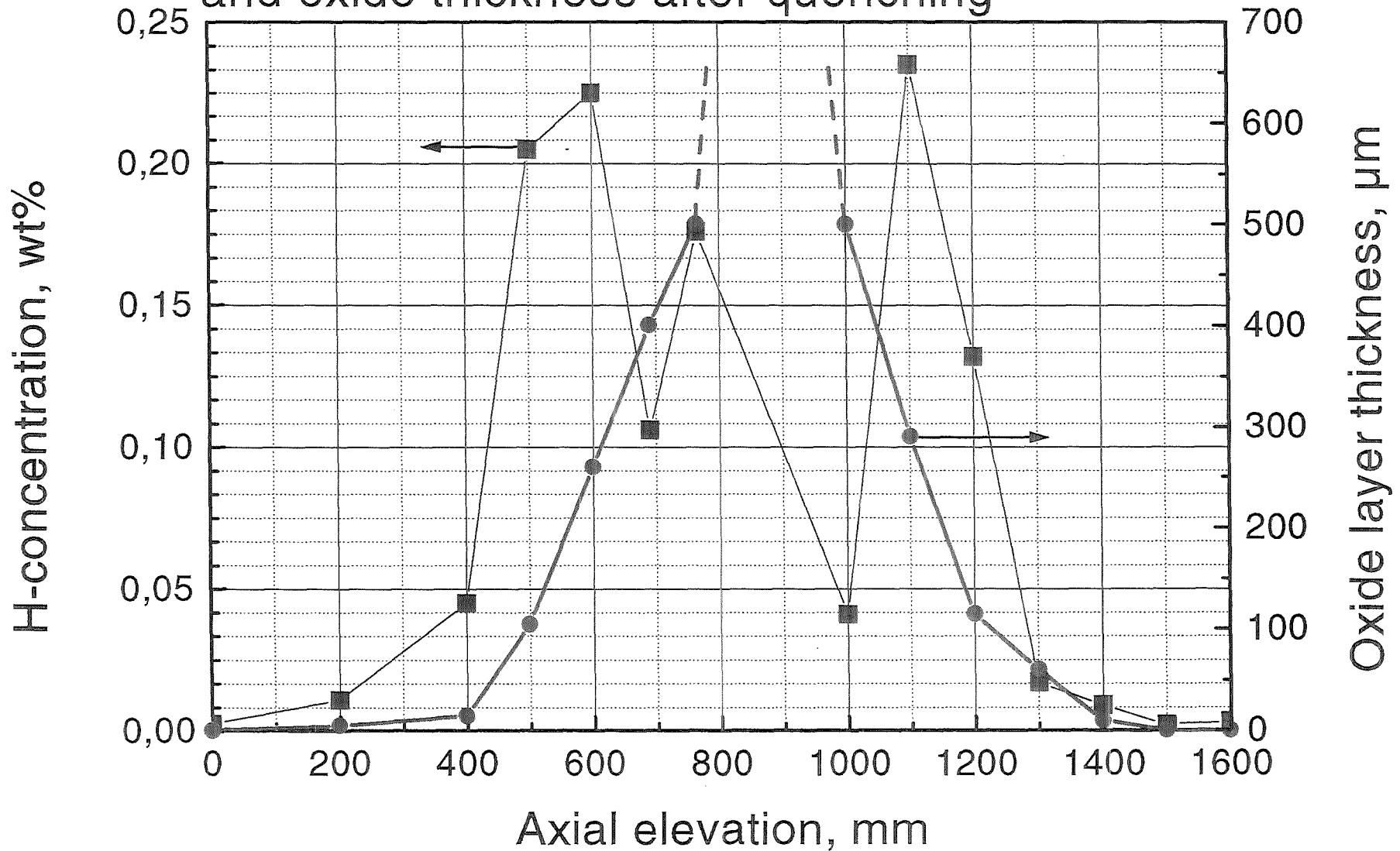


Fig. 43

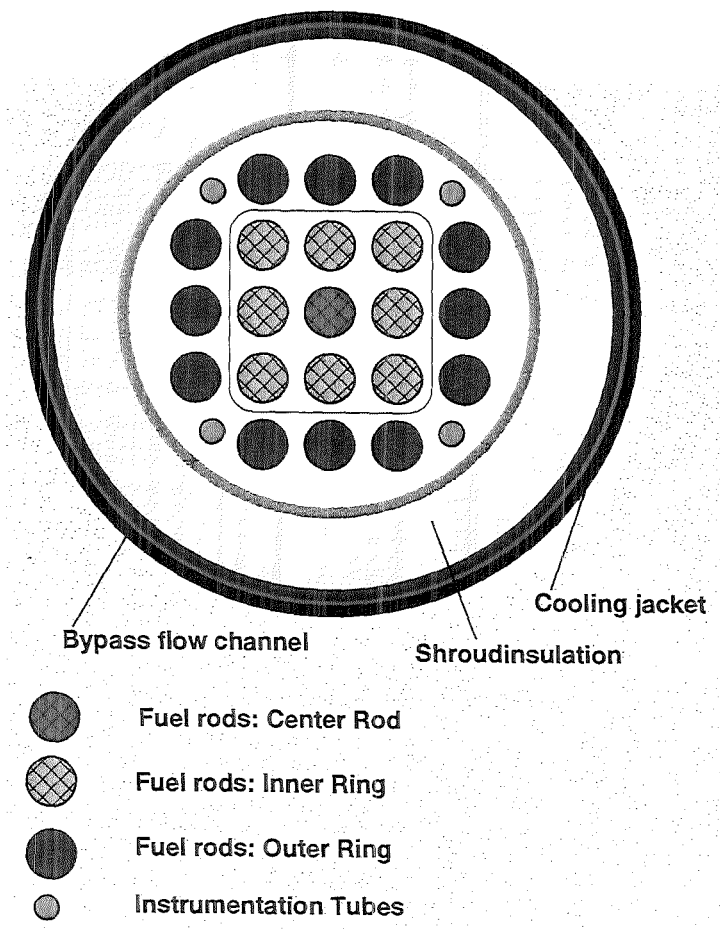
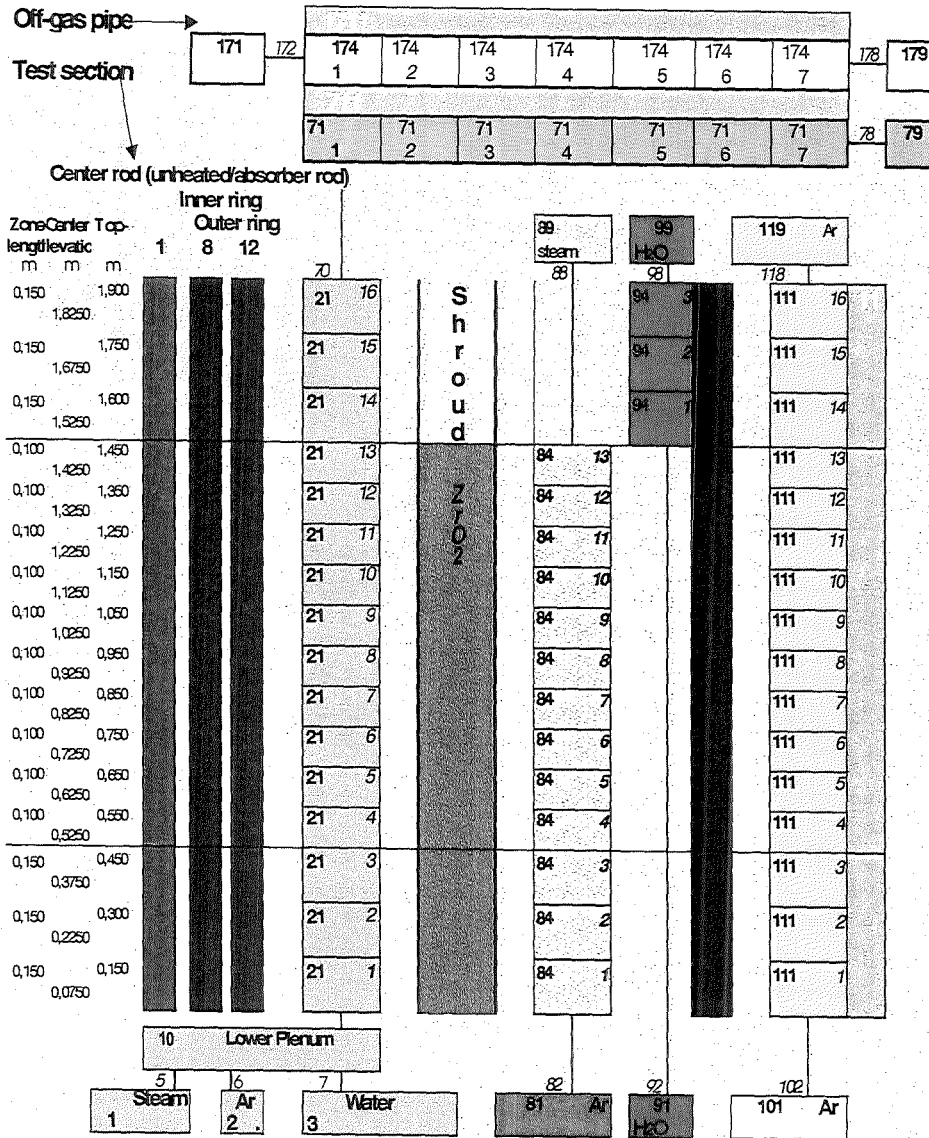


Fig. 44

QUENCH qnch2f14

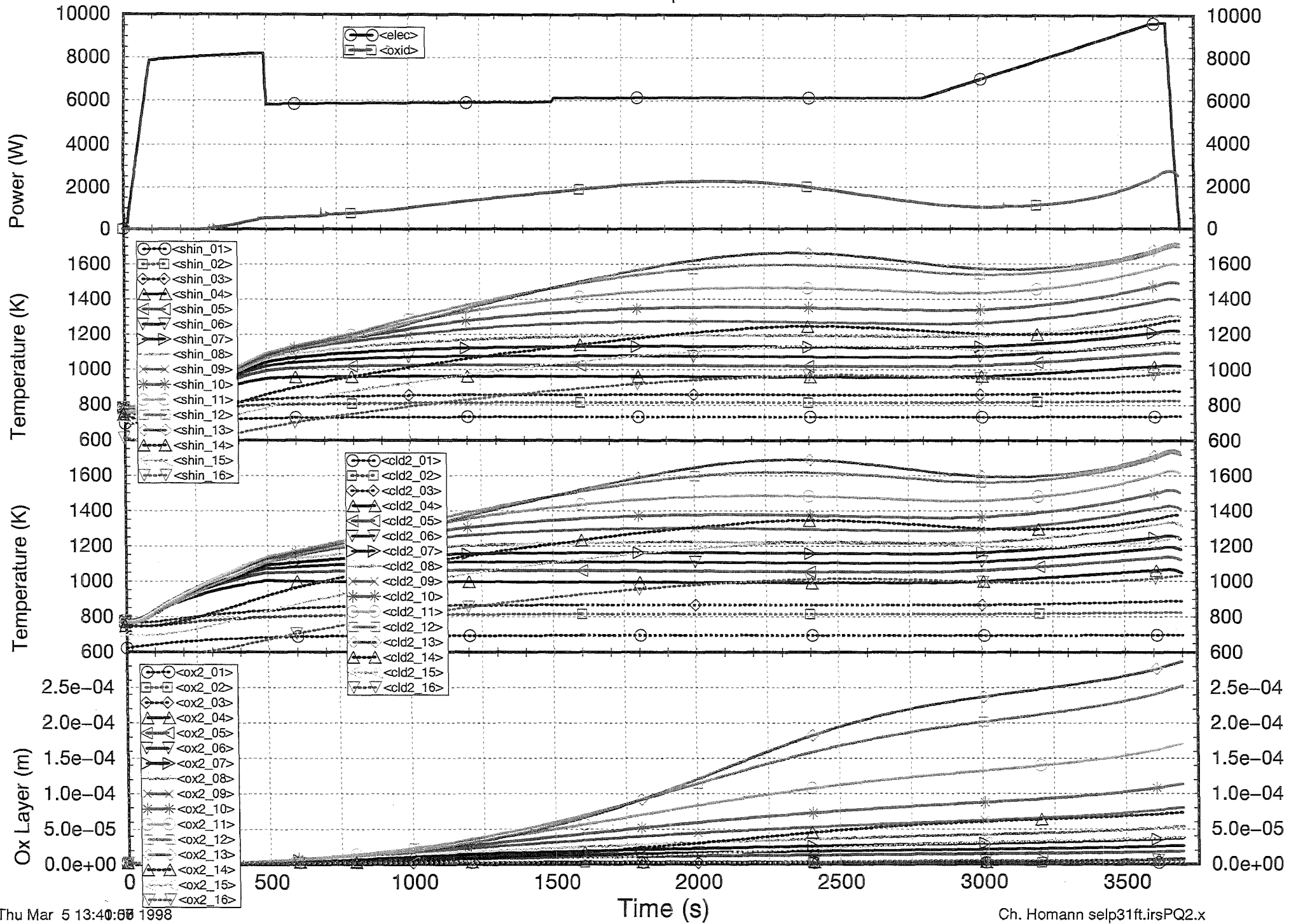


Fig. 45

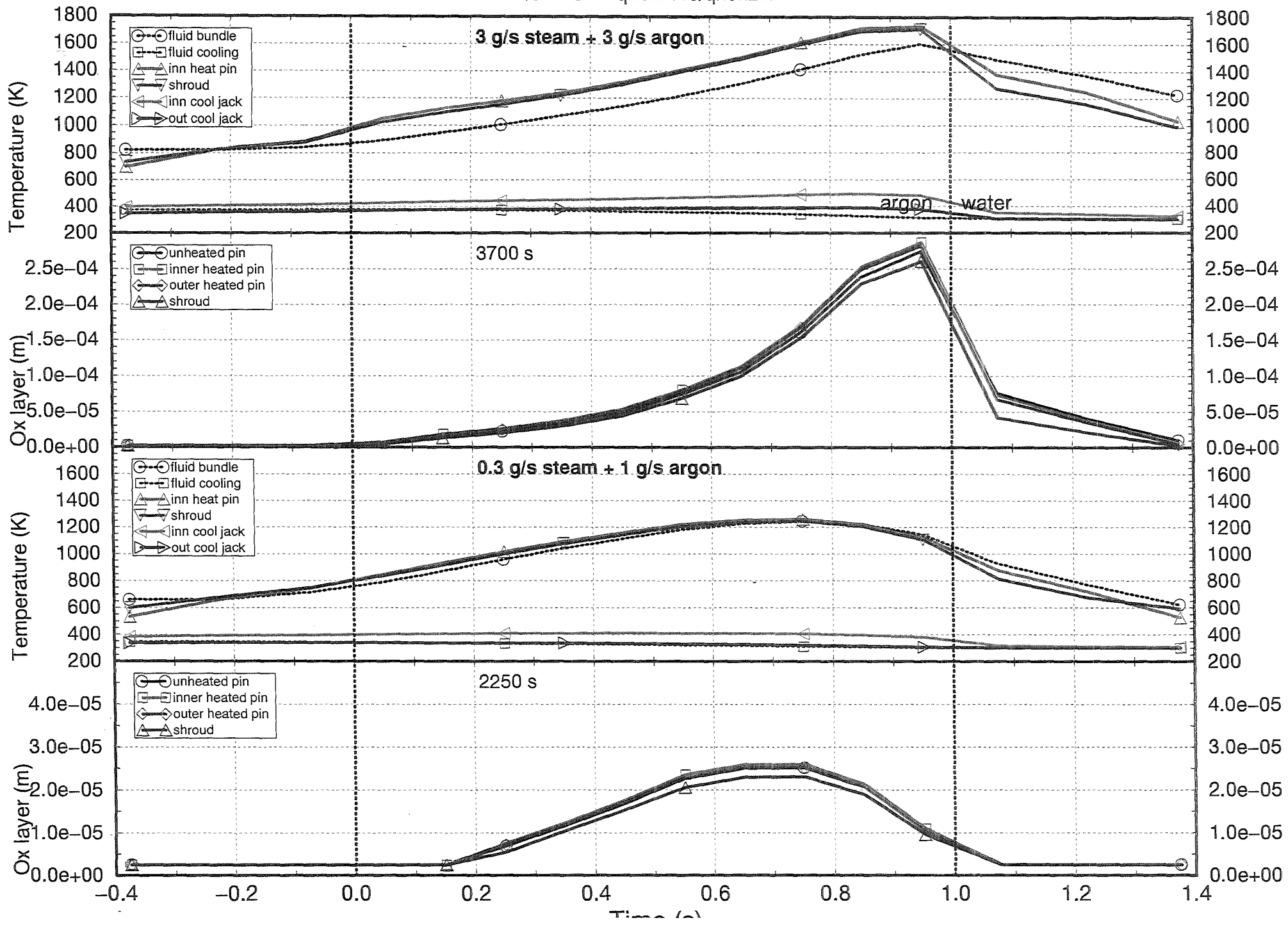


Fig. 46

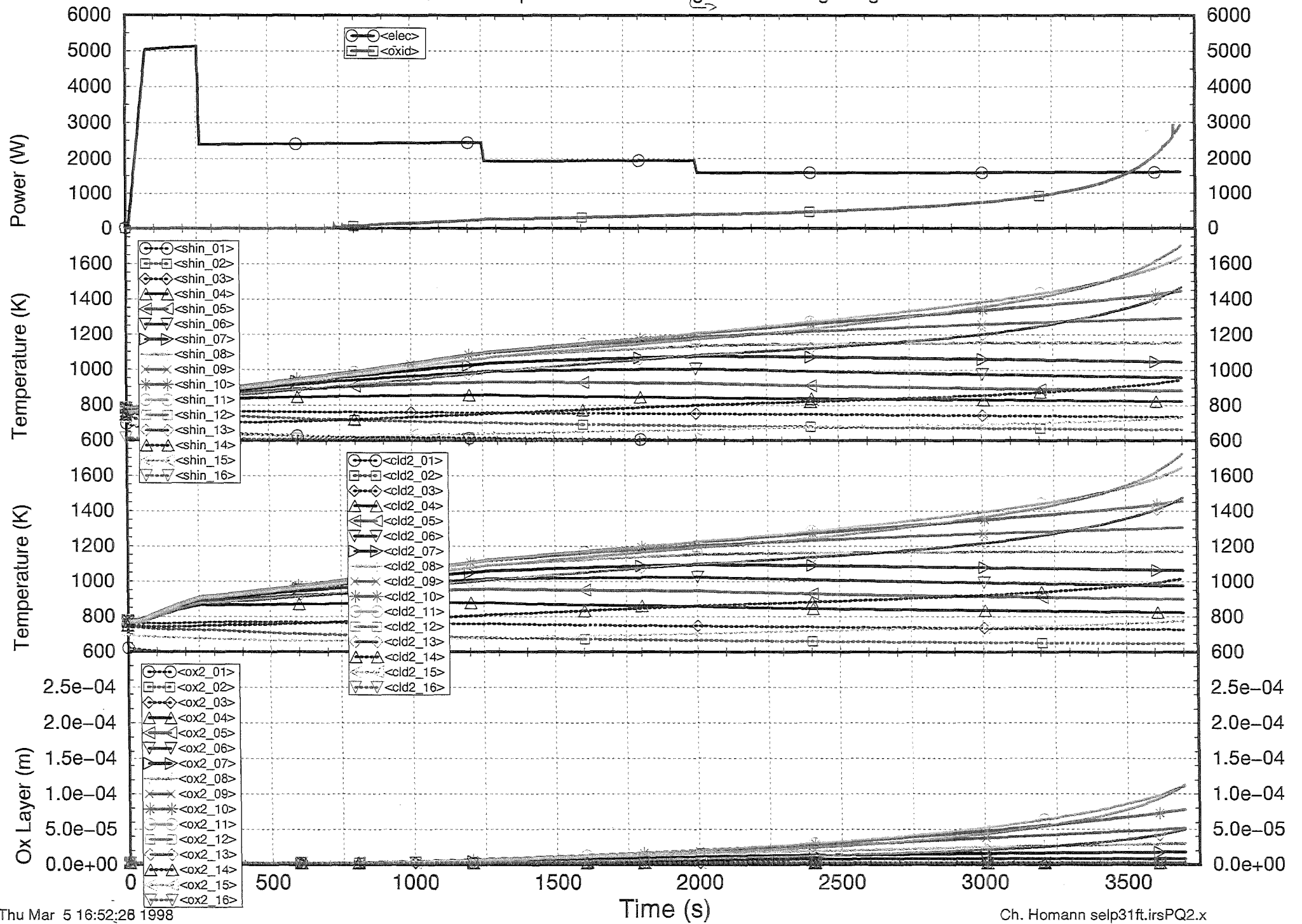


Fig. 47

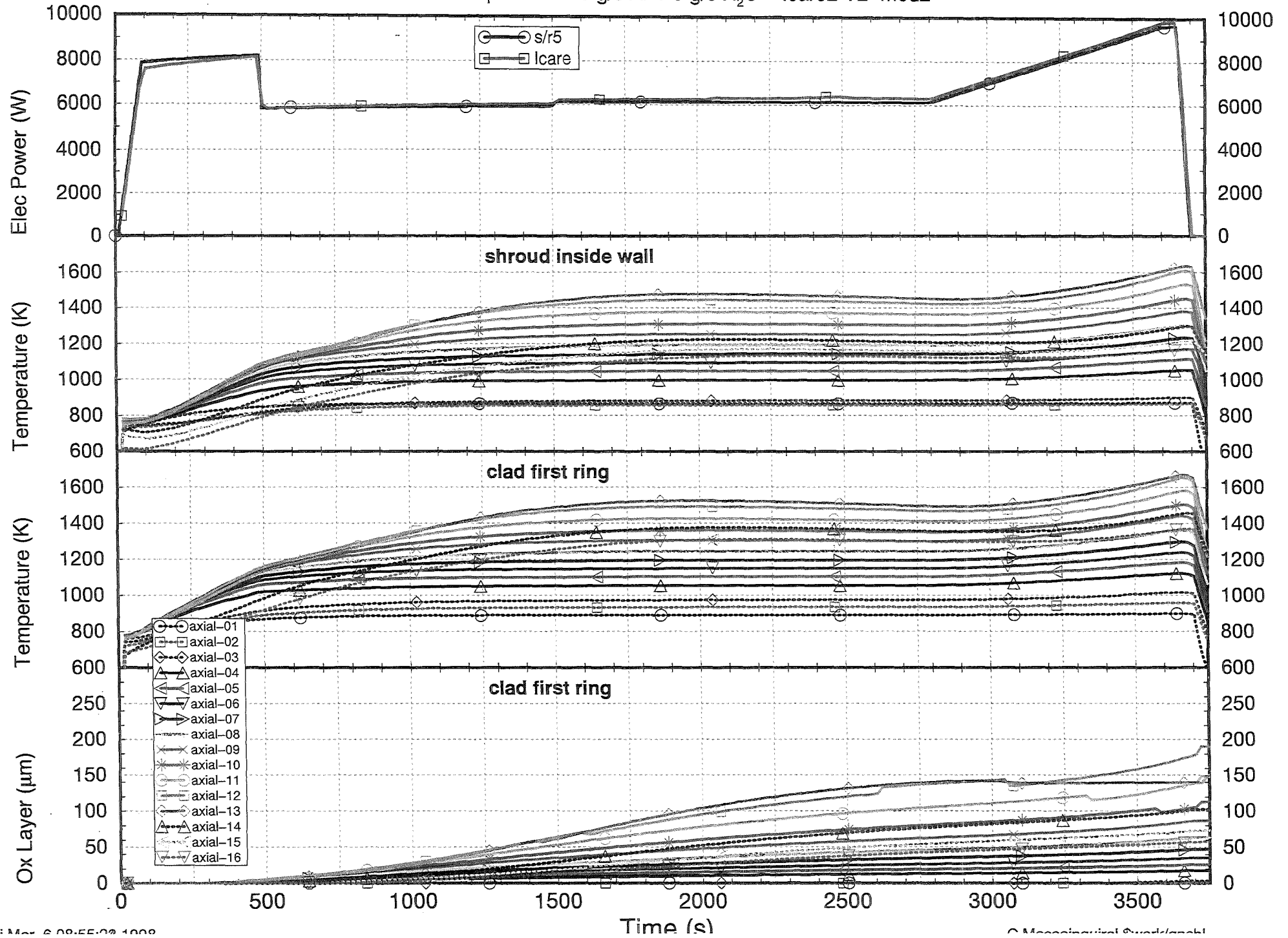


Fig. 48

QUENCH qnch2f14 test4 3 g/s Argon + 3 g/s H₂O

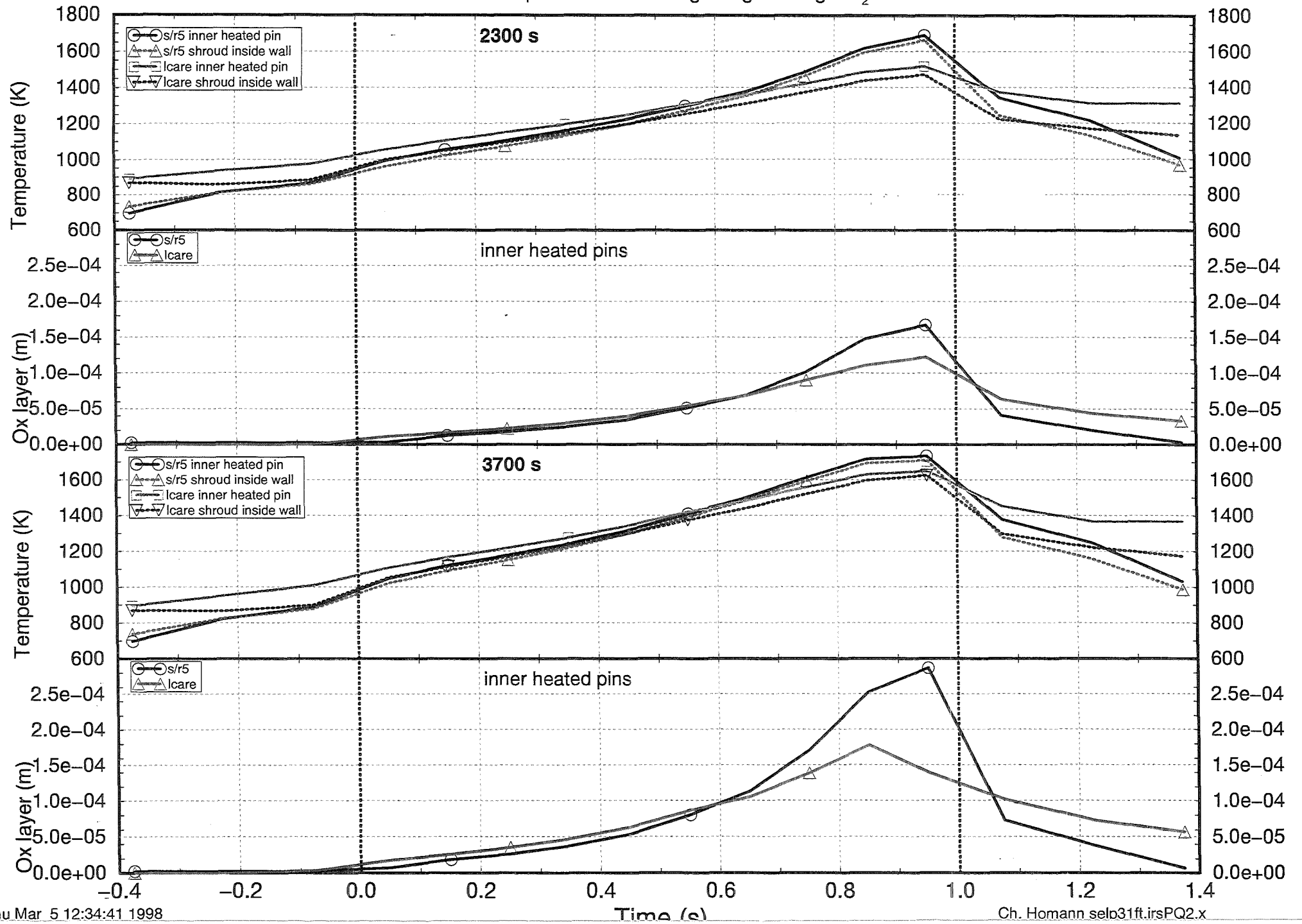


Fig. 49

QUENCH qnch3a06 3 g/s argon

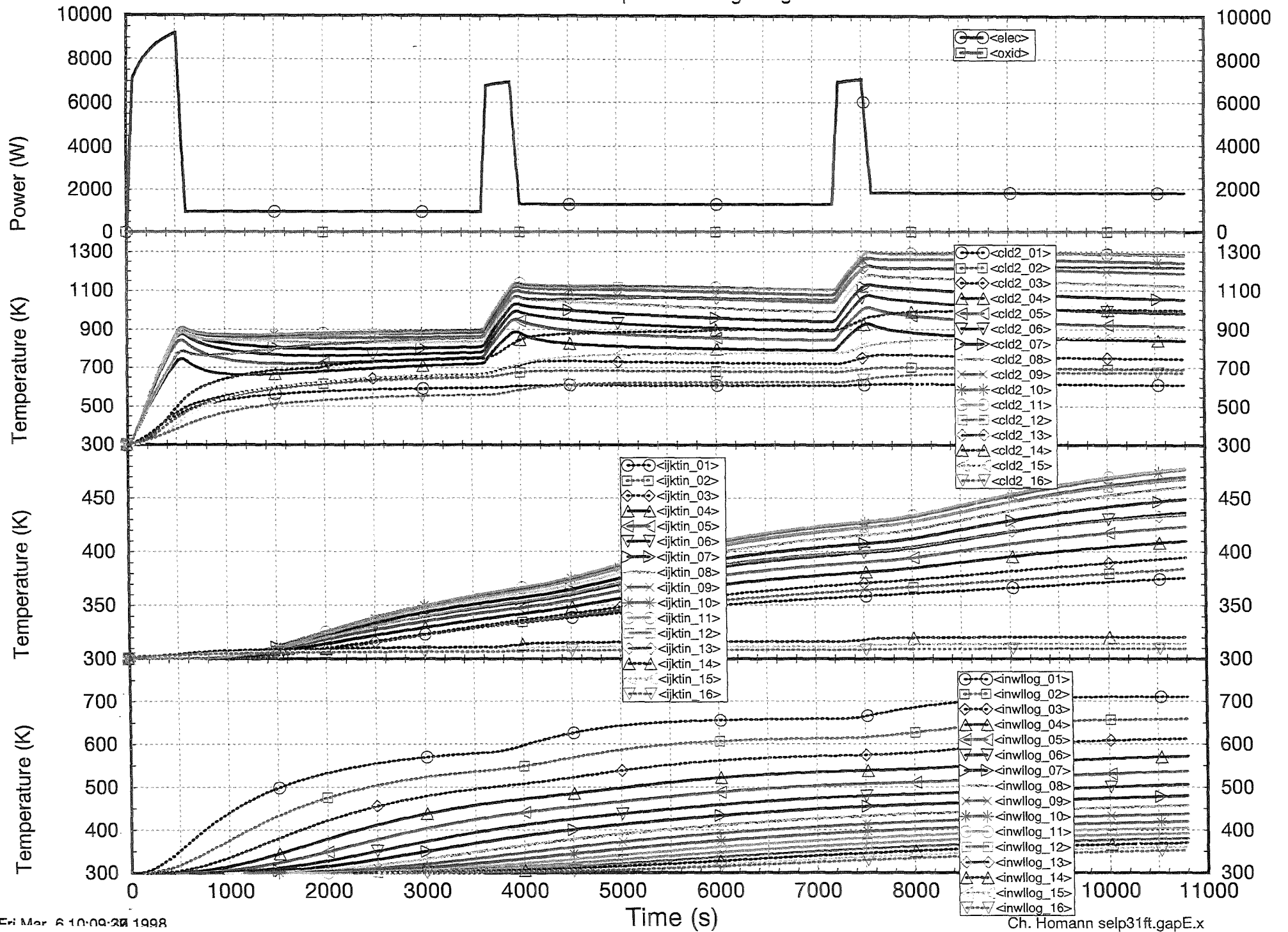


Fig. 50

QUENCH qnch3a06 3 g/s argon

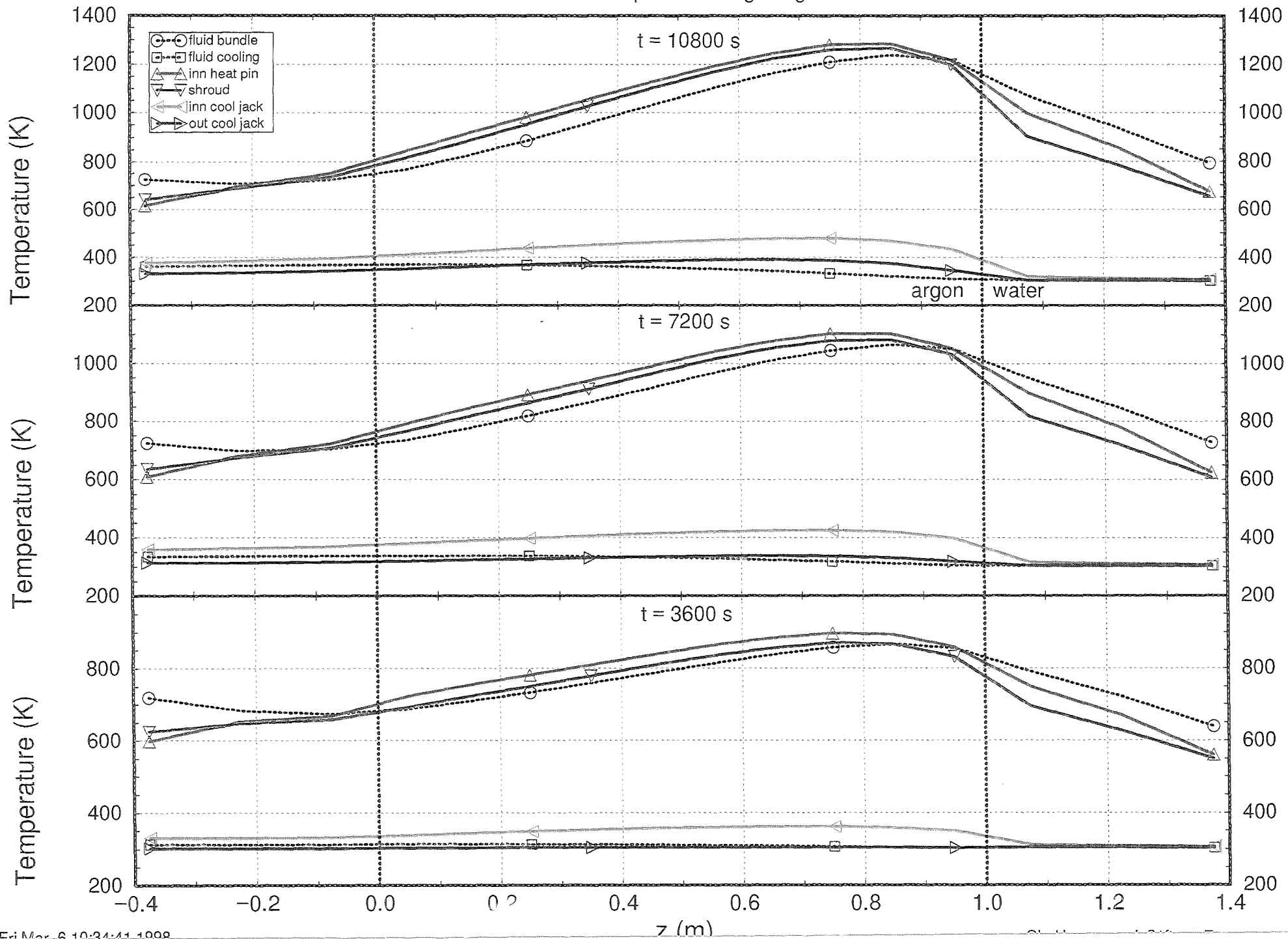


Fig. 51

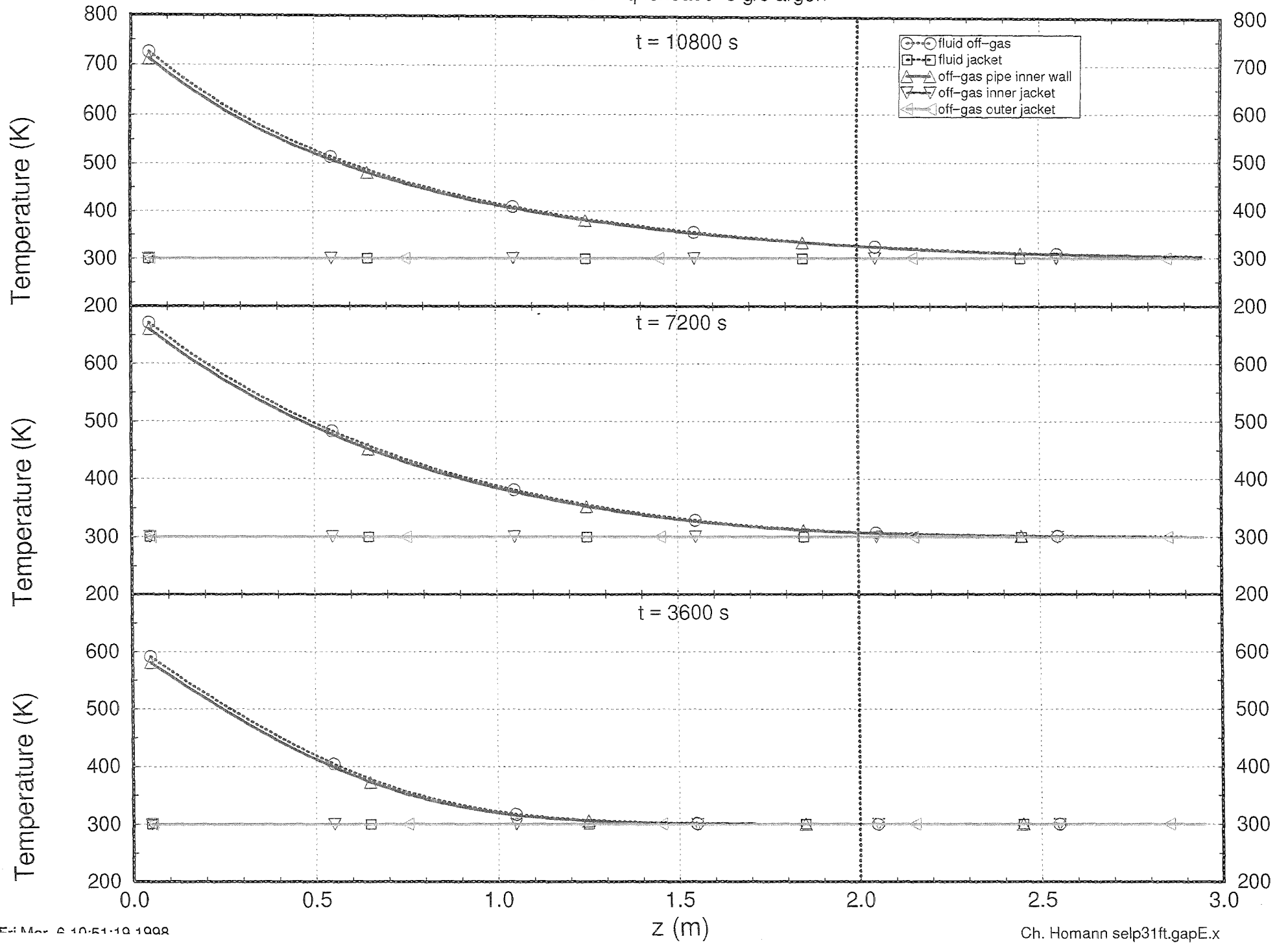


Fig. 52

QUENCH qnch3b03 3 g/s steam + 3 g/s argon

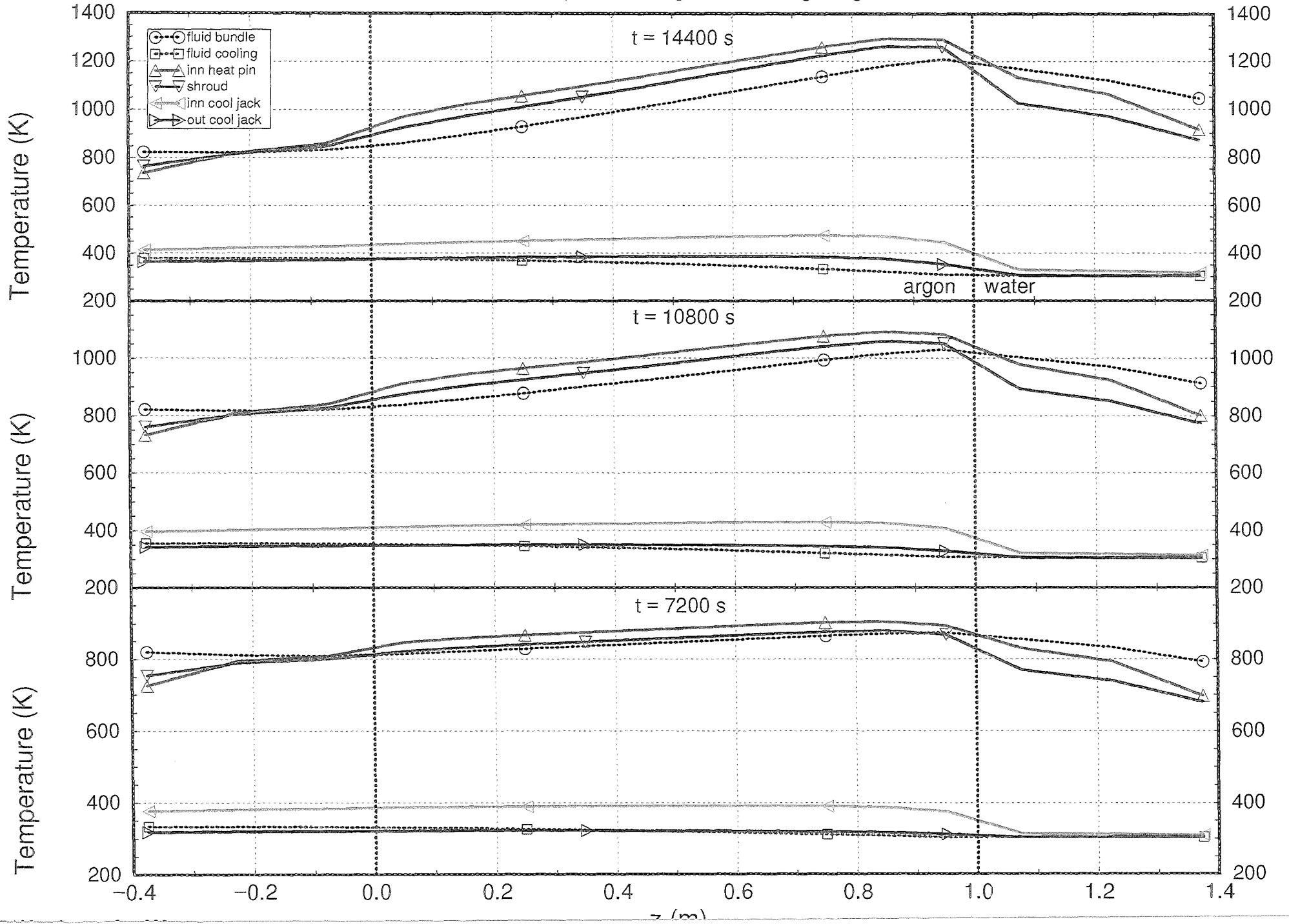


Fig. 53

QUENCH qnch3b03 3 g/s steam + 3 g/s argon

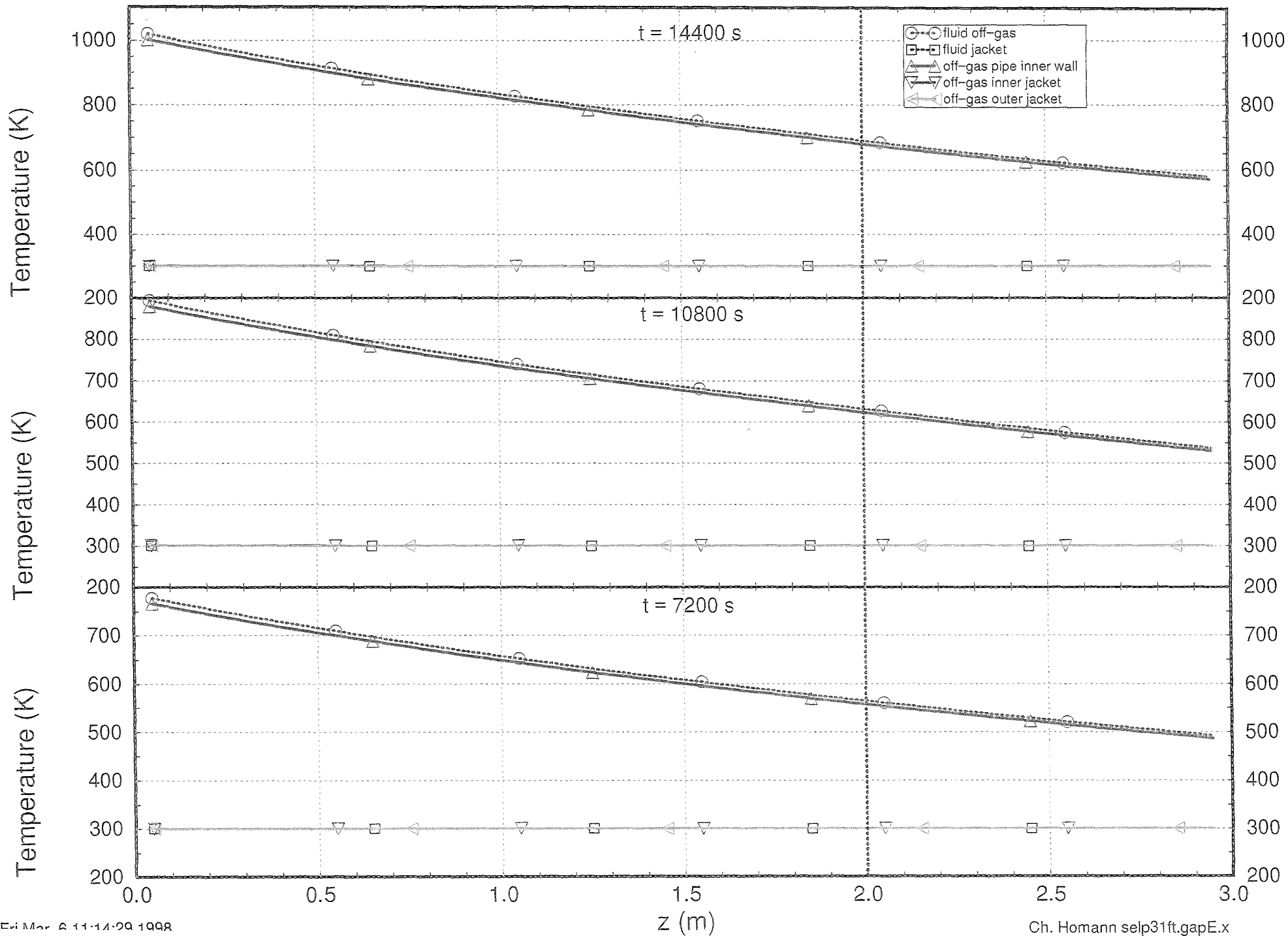


Fig. 54

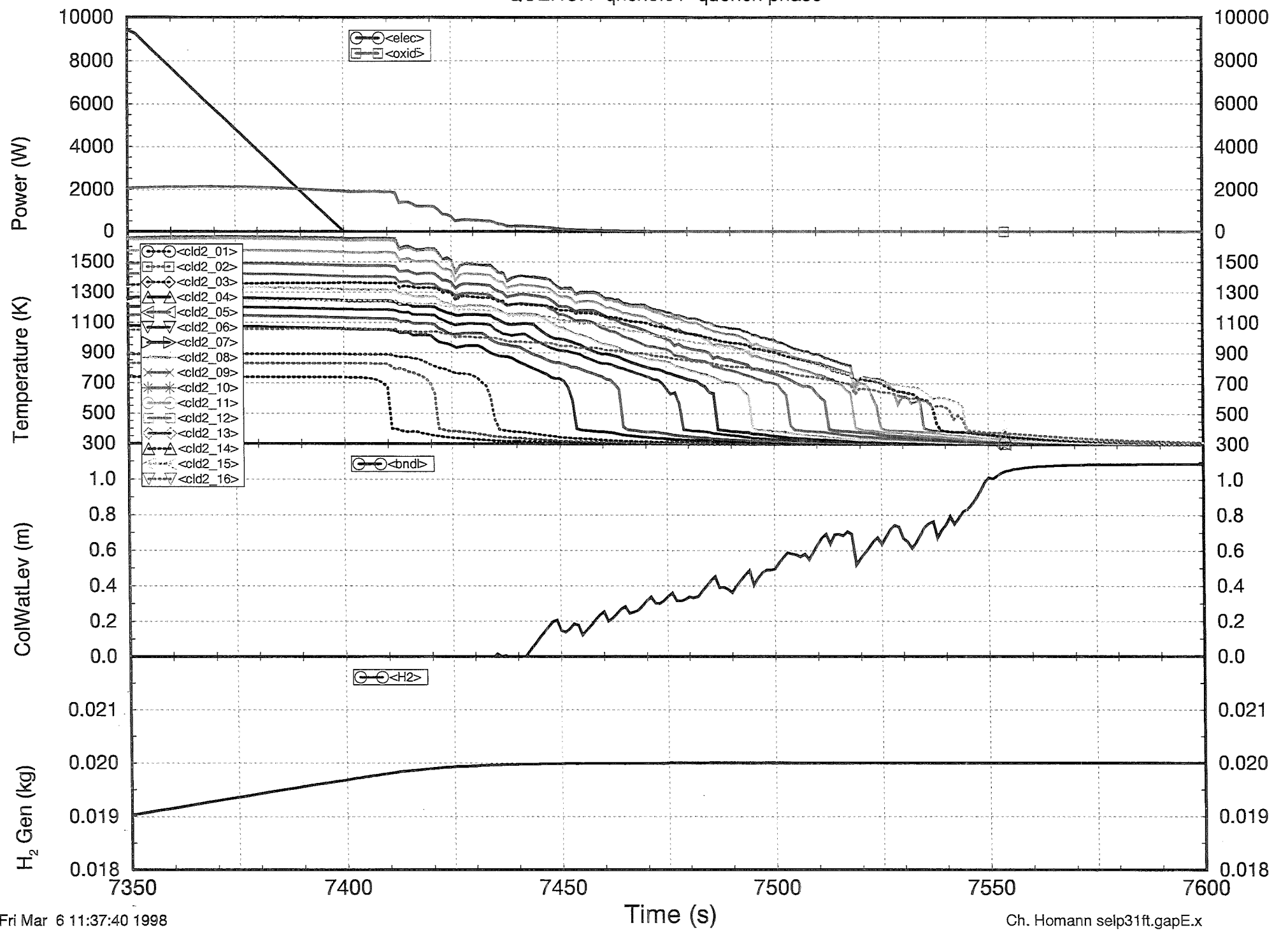


Fig. 55

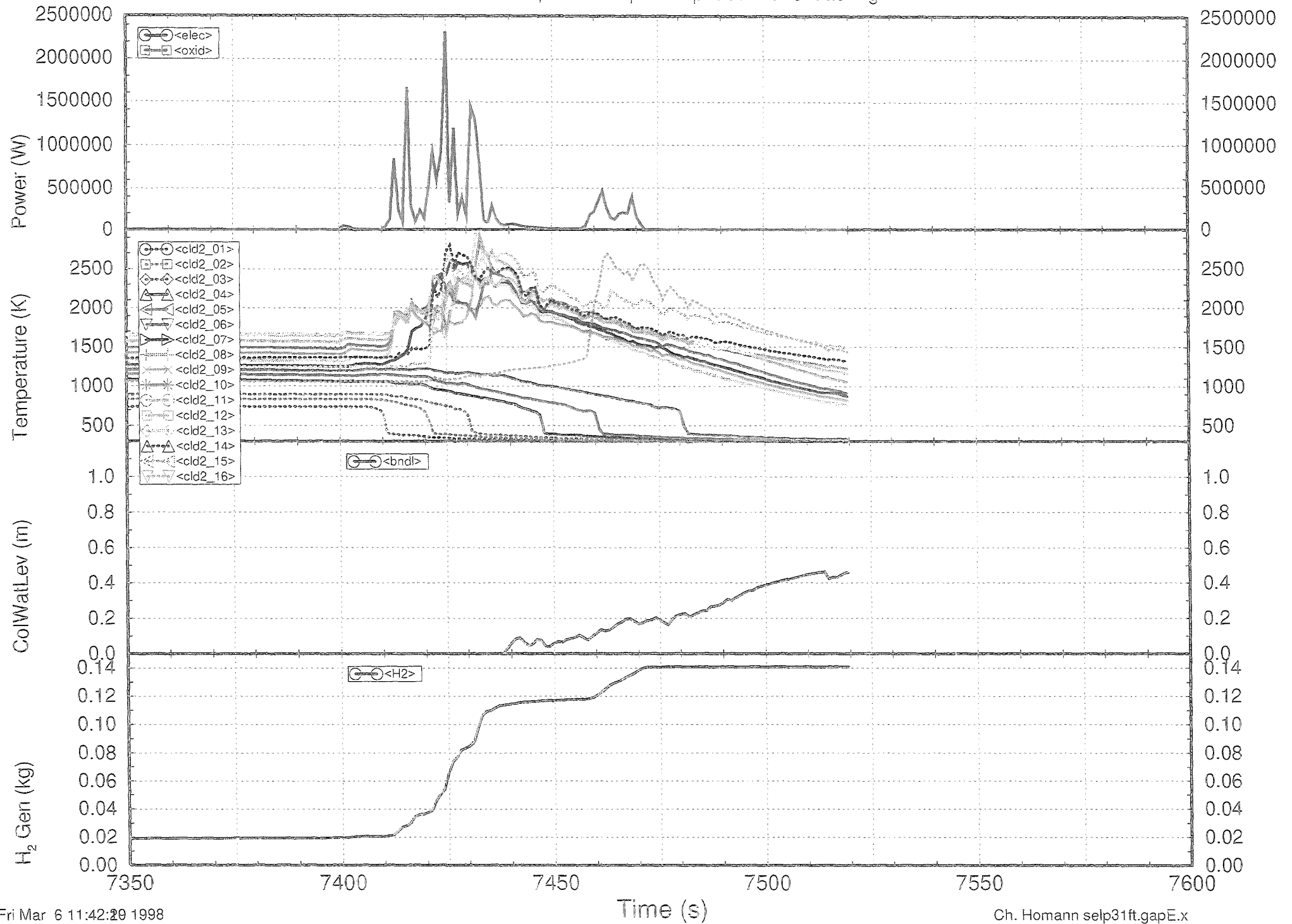


Fig. 56

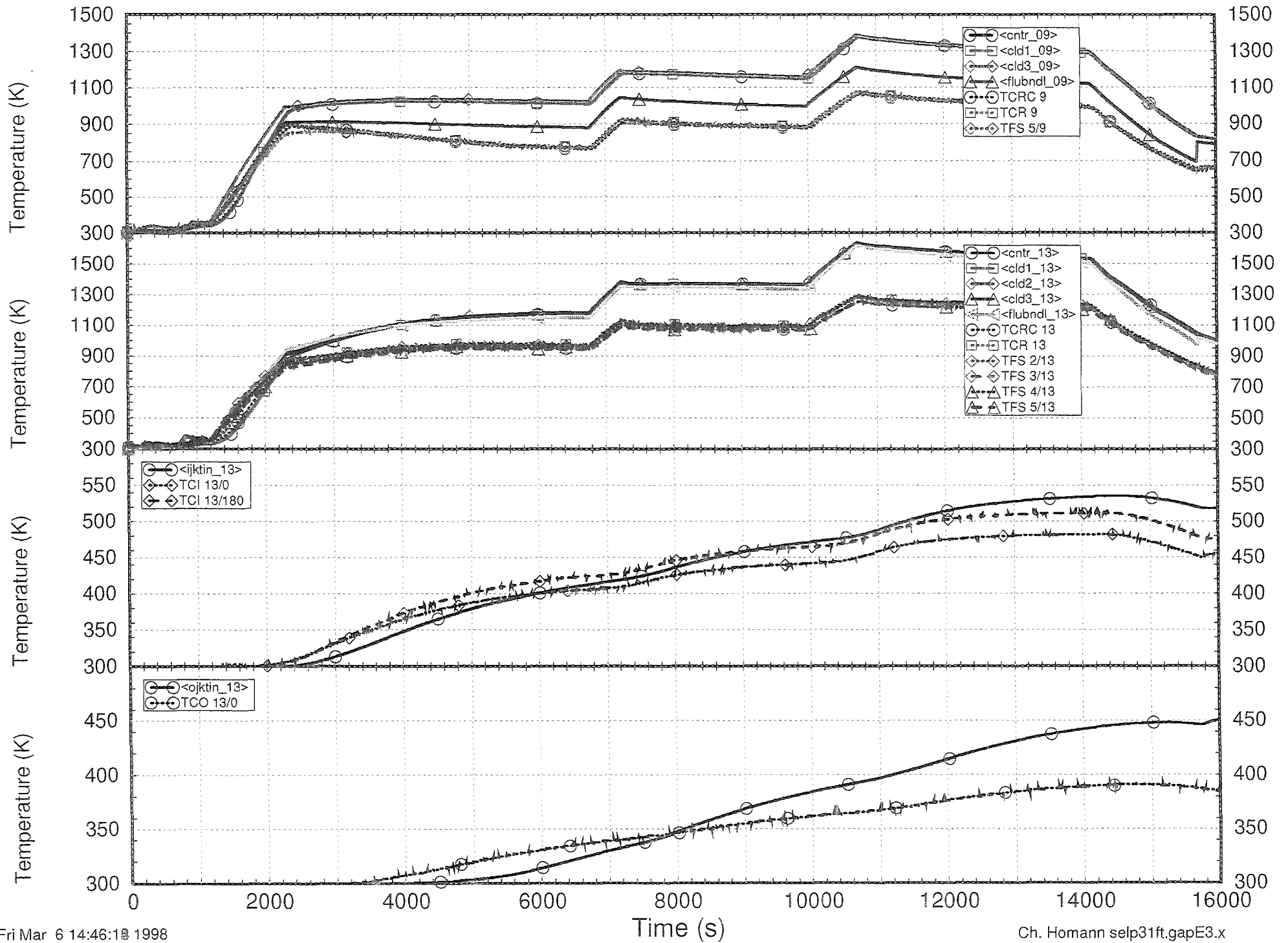


Fig. 57

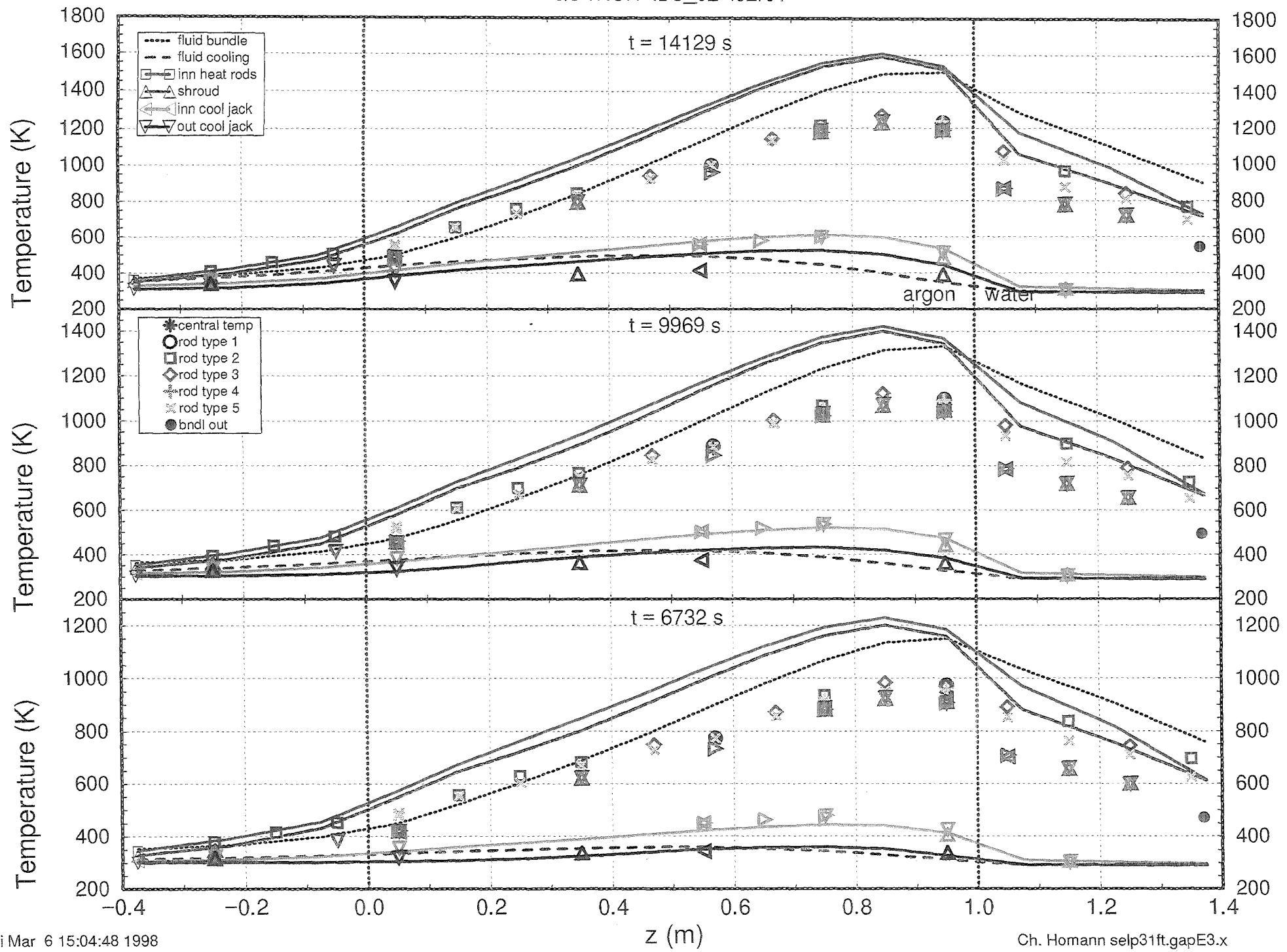


Fig. 58

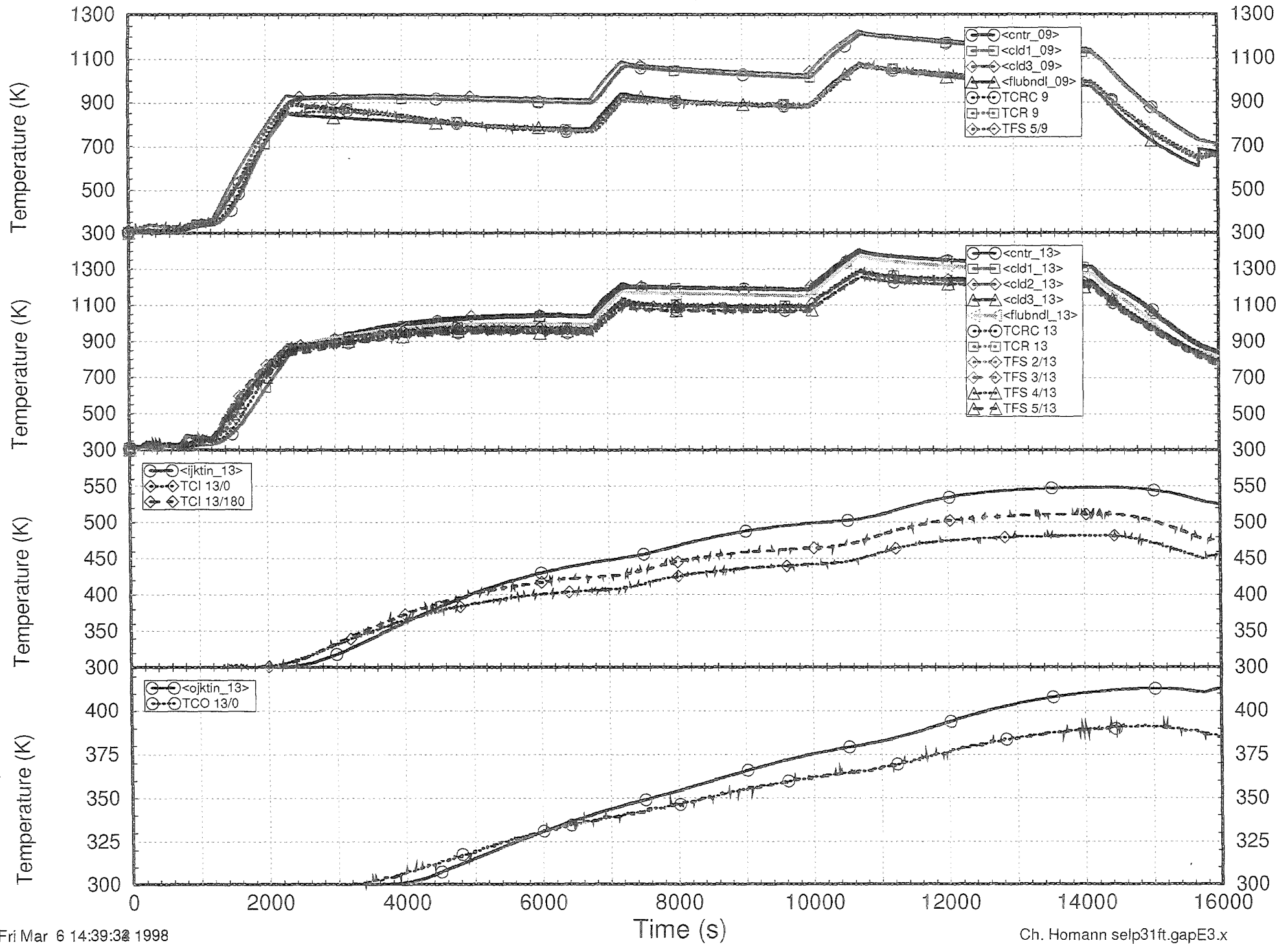


Fig. 59

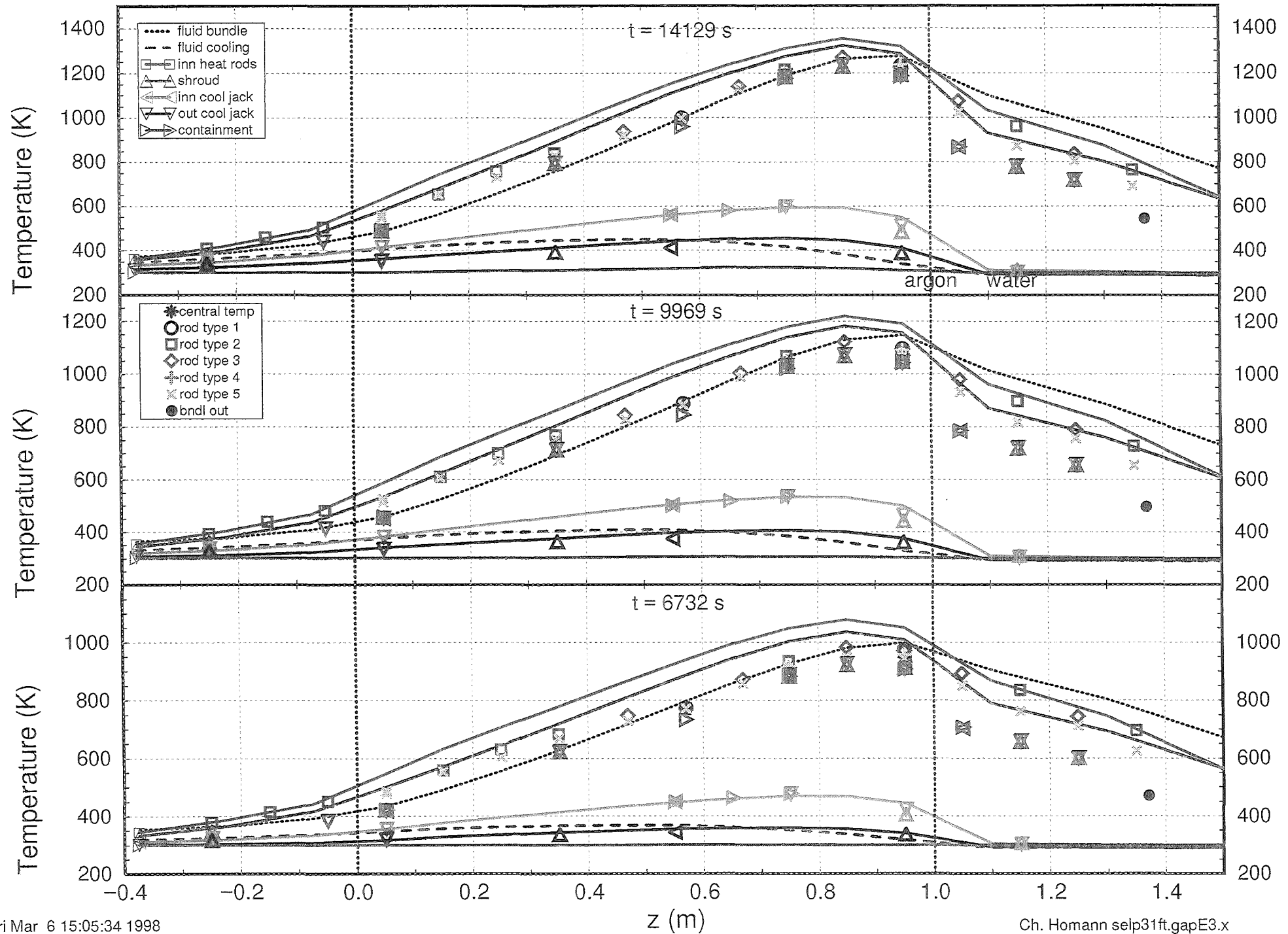


Fig. 60

Material Property Data

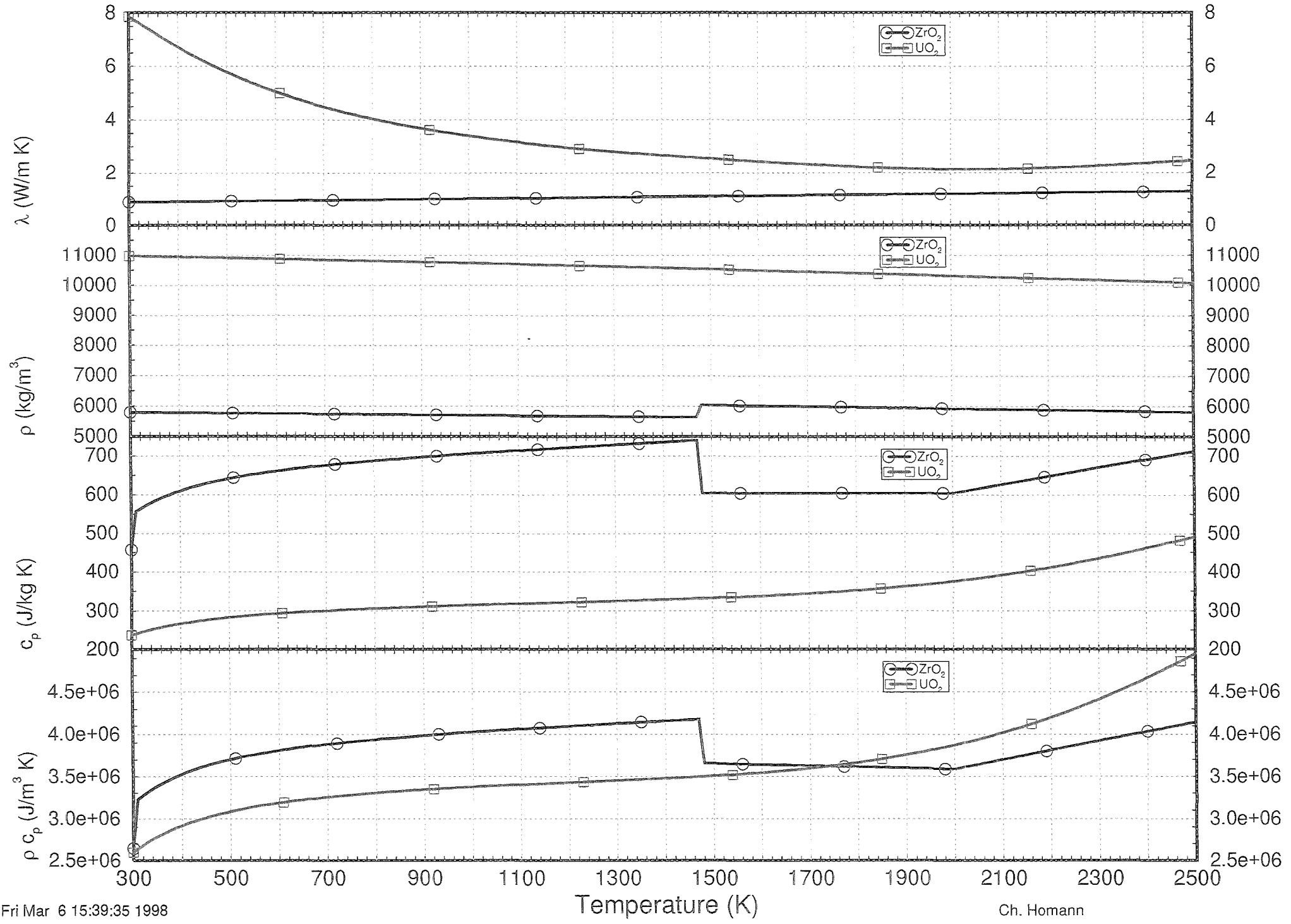


Fig. 61

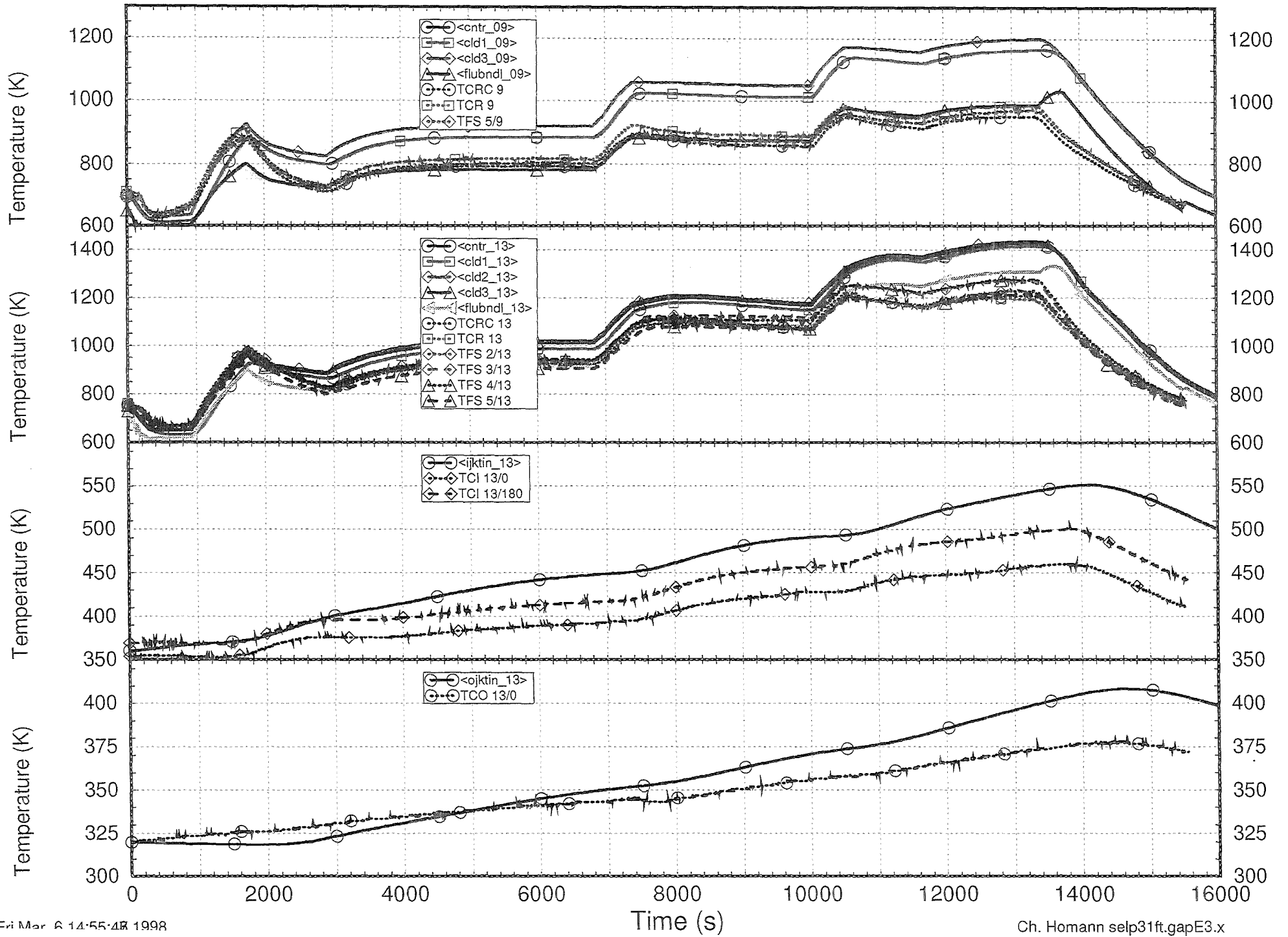


Fig. 62

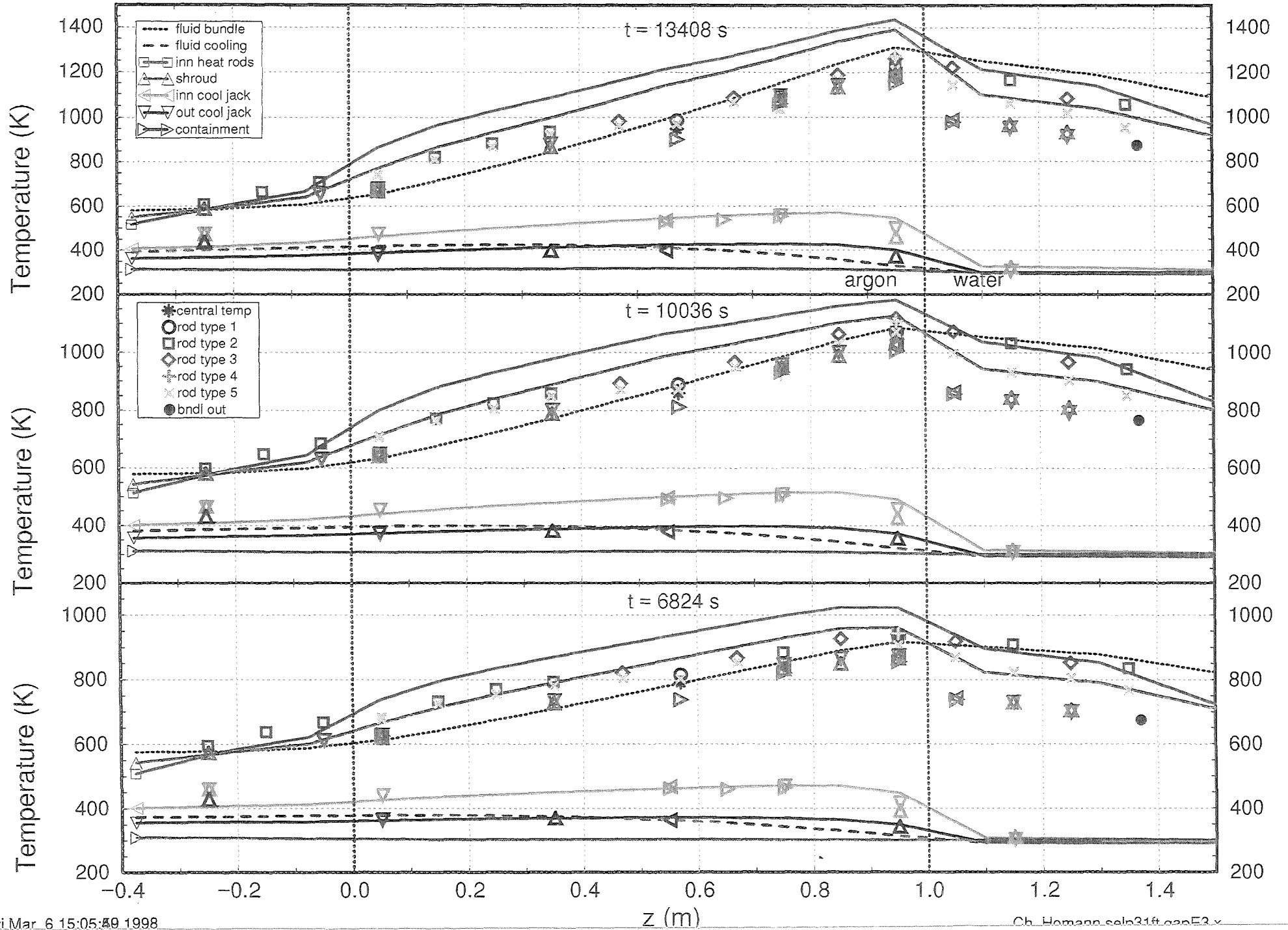


Fig. 63